LOW-COST PASSIVE WIRELESS SENSORS FOR AGRICULTURE AND ENVIRONMENT MONITORING

A Dissertation

by

ONDER DINCEL

Submitted to the Office of Graduate and Professional Studies of
Texas A&M University
in partial fulfillment of the requirements for the degree of

DOCTOR OF PHILOSOPHY

Chair of Committee,	Jun Kameoka
Co-Chair of Committee,	Laszlo Kish
Committee Members,	Kamran Entesari
	Chu Kung-Hui
Head of Department,	Miroslav Begovic

August 2021

Major Subject: Electrical Engineering

Copyright 2021 Onder Dincel

ABSTRACT

This research aims to investigate chipless, wireless passive sensors for agriculture and environmental monitoring where commercially available wireless sensors and their fabrication setups are expensive. In most cases, sensor use is limited by their high cost per unit. Our research targets and tries to solve the cost and reliability issues with multiple novel techniques. This work investigates the principles of chipless and wireless sensing elements and their producibility on low-cost substrates. We have developed sensors, and antenna circuitry on paper and further available for any substrates to ensure our work has the unique and easy-to-follow detailed process and experiments with its limitations, problems with their possible solutions. In addition to being wireless, our sensors have a multiplexing ability that allows multiple sensors to be built on substrates on the same tag, and the data can be received and processed wirelessly in an efficient way on the same substrate plane. Our chipless tag sensors have wireless moisture and temperature multiplexed measurement ability inside the soil, wireless ammonia detection and concentration measurement, wireless abiotic stress detection, differentiating biotic and abiotic stress on plants to ensure effective agricultural and environmental monitoring can be achieved by a low-cost chipless wireless and non-invasive tags. We have achieved sensors and sensing elements targeting wireless, compatible, easy to fabricate, and low cost. Our sensors can be built on any substrates with an additional ability to be multiplexed on the same tag. This research has detailed procedures of the design and fabrications. They

are provided for those who want to design and fabricate their chipless and wireless sensors on any low-cost substrates.

DEDICATION

My doctoral dissertation is devoted to my family. Especially, the presence and support of my parents and sister has brought me to this day and my wife and children have always motivated me to move forward.

This thesis has been prepared with the aim of shedding light on researchers in the scientific community. I would also like to dedicate my doctoral dissertation to those who have devoted their life to science and research.

ACKNOWLEDGMENTS

I would like to give my deepest gratitude to my advisor and committee chair, Dr. Jun Kameoka, who supported and motivated me for my future scientific career. Without his guidance, I would not be able to study sensors. I am thankful for his unlimited support, kindness, and patience. I would like to thank my committee co-chair, Dr. Laszlo Kish, for his kind and positive support. Without my chair and co-chair, I would not consider pursuing my doctorate degree. I would like to thank Dr. Kamran Entesari for his help and guidance in my research. I would also like to thank my committee member Dr. Kung-Hui Chu for her supportive scientific analysis. I want to thank Dr. Won-Bo Shim for his support and kind help in my plant health experiments.

I am immensely thankful to my lab mates Sina Baghbani, Jaskirat S. Batra, Po-Jung Huang, Ting-Yen Chi, Zheyuan Chen. I would like to thank my colleagues Reza Ebrahimi Ghiri, Yusuf Dogan, and Sinan Yigit for their valued knowledge and support. My thanks also go to our department staff graduate advisor Melissa Sheldon for her kind help and support. I also want to thank my all-other friends and colleagues and the department faculty and staff for making my time at Texas A&M University a great experience. I also want to extend my gratitude to the Turkish Ministry of Education for monetary support and giving me the opportunity to have my Ph.D. in Electrical Engineering at Texas A&M University.

Finally, thanks to my parents Muruvvet and Hasan Dincel, for their encouragement and advice. I also thank to my sister Ozge for her great supports. Beyond all, my daughters

Oyku and Ceren-Ozgu are my love, and my works are dedicated to them and last but not least, my wife, Gunes Dincel; you were the inspiration and gratitude along my Ph.D. adventure. Thank you very much for your kind patience, support, and love.

CONTRIBUTORS AND FUNDING SOURCES

Contributors

This work was supervised by a dissertation committee consisting of Prof. Jun Kameoka (Advisor), Prof. Laszlo B. Kish (Co-Advisor), Prof. Kamran Entesari (Member) of the Department of Electrical and Computer Engineering at Texas A&M University, and Prof. Kung-Hui Chu (Member) of the Department of Civil Engineering at Texas A&M University.

The Anechoic Chamber room measurements of UWB antennas are made by Prof. Entesari's research group, and the results are presented to us. Super high frequency (SHF) measurements up to 20 GHz frequency level have done with Prof. Entesari's research group and used his Vector Network Analyzer for those measurements of more than 10 GHz.

Some anechoic chamber measurements were made by Prof. Entesari's Ph.D. student Reza Ebrahimi Ghiri.

Fujifilm Dimatix Material printer was used from Prof. Arum Han's lab, and we have used their oxygen plasma treatment equipment for the surface treatment of the polyimide tape.

Prof. Won-Bo Shim provides us infected and healthy plant samples (corn and cotton).

All other works conducted for the dissertation were completed by the student independently.

Funding Sources

This work was also made possible in part by Bill and Melinda Gates Foundation under Grant Number OPP1199456, and Turkish Ministry of National Education on behalf of Bozok University along with his research and education Under Grant Number: 1416-11/2.

NOMENCLATURE

3D	Three-Dimensional
A	Ampere
AC	Alternative Current
AM	Amplitude Modulation
B	Susceptance
C	Celsius
C,c	Capacitance
c	Speed of Light
CAD	Computer-Aided Design
dB	Decibel
DC	Direct Current
DI	De-ionized
EDX	Energy Dispersive X-Ray
Eq	Equation
EM	Electro Magnetic
EMF	Electro Magnetic Field
F	Farad
f	Frequency
FM	Frequency Modulation
g	Gram

G	Conductance
GHz	Giga Hertz
HCl	Hydrogen Chloride
HF	High Frequency
Hz	Hertz
hr	Hour
IC	Integrated Circuit
IPA	Isopropyl Alcohol
K	Kelvin
kHz	Kilo Hertz
kΩ	Kilo-Ohm
λ	Wavelength
l	Length
L	Inductance
LCR	Inductance Capacitance Resistance
LF	Low Frequency
LoB	Limit of Blank
LoD	Limit of Detection
μA	Micro-ampere
μF	Micro-Farad
μm	Micro-meter
μV	Micro-volt

m	Meter
mA	Milliampere
MEMS	Micro Electro-Mechanical System
mΩ	Miliohm
MΩ	Megaohm
mg	Milligram
MHz	Mega Hertz
min	Minute
MIP	Molecularly Imprinted
mL	Milliliter
mm	Millimeter
mV	Milli-Volt
nA	Nano-Amper
NCSOm	Nitrite Ceramic Silver Oxides Mixture
nF	Nano-Farad
NFC	Near Field Communication
nm	Nanometer
Ω	Ohm
P	Power
PANI	Polyaniline
PCB	Printed Circuit Board
PDMS	Polydimethylsiloxane

PET	Polyethylene Terephthalate
pF	Pico-Farad
pL	Pico-Liter
PP	Polypropylene
ppm	Particle per million
PVA	Polyvinyl Alcohol
Q	Quality Factor
$\boldsymbol{\rho}$	Resistivity
R,r	Resistance
r	Radius
RF	Radio Frequency
RFID	Radio Frequency Identification
RH	Relative Humidity
RMS	Root-Mean Square
RX	Receiver
$\boldsymbol{\sigma}$	Conductance
s	Second
S	Siemens
SAW	Surface Acoustic Waves
SEM	Scanning Electron Microscopy
SHF	Super High Frequency
SNP	Silver Nano Particles

t	Time
ti	Thickness
T	Period
TDR	Time Domain Reflectometry
TX	Transmitter
UHF	Ultra High Frequency
uL	Micro liter
um	Micron
UWB	Ultra-Wide Band
UV	Ultraviolet
UVA	Ultraviolet A
ω	Angular Frequency
W	Watt
w	Weight
wt	Width
V	Volt
v	Volume
VNA	Vector Network Analyzer
X	Reactance
X_c	Capacitive Reactance
X_L	Inductive Reactance
Y	Admittance

Z	Impedance
Z_o	Characteristic Impedance

TABLE OF CONTENTS

Page

ABSTRACT ii

DEDICATION iv

ACKNOWLEDGMENTS v

CONTRIBUTORS AND FUNDING SOURCES vii

NOMENCLATURE ix

TABLE OF CONTENTS xv

LIST OF FIGURES xvii

LIST OF TABLES xxii

1. INTRODUCTION 1

1.1. Objective and Motivation 1
1.2. Passive RFID Tags and Wireless Communication 4
1.2.1. Passive RFID Tag Components 5
1.3. Sensing and Sensor Fabrication 10
1.3.1. Sensing Principles 11
1.3.2. Sensor Fabrication 12
1.4. Experimental Measurement 13
1.5. Previous Research 13

2. DESIGN AND FABRICATION 15

3. MULTIPLEXED UWB (ULTRA WIDE-BAND) SENSOR 33

3.1. Introduction 33
3.2. Materials and Methods 35

4. UHF TAG SENSORS 43

4.1. Molecular Imprinting 43
4.2. Electrodes Printing 45
4.3. UHF Tag Sensor Setup 46

4.4. Wireless UHF Tag for Plant Drought Stress 52

5. LF LEVEL PLANT HEALTH MONITORING 57

5.1. Introduction 57
5.2. Abiotic and Biotic Stress Sensor and System Design 58

6. RESULTS AND DISCUSSION 66

6.1. Wireless Multiplexed Temperature and Moisture Sensors Measurements 66
6.1.1. UWB Antenna Tests and Measurements 66
6.1.2. Stub Resonators Design and Measurement Results 69
6.1.3. Wireless Soil Measurements for Super High-Frequency Levels 74
6.1.4. SHF Salinity Measurement 79
6.2. UHF Level Sensing and Measurement Results with Discussion 80
6.2.1. UHF Wireless Gas Sensing 82
6.2.2. UHF Level Wireless Plant Stress Monitoring 85
6.3. LF Level Plant Health Sensing 88

7. CONCLUSIONS 93

REFERENCES 94

APPENDIX A EDX AND SEM IMAGES 103

APPENDIX B ENHANCEMENTS IN FABRICATION 106

APPENDIX C DEVICES USED IN FABRICATION 108

LIST OF FIGURES

Page

Figure 1: Radio Frequency Levels and their classifications.....4

Figure 2: An RFID tag and its components.....5

Figure 3: Basic equivalent circuit of a tag.....6

Figure 4: Fabrication Steps for low-cost sensors/tags/antennas.....16

Figure 5: Fujifilm Dimatix material printing method. 18

Figure 6: 3D Design and fabricated versions of the commercial sensor probe covers to perform reference measurements.....19

Figure 7: UVA Exposure (Green Line) and Photoflash Bulb Spectral illumination resistivity improvements in ohm.cm (Blue Line) 20

Figure 8: Printing issues for Fujifilm Dimatix Material printer.....22

Figure 9: PP substrate Silver Nanoparticle ink deposition post curing.....23

Figure 10: Silver nanoparticles are deposited on PET substrate and its SEM images.....24

Figure 11: EDX SEM Image and measurement for the inkjet ink to understand what types of compounds have been used.....25

Figure 12: Preliminary data collection probes for plant health monitoring wired structures to perform multiple probes to avoid physical pressure point and force effect without having high ohmic contact resistivity.....26

Figure 13: Microstrip lines designed on PET and polyester film in several thicknesses.27

Figure 14: a) Designed 3D schematics of the resonator on a microstrip line, b) impedance and 2D structural position of the stubs, c) their equivalent circuit affecting the resonance frequency and their quality factor.....28

Figure 15: Stubs resonant frequencies by the numbers of the stubs allocated on the same substrate and their quality factors defined by their resonance frequency and 3dB signal decrease method.....30

Figure 16: Multiplexed resonators and their frequency vs gain responses 31

Figure 17: a) Fabricated five stubs microstrip line resonator on pet substrate b) Schematical representation of the stubs impedance and conductance c) Equivalent circuit schematics of the printed circuit network for multiplied stubs 36

Figure 18: a) Testing setup for the multiplexed soil sensor, b) The sensor before dipping into the soil, c) Cross-sectional cut view and layers depositions on the PET substrate. 38

Figure 19: a) Printed and prepared wireless sensor unit, b) Cross-sectional view and parts of the paper sensor, c) Experimental setup for the wireless measurement 40

Figure 20: All RF Absorber covered box 40

Figure 21: a) Experimental Setup with other sensor probes b) Experimental Setup monitoring sensors removed and ready to perform the wireless measurement 41

Figure 22: a) Salinity experiment setup, b) UWB antenna design and the water droplet illustration 42

Figure 23: Molecular printing principles and methods a) solution mixed with the functional monomers (blue) and template materials, b) Co-polymerization of Functional monomers with templates. Molecular recognition modification has been made and, c) Removing the template material © 2020 IEEE "Adapted from [45]". 43

Figure 24: Fujifilm Dimatix material printer electrode printing process schematics. Silver nanoparticles are deposited on the polyethylene terephthalate and/or any other polyester materials. In a conventional oven it has been cured for 120°C for an hour. Sintering helped to evaporate the solvents in the ink. Polyaniline strips are integrated with the silver electrodes. Conductive silver flakes paste has been applied added on the corner parts to avoid any discontinuity © 2020 IEEE "Modified from [45]" 45

Figure 25: Wireless and battery-less paper sensor, schematic diagram of wireless and battery-less paper sensor. Dipole antenna receives the signal from the source antenna, and RF signals proceed through the MIP sensing element and back to the source antenna 47

Figure 26: a) Designed and first worked UHF tag with better quality factor and resonance at 1100MHz b) Ultimate version of the UHF tags where it can operate at 940MHz 48

Figure 27: UHF level tag design and its dimensions in detail for reproducibility and comparison. 49

Figure 28: a) Printed UHF tag b) MIP PANI deposited on the gap between dipole antennas 50

Figure 29: Image of the VOC detection experiment set up. Wireless paper sensor is located on the inside of the chamber wall to monitor the VOC concentration from food spoilage. 51

Figure 30: Metal template for plasma treatment before printing and high temperature oven curing a) Printed sticky front side b) Opposite side view of the tape. 53

Figure 31: UHF level wireless IDT sensor design for sensing plant abiotic stress (drought) 54

Figure 32: UHF Plant Stress Monitoring Tag Experimental Setup 55

Figure 33: Stress reasons in plants 57

Figure 34: Schematic of a handheld with described parts 60

Figure 35: Printed handheld probes for precise measurement 61

Figure 36: Experimental setup for plant health monitoring (cotton) testing setup of the handheld device with complete wireless configuration and connection through portable wireless VNA 62

Figure 37: Cotton seedlings for plant abiotic and biotic stress monitoring 63

Figure 38: Cotton seedlings for drought test b) Cotton seedling sample in a petri dish .. 64

Figure 39: Graph for antenna reflection S11 data and the printed antenna. 67

Figure 40: Anechoic chamber measurements of the UWB antenna 68

Figure 41: Anechoic Chamber measurements of the UWB antenna and its radiation pattern at three planes (yz, xz, xy) 69

Figure 42: Stub type resonator simulation and measurement (5 Stubs) 70

Figure 43: Stubs resonance frequencies vs to gain and their quality factors 72

Figure 44: a) Not multiplexed stubs group temperature sensor performance b) not multiplexed sensor response to the water content in soil c) Multiplexed

version of the stubs group temperature sensor response to the temperature changes in the soil d) multiplexed sensor response of the moisture sensor.....73

Figure 45: Multiplexed Resonators and their frequency and gain responses.....75

Figure 46: S21 Response of the antenna for wireless sensing and its temperature, moisture and control resonance frequency peaks 77

Figure 47: Water content and temperature changes in magnitude and frequency, respectively, for wireless sensing. 78

Figure 48: Wireless S21 changes in the gain by the salt content in the water droplet. 79

Figure 49: Fabricated UHF tag version 1 (shorter dipole antennas) 81

Figure 50: Nitrogen only and nitrogen with ammonia measurements from the setup at a particular concentration.....83

Figure 51: Molecular imprinted wireless sensor measurement in several ammonia concentrations 84

Figure 52: Stressed and healthy corn response in wireless measurements. 85

Figure 53: Healthy and stressed plants averaged magnitude results from UHF wireless sensing tag 87

Figure 54: Measured resistance from the cotton samples 88

Figure 55: Measured capacitance from the cotton samples 89

Figure 56: Resistance Measurements for abiotic drought stress on cotton seedlings 90

Figure 57: Capacitance measurement of abiotic drought stress on cotton seedlings 91

Figure 58: Measured resistance at 100 kHz of abiotic drought stress on cotton seedlings 92

Figure 59: EDX measurement and SEM images with Silver, Chloride, Oxygen, Carbon atoms in the sample.....103

Figure 60: Silver, Chloride, Carbon and Oxygen atoms in the ink sample.....104

Figure 61: Polyurethane, Ethylene glycol, Flourosurfactant (Benzalkonium Chloride), and Glycerol Chemical Structures 105

Figure 62: Ultra wide band antenna design on PDMS and PDMS Ecoflex mixed samples 106

Figure 63: a) Stereolithography 3D printer b) Material inkjet printer c) Spin coater 108

Figure 64: Devices are used for cleaning and curing processes a) Ultrasonic Cleaner b) Optical Curing Flashing Machine c) Hand Vacuum d) Scale e) Oven 109

LIST OF TABLES

Page

Table 1.1 Material Printer Settings Table in Section 2 ”Adapted from [34]”.....17

1. INTRODUCTION

1.1. Objective and Motivation

The World evolves through data collection and processing. Data is the barest value that comes from outputs in the form of a quantity and/or a phrase. In terms of data mining, for a physical or chemical changing data collection, sensors are required. They monitor/read changes in the targeted agent and provide data for further understandings. Sensors are the input data loggers for networks that give more knowledge about the target [23]. However, in today's world, expensive and unfeasible sensors refrain the widespread applications and usability [24]. Therefore, being low-cost and easy fabrication with simplicity make sensors available for everybody.

In the semiconductor industry we have plenty of silicon wafer based electrical and optical sensors. Although they are cultivated their limited fabrication and applications restrain their implementations. Particularly in agriculture, the sensors are extraordinary limited and ineffective.

Starvation and human population increase have forced the industry to invent and invest on high yield agriculture. To improve the yield, you can adjust given nutrients to the plants, genetically modify, and change environments [21,22]. Changing climate and soil is not a cost-efficient way; therefore, industry focused on GMO or nutrients support [20]. GMO is a way that is related to the plant seed. However, for growth, external nutrient support and dosages are very crucial. To increase the yield, precise agriculture is required. To get precision, proper monitoring is the key. In the agriculture industry there are plenty

of companies focused accurate monitoring and testing. However, they don't provide any ultra-low cost monitoring methods that can give an ability to monitor the vast fields. Our motivation and the proposed idea is to provide those sensors with for a meager cost and very easy to fabricate for data collection and simultaneous monitoring for more efficient and precise agriculture.

Sensors are typically used to monitor data in various applications, such as agricultural applications and in the health care industry [25-27]. In agricultural applications, sensors may be used to monitor crop fields in order to apprise farmers of various conditions present in the crop field. In agricultural applications, large areas, such as hundreds of acres need to be monitored. For example, soil conditions are monitored to ensure that the soil conditions are conducive to growing crops. Typically, the soil conditions are manually monitored, where a user moves around crop fields with a probe for insertion into the crop field. Often times, this method of manually monitoring soil conditions is time prohibitive since users need to probe hundreds of acres manually.

Moreover, in some implementations, battery-powered sensors may be used for agricultural applications [28-30]. In these implementations, the sensors are placed in areas that require monitoring and gathering all data to determine soil conditions. However, these sensors typically are expensive, need a battery, and, if the battery does not die first, tend to decay over time due to exposure to the elements. Additionally, for large areas, such as hundreds of acres, many of these sensors are required. Thus, using these types of sensors is cost prohibitive. Furthermore, similar to using the probes mentioned above, no

automated method exists for gathering data from these sensors. Instead, the data must be manually gathered, which creates problems similar to using probes.

Many researches and designs have been made and represented about RFID tags on any substrates in literature for wireless sensing purposes [37-42]. RFID tags are generally used as price tags to provide faster checkout or security tags [43,44]. However, there are many types of research made on the tags to proof of the concept using them as a wireless sensing element [41,42]. RFID tags, in literature, generally are focused on sensing or coding uses [37,39,40,41].

In today's world, we have advanced technology on sensors. Their sensing capability and quality factors are truly high. However, costly fabrication and expensive setups are not only decreasing their value but also the availability for all the consumers. The producer avoids setting thousands of dollars on just monitoring their crops/plants while struggling with undesirable expenses.

In addition, wireless sensors are in the literature for decades [7,8,29,30,39,42]; however, their simplicity are decreased by the usage of the chips to regulate/filter/amplify the sensing data by adding additional cost to the device. Therefore, we don't see many sensory tags around in the market as long as the product is pricey.

Our motivation is to provide low-cost wireless sensors for the broad of usage multiple sensing and increase the feasibility and prevalent usage. Our targeted experimental examples are for agricultural, environmental, and biological monitoring.

In addition to all sensing capabilities, also their durability in outdoors and being non-invasive are crucial features for the harsh environment and able to implement measurements for the seedlings.

1.2. Passive RFID Tags and Wireless Communication

Radio Frequency Identification (RFID) has increasing popularity in our digital world. These RFID tags are in almost all industries, especially for tracking and barcoding purposes. There are three types of tags: passive, semi-active, and active. We are not going to discuss active or semi active RFID tags. Because these tags, Programmable chip integrated RFIDs, are costly and complicated structures with an expensive fabrication process.

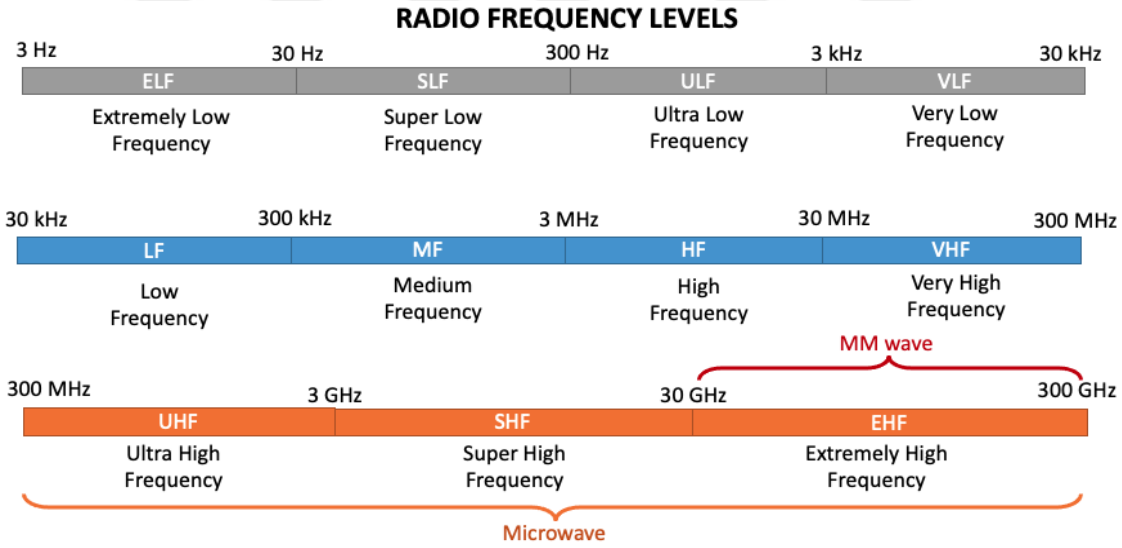

Figure 1: Radio Frequency Levels and their classifications

As seen from the figure there are several bands in radio frequency. We have our measurements at Super High Frequency (SHF), Ultra-high frequency (UHF), and Low-frequency levels (LF), where their operational frequency ranges are from 30 GHz to 3

GHz, 300 MHz to 3 GHz, and 30 kHz to 300 kHz respectively. Our passive batteryless and chipless wireless sensors work at microwave levels.

1.2.1. Passive RFID Tag Components

The main parts of the RFID tags are the antenna, integrated circuit, and substrate, as shown in figure 2.

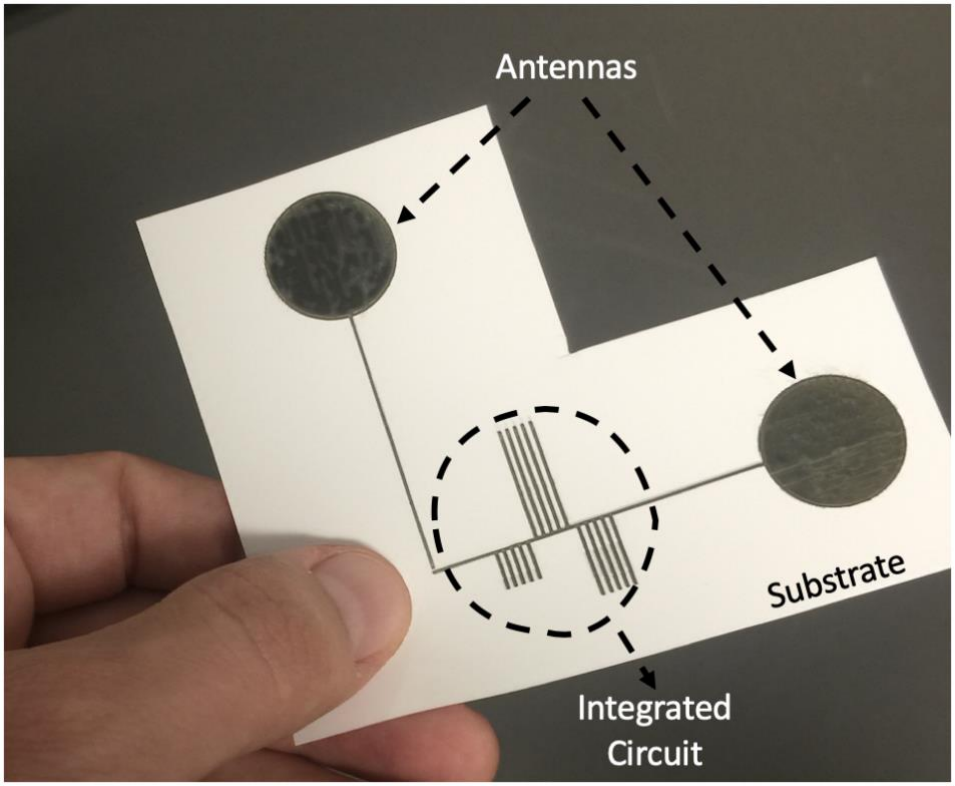

Figure 2: An RFID tag and its components

A tag has three main parts to perform its wireless detection capability as seen from figure. Antennas are required to receive and/or reflect the signals. Integrated circuit is the circuit components of the whole tag where it modifies the received signal between

antennas. And the substrate is the part of dielectric isolation, affecting design and fabrication. The primary circuit equivalent of the tag is in figure 3.

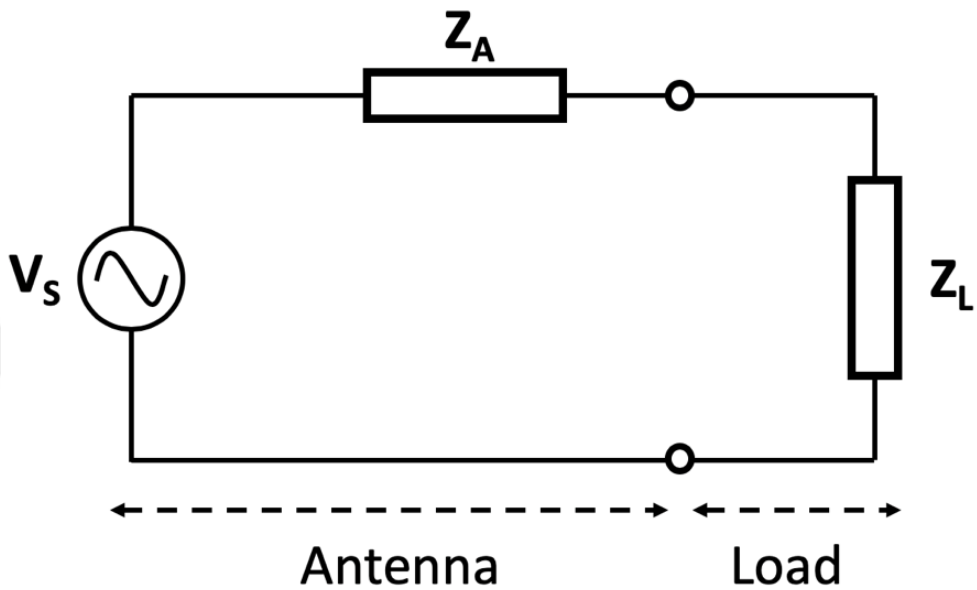

Figure 3: Basic equivalent circuit of a tag

V_s is the voltage generated across the whole tag; impedance of the load includes all the circuit elements integrated into the tag. The impedance of the antennas is important to match with the impedance of the load and the whole testing/transmitter and receiver systems to maintain the highest power transfer between a transmitter and a receiver. The maximum power reflection coefficient can be calculated by the equation given below.

$$|s|^2 = \left|\frac{Z_L - Z_A^*}{Z_L + Z_A}\right|^2 \ , \ where\ Z_A = Z_L^* \ , \ 0 \leq |s|^2 \leq 1$$

For the maximum power transfer, the imaginary part of the load should be equal to the real part of the antenna, and if the imaginary part of the antenna equals to antenna's real impedance part, the impedance matching will be the maximized and higher power transfer will be possible.

1.2.1.1. Tag Antenna

The passive tag antenna is responsible part to receive and transmit the signals. According to the operation frequency level and range, this part is the most space consuming part of a tag. In addition, they also have a circuit equivalent that interferes with the integrated circuit part of the tag. Besides, in some applications, the RFID tag can only have a backscattered structure, and whole system act as a specified reflector. Our experiments have used four UWB (Ultra-Wide Band) Antenna to transmit and receive the signals from the tag and on the tag itself. The principles for these methods are called inductive coupling and backscattering coupling. UWB antennas are commonly using in wideband applications like coding and wideband multiple sensing. Wideband multiple sensing is the concept we would like to prove its integration and feasibility. Further explanations and discussions are going to be made in the design part.

1.2.1.2. Integrated Circuit

This part of the tag has a component network that contributes to the impedance of the whole structure. Some tags have an IC chip attached to the circuitry, which provides data memory, regulation, switching, amplification, filtering, delaying, or other circuit components' capability. Our purpose is to create Chipless and Batteryless RFID sensors on paper. Therefore, we are going to explain design principles and calculations in the design and fabrication sections. IC part in our experiments acts as a regular RLC components network that affects the reflected, received, and transmitted signals.

Integration of the passive circuit elements are mostly for sensing and matching impedance of the systems such as 50 Ω and 75 Ω. Our cables, transmitters, and receivers

have a 50Ω characteristic impedance value. Therefore, we aimed to match with the impedance in our designs and fabrications.

There are 3 Circuit Matrix Types:

1- Z parameters, 2- Y parameters, 3- S parameters

where Impedance → Z= R+JX = |Z|e^(j$\boldsymbol{\theta}$), Admittance → Y=G+JB = |X|e^(-j$\boldsymbol{\theta}$) also admittance known as 1/Z. Y admittance, G conductance, and B susceptance are in siemens.

D (Dissipation factor) = tan$\boldsymbol{\delta}$ (Loss Tangent) = 1/Q (Quality Factor),

X=$\boldsymbol{\omega}$Ls inductive reactance where $\boldsymbol{\omega}$=2 π/T or $\boldsymbol{\omega}$=2 πf, and x⩾0, B⩽0 , 0 ⩽ $\boldsymbol{\theta}$⩽π/2, X=-1/$\boldsymbol{\omega}$Cs capacitive reactance where x⩽0, B⩾0 , 0 ⩾$\boldsymbol{\theta}$⩾-π/2, Resistance R (The Real Part of the impedance), Reactance X (The Imaginary Part of the impedance), Measuring R and X from Z= R+JX

X_c→ Capacitive Reactance where the voltage lag to current

X_L→ Inductive Reactance where the voltage lead to current

X_c=1/(2πfC) and X=X_L+X_c= $\boldsymbol{\omega}$L-1/($\boldsymbol{\omega}$C)

Characteristic Impedance=Zo=(Z_{open}*Z_{short})^1 when f<$\boldsymbol{\lambda}$/4

$\boldsymbol{\omega}$o=1/(LC)^1 Q=(L/C)^1/R.

We have used s parameters and measurement from the vector network analyzers, especially S11 (known as input reflection coefficient or return loss) and S21 (Forward transmission coefficient). S11 is the reflected, and S21 is the transmitted signal through the connected circuitry.

$$VSWR = \frac{1 + |S11|}{1 - |S11|}$$

Voltage standing wave ratio is related to return loss and is defined by the equation above. The ideal scenario is one where there is no loss on the antenna/circuitry. This gives an idea about how well the design of the circuitry or the antenna match with the characteristic impedance of the machinery, other system characteristic impedances. One is a perfect match with the systems' characteristic impedance with a zero loss, which is an ideal condition.

1.2.1.3. Substrate

Printing, PCB, or clean-room fabrications are made on several substrates where their electro-magnetic characteristics are crucial to design and simulate. In most of our experiments, we focus on their dielectric constant, loss tangent, and phase changes. Therefore, before using a substrate either we would like to use defined properties or measure and define their required characteristics. These properties are used to determine our design and simulations before fabrication.

For the dielectric constant measurement, the used equation is[62]:

$$\boldsymbol{f_0 = \frac{nc}{2\pi r_m \sqrt{\varepsilon_{eff}}}}$$

Where the c is the speed of light and n is the resonant frequency order r_m is the ring the mean radius for the microstrip ring resonators.

For the dielectric loss tangent measurements we have used,

$$\boldsymbol{tan\delta = \frac{\alpha_d \alpha_0}{\pi \varepsilon_r (\varepsilon_{eff} - 1)} \sqrt{\varepsilon_{eff}(\varepsilon_r - 1)}}$$

Where the α_d is dielectric loss and other dielectric and effective dielectric constants have been used. If the substrate surface was hydrophobic, to increase hydrophilicity, we have used plasma treatment and chemical surface treatment methods to deposit any material to process the patterning effectively.

The substrates we have used are

1- FR4 (Basic low-cost copper printable circuit board for fabrication and testing of ultra-wide band transmitters and receivers)
2- PET (Polymer substrate for ultra-wideband antennas and ultra-high frequency applications.
3- PI (Polyimide, Plant health monitoring ultra-high frequency tag applications and high temperature curing fabrications)
4- Copper Tape (Plant health monitoring electrode and measurement tool connection)

1.3. Sensing and Sensor Fabrication

Sensing elements vary from biological to chemical, thermal, optical, and so forth. In our research, we have used, are chemical, electromagnetic, force, and thermal. Our sensors are built on resonators that can resonate at a particular frequency we have defined. Therefore, their abilities are depended on their electrical interaction with the substrate and the deposited material as a sensing factor. Also, the changes in the wireless elements can be in the frequency domain RFID sensing or time-domain RFID sensing.

For the sensor fabrication, we have used inkjet material deposition technique, spin coaters, pipetting, direct immobilization, and electrochemical deposition. Details and general knowledge will be given in the sections we have used.

1.3.1. Sensing Principles

There are many ways to process chipless and wireless sensing efficiently on a substrate: Reactive Load Transmission line, ladder network, RF-SAW techniques, piano, and Hilbert curve fractal resonators, radar cross-section, thin-film transistor methods, capacitive gap coupled dipole array. We mainly focused on the capacitive gap coupled dipole array method and reactive load transmission line techniques in our works because of its simplicity, low-cost setup and fabrication, and capability to modify or deposit materials on them. Sensing techniques have an amplitude and phase of the spectral changes in their received and reflected signals, or backscattered spectral signals, and their time domain analysis are the another method to observe sensing phenomena. Time-domain reflectometry (TDR) or frequency modulation (FM), or phase encoding method, is the most common method to perform signal processing.

We have measured and calculated the limit of detection (LOD) for our sensors if it is possible. For this calculation, we used the standard error of interception is found by the data analysis of the excel worksheet doing its regression analysis.

$$\boldsymbol{SD = SE\ x\ N^{0.5}\ and\ LOD = 3.3x\frac{SD}{Slope}}$$

Where SE is the Standard error of interception, SD Standard Deviation, N is the number of samples/measurements.

For quality factors, we have used the 3dB bandwidth method roughly estimating the quality of the signal resonance peaks. Signal peak has recorded and divided by the difference of -3 dB high frequency and -3 dB low frequency values from return loss measurements (S11). Simply,

$$Q = \frac{f_p}{f_{3dBh} - f_{3dbl}}$$

From the equation, we have calculated the resonator quality factor from the S11 measurements.

1.3.2. Sensor Fabrication

The technique we have used for the sensor fabrication is using smart sensing materials in our printed circuit elements to perform changes in the generated/excited signal and receive them back or just using the reflection of the generated signal. For temperature sensing, we have used crystals, and metal oxide materials blend to change the electrical characteristics of the resonators on the surface that results in shifting the resonant frequency. On the other hand, for humidity sensing, Kapton tape, PVA, and polyester have an advantage over other materials because their relative permittivity changes by the humidity fluctuations. As an example, Kapton tape has,

$$\boldsymbol{\varepsilon_r = 3.05 + 0.008\, x\, RH}$$

Kapton has a relatively linear response to the humidity changes.

For the characterization and observation of the smart materials and the materials, we have deposited silver, and we have used EDX in SEM imaging techniques to understand what materials contribute or change the current density.

Beyond, we have designed a new method to provide a layer for the sensor substrate and create a new sensing area on resonators. This area has the effect of changing the dielectric and the impedance of the **stubs**. The changes are examined, and the technique with the phenomena has discussed below.

For sensor and antenna fabrication methods

1) Inkjet Material Printing
2) 3D Printing
3) PCB Fabrication

1.4. Experimental Measurement

To excite and receive any reflection from an RFID tag, there should be a transmitter and receiver. We have used commercially available UWB antennas and wide band UHF(Ultra High Frequency) and inductive coupling inductors for HF (High Frequency), LF (Low Frequency) sensing application purposes.

1.5. Previous Research

There are several publications having a valuable method for sensing and wireless transferring at low frequency levels [1-4]. However, their problem is the lack of a control group which provides appropriate working information about sensor operation and measurements. They need to be integrated with an additional load which will affect their collected data from the primary sensor and cannot be transferred without modulation or storing (where analog input chips are required with a battery) [12-15].

In agriculture, companies do not believe much profit in advanced monitoring; therefore they don't invest in sensor development for agriculture. Instead of limited budget and investments, there are several noticeable publications and works in this field [7-11]. However, their primitive sensors and incompetencies are far behind today's requirements and demands [19].

Today's sensors requirements are basically

1- Low-cost fabrication

2- Durability in harsh weather conditions

3- Easy to fabricate and resources availability

4- Wireless

5- Accuracy with a Control Unit

6- Batteryless

7- Plant and Environment Friendly

8- Chipless

9- Flexible

10- Low power

11- Low-cost measurement setup

12- Multiplexed

Most of the wireless sensors in the literature fails at the accuracy with a control unit and durability in harsh weather conditions. Plexiglass acrylic UV blocking thin film is being to be used on the antennas to avoid UV degradation, and water-proof unique inkjet printers silver nanoparticle solutions are used for the fabrication. Not only UV is blocking but also using coating techniques to avoid any humidity or sharp object touching or deformations. Our proposed designs and fabrications have been proved and ensured that passive wireless sensors can be effective in sensing and can measure electrical and magnetic changes with several methods discussed in this dissertation.

2. DESIGN AND FABRICATION

In this section, we have used several fabrication methods to define the most cost-efficient and empirically effective way for mass production. We have found direct inkjet material printing is an effective method for high frequency and small applications [18]. However, it has its own issues we have addressed and solved. And also, we have suggestions for the professional material printer companies working in this field. Furthermore, in some cases, for example, round and curved shaped designs and precise alignment required designs, the screen printing method is an easy and appropriate technique to fabricate the conductive parts [31,32]. However, the deposition thickness inadjustability and every time new masks for each design requirement are drawbacks of the screen printing. We have optimized our printing towards to have low loss high frequency capability. Therefore, we had to investigate our printing and with improving its quality by adding or adjusting procedures, optimization of all fabrication steps. Actually, to make it more clear for anyone who is willing to perform these methods, we have shared all detailed recipes and fabrication tricks and techniques.

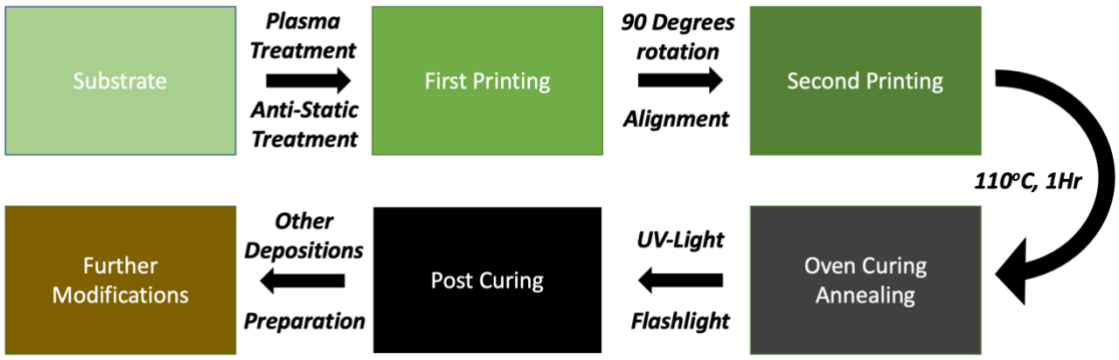

Figure 4: Fabrication Steps for low-cost sensors/tags/antennas

As it seen from the figure above, the PET, polyimide etc. substrates have first treatments as a anti-static treatment from staticide spraying on the surface and/or oxygen plasma treatment to adjust surface hydrophobicity. First part printing that includes only horizontal lines, and then the second printing includes vertical drawings but as a horizontal printing on the surface of the substrate with a sample alignments. After the second part of printing, we perform the oven curing for 1 hour at 110C. Then, curing with a high range wavelength flashlight curing and UV-Light curing for couple of minutes. (Further methods are discussed in details in the fabrications and discussion section) PDMS (polydimethylsiloxane) and/or ceramic oxide materials or molecularly imprinted material deposition.

The printer has operated at the highest deposition settings as much as possible since the fabrication quality and the deposition amount matter at a higher frequency related to fabrications and applications.

Table 1.1 Material Printer Settings Table in Section 2 ”Adapted from [34]”

Parameter	Nozzle Spacing	Nozzles Activated	Nozzle Diameter	Frequency	Cartridge Size
Value	254µm	16	21µm	30kHz	10pL
Parameter	Substrate Temperature	Jetting Frequency	Applied Voltage	Drop Spacing	Drop Angle
Value	30°C	5Hz	30V	20µm	4.4°

According to the table 1, the printer setup has the highest deposition rate in a single printing [34]. We avoided to have multiple printing to avoid any mechanical impurity, and the printer deposition only x direction; therefore, x-direction printing is not good enough at y direction. Consequently, we had two different versions that only x direction and combined into one. We also optimized the droplet size and volume by the applied voltage.

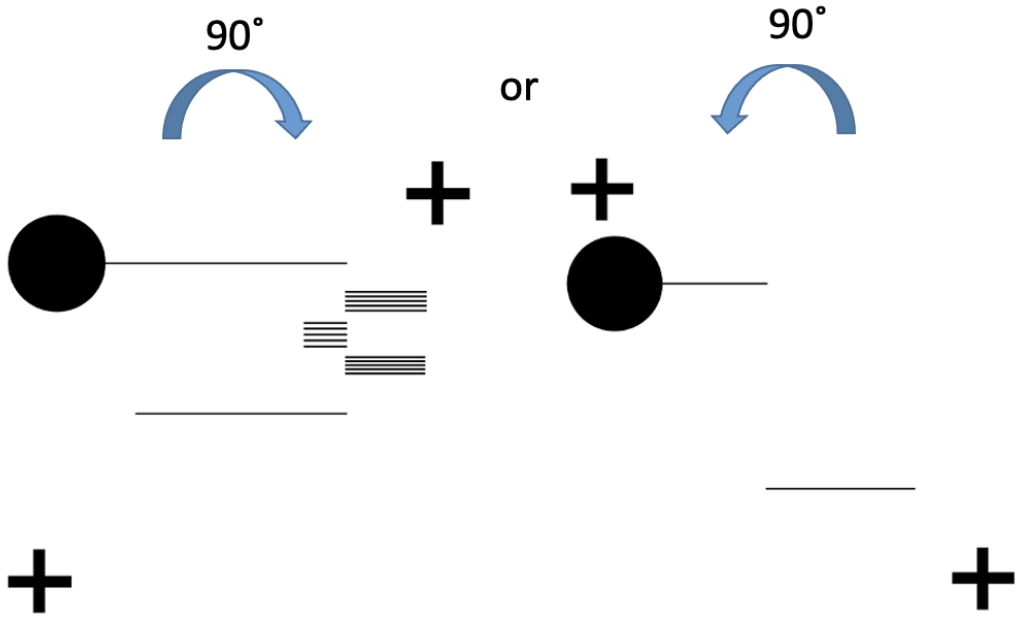

Figure 5: Fujifilm Dimatix material printing method.

We have used material printing for the fabrication of the electrodes. However, we observed problems when the printer drops one by one the ink on the substrate. Therefore, the material printer does not work in the vectorial form; it prints only one direction. The quality in x direction is more exemplary than the y direction. To avoid any deposition issues, edge problems or surface bump any many other issues, we have found a way to rotate the printed sample to print other design part as seen in figure 5. Printings issues will be discussed shortly, but in this way, we had better printings.

To avoid multiple depositions, we kept the deposition at its highest printing and deposition limits to prevent any line misalignments and reprinting issues. Also, we decreased the fabrication duration with more homogeneous lines where they can operate

in ultra-high frequencies (up to 19 GHz) where the most alternatives can not achieve such a frequency and the gain.

As a control part we have used commercially available wired precision monitoring sensors to compare the data we have collected from our sensors and compare our data with the data that comes from the commercial sensors. Some commercial sensors are not agriculture friendly and can not be used to monitor under the soil. We have designed, and 3D printed a case to overcome this limitation and used advanced precision sensors under the soil to characterize the results we obtained [33].

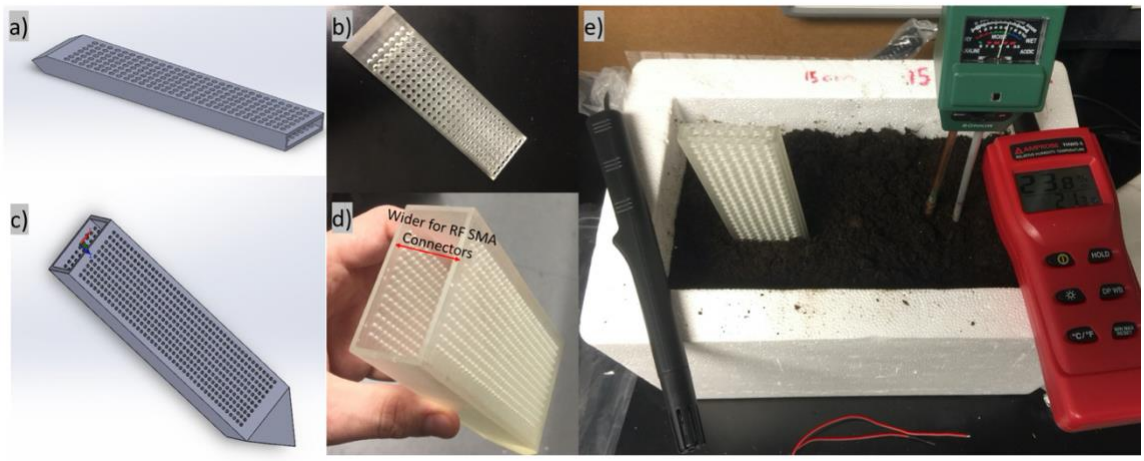

Figure 6: 3D Design and fabricated versions of the commercial sensor probe covers to perform reference measurements

As it is seen in the figure above, the 3D printed structures has been used for continuous soil properties monitoring and characterization of our sensors. There are very limited sensors in agriculture available commercially; therefore, we have modified existing advanced wired sensors applicable to the soil monitoring by printing soil protective cases and holders. In the figure, it is noticeable that the case has holes along

their bodies to provide efficient gas, humidity, and heat circulation without contaminating and breaking the commercial probes. We have designed and fabricated several probe cases related to the brand and the material we would like to monitor. We have used Amprobe precision temperature and humidity monitoring probe to measure humidity increments and logging temperature changes. In the figure, polyethylene or ethylene and vinyl acetate foam bottles, bowls, and boxes are used as containers of the soil we have tested. Related materials and equipment will be seen in the figures we have presented for soil monitoring and characterization.

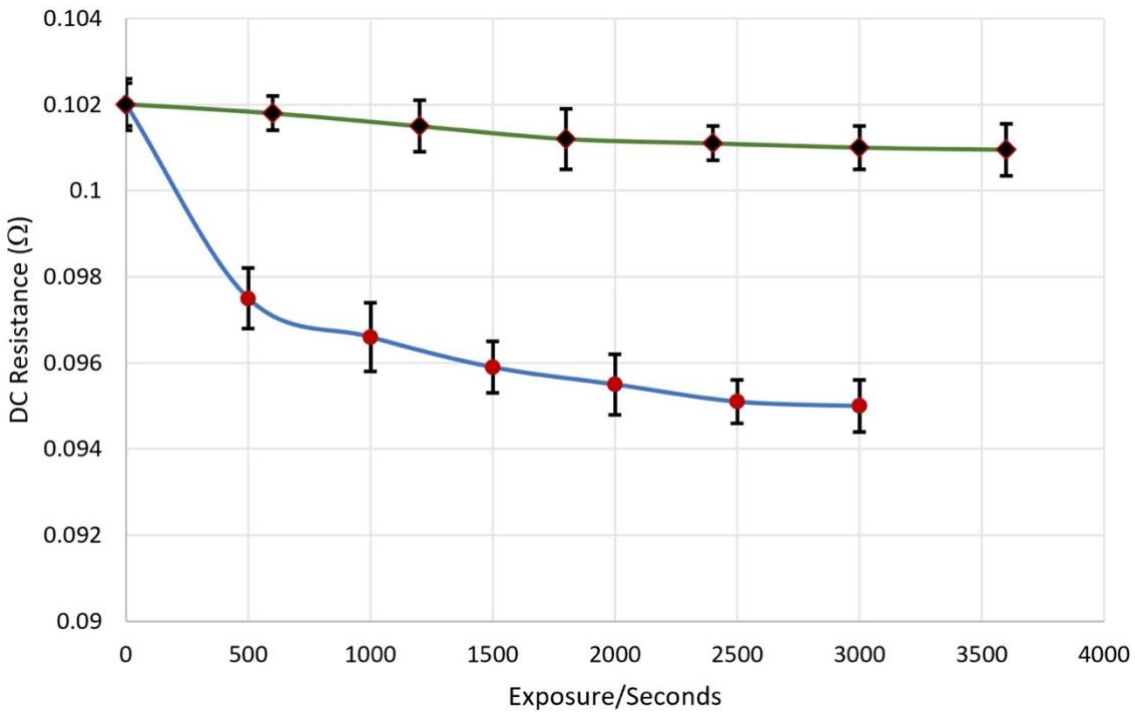

Figure 7: UVA Exposure (Green Line) and Photoflash Bulb Spectral illumination resistivity improvements in ohm.cm (Blue Line)

As shown in the figure, UVA and photoflash spectral illumination treatments improved the printed nanoparticle silver conductivity. We have observed up to 6%

improvement in conductivity combined. According to our experiments, 2000 to 3000 exposure decreased the resistance 5% to 4% and a 30 min UVA exposure reduced the resistance by 0.8 % to 0.9%. Furthermore, the oven sintering process needs to be optimized for higher conductivity. Therefore, longer oven curing increases the conductivity. However, the curing period is limited by the polymer we have ink deposited on. PET substrate can handle up to 150°C degrees for a limited time, the degradation starts in such temperatures. PET substrate reaches 140°C only for a minute inside an oven. However, we keep the sensor attached on a dense cellulose tray by polyimide tapes and curing 140°C degree 10 min curing is recommended. However, I found longer is better; my final curing method is 140°C for 10 min then 110° for 1 hr. Photoflash lamp 10 flashes per second 300nm to 700nm spectral distribution. All curing required to be cooled down at room temperature for a while.

In addition to all curing improvements, the printer and fabrication need to be optimized for an effective electrode and circuit component design. Therefore, we had more investigations and solutions for printing and fabrication issues.

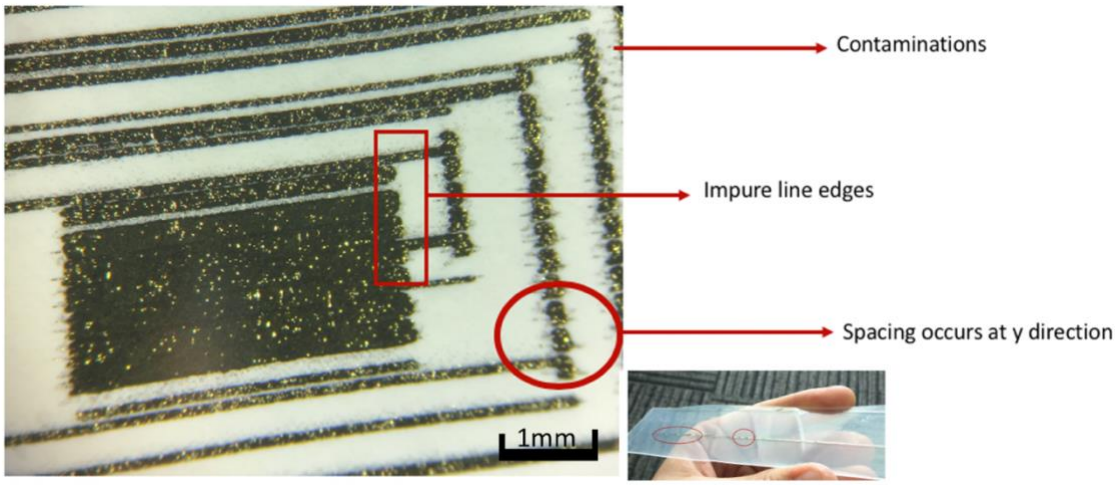

Figure 8: Printing issues for Fujifilm Dimatix Material printer

Improper unoptimized printings can cause loss and inadequate responses in the designs. As it is seen in the figure, the lines are not acceptable for high-frequency component printings. Therefore, given problems in the figure are discussed and solved separately. First, we observed tiny particle contaminations on the PET substrate. These silver particle contaminants are caused by the static electricity of the substrate and surface charges. We have used Staticide liquid to neutralize the surface charges to avoid particle contamination while piezo pumps are jetting (spraying) the silver nanoparticle ink. Impure line edges are decreased by optimizing jetting frequency and the volume defined by the voltage on the piezoelectric jetting components. Spacing at y-direction is caused by the cartridge angle adjustments, and we have optimized the angles.

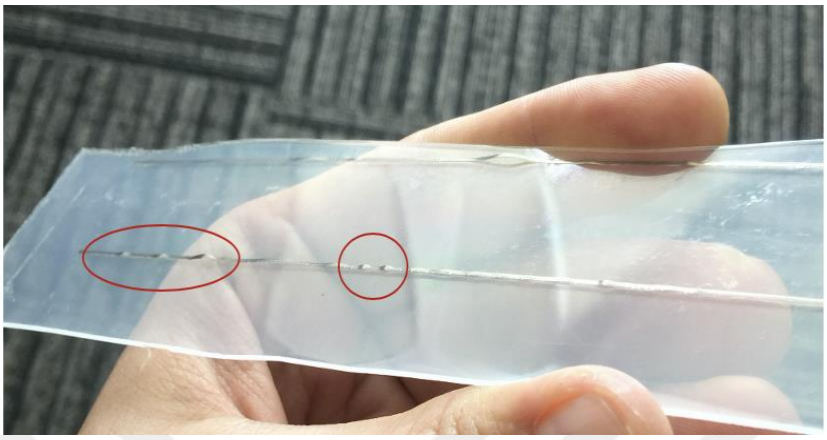

Figure 9: PP substrate Silver Nanoparticle ink deposition post curing

We have tried multiple substrates that some of which failed to be cured at 110C degrees, and some of them had deformation on the film/layer where it caused unexpected cracks or bumps as seen in figure 9. To avoid these problems we specifically chose substrates less thermal expansion or shrinking factor. Bending is also one of the problems. For bending issues, we have secured our substrates with high temperature tape on a metal tray and cured after all. We haven't kept the samples in the oven at higher temperatures since PET, and other low-cost substrates are deforming a lot even we secure them and/or add some weights.

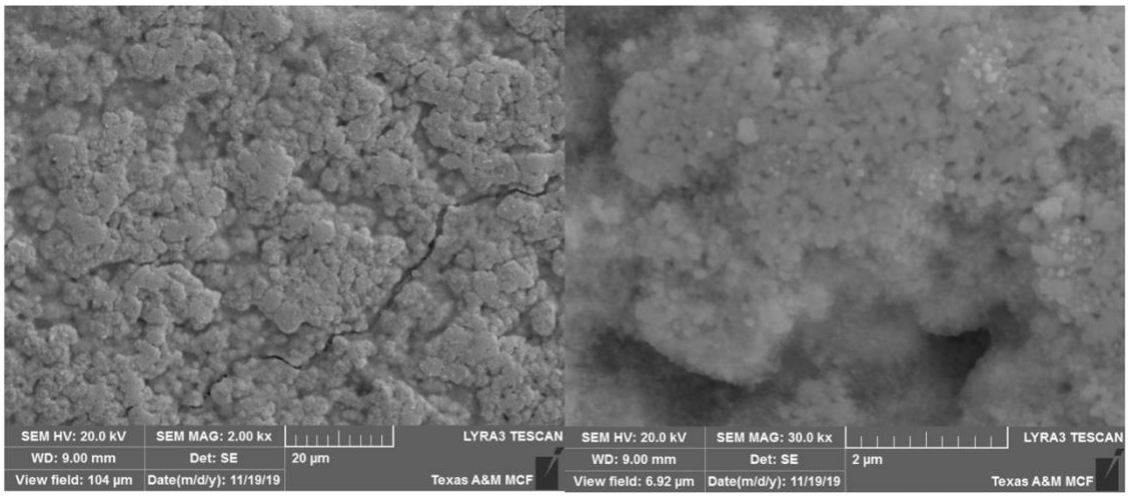

Figure 10: Silver nanoparticles are deposited on PET substrate and its SEM images.

In the figure above, silver nanoparticle clusters are observed, and their deposition on a PET substrate is investigated. Surface roughness has defined from a profilometer as a 0.21thou/mil. However, edge deposition effects are ignored. We have seen some crack lines through the sample. These cracks are caused by the ink we have used when it is cured long time and bending is a problem. This is an unwanted situation, but the ink has a solid environmental durability and water resist capability that we sacrifice from being flexible. Therefore, for agriculture, less vulnerable sensors are required and need to be fabricated.

In this particular ink, Novacentrix, the ink manufacturer, is used polyurethane to provide strong attachment (adhesion).

We have performed EDX-SEM imaging and measurement to ensure the ingredient compounds of the used nano silver ink.

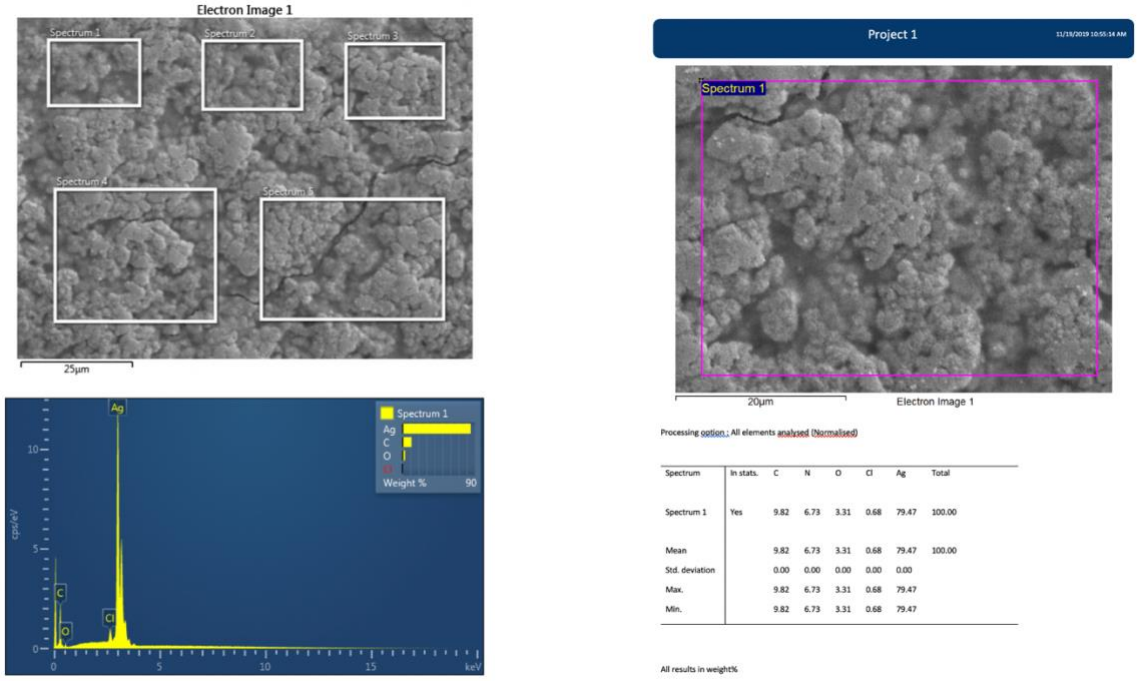

Figure 11: EDX SEM Image and measurement for the inkjet ink to understand what types of compounds have been used.

From figure 11, EDX measurements and analysis have been done since we wanted to investigate the silver ink we have used to not interfere with the our other chemical characterizations and experiments for molecular imprinting. We have found there are chlorosurfactant which is benzalkiumchloride, polyurethane, ethyl-glycol, and glycerol inside of the ink. Further analysis and measurements are in the supplement A section.

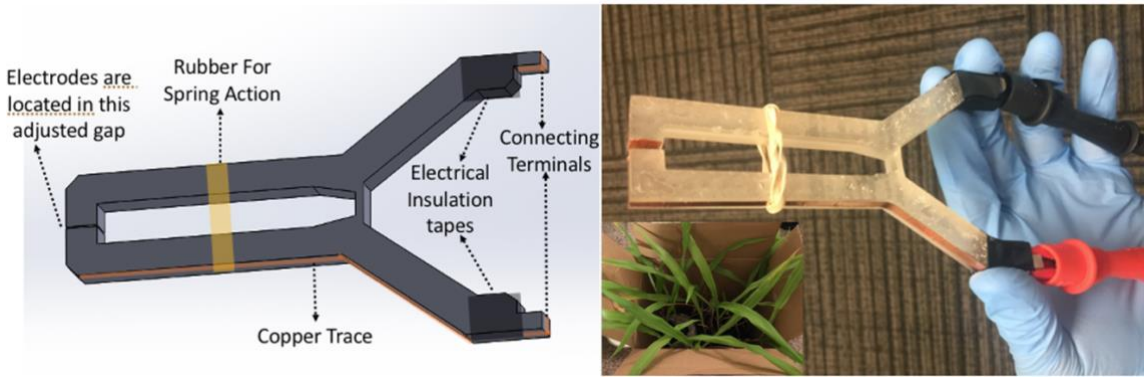

Figure 12: Preliminary data collection probes for plant health monitoring wired structures to perform multiple probes to avoid physical pressure point and force effect without having high ohmic contact resistivity.

According to the figure 2, we have designed an effective way to measure the plant health without defecting the leaves and interfere our data with other physical changes like pressure point changes and pressure force changes. To provide homogenous pressure on the tip of the probe, we have designed the tip to have a predefined gap after adding a sensor probe that could match with another probe that the targeted leave sandwiched. We monitor corn leaves at their very early stages especially when they have their first leaves, which are very delicate and sensitive to any forces. To avoid weak probe contact, we have designed the end parts that are appropriate for high frequency crocodile head cables. For adequate pressure on the leaves we have added a plastic spring on the probes to have an adequate pressure for the measurements. Electrically insulated holding parts are to avoid any static and magnetic interferes from the experiencer hands. This probe is appropriate for low frequency measurements up to 30MHz, for higher frequency measurements we use direct contact and adhesives materials to attach on the leaves and measure them by very thin probes is recommended.

Our multiplexed sensor has a unique approach on the processing the data from the resonators and have better quality factor than any other stub type resonators ever designed. Our approach has basic stubs parallel to each other at a certain distance and resonates at the frequency determined and calculated by their length;

$$f_0 = \frac{Y_i}{4l\sqrt{\varepsilon_e}} \qquad Eq.1$$

Where Y_i, l, ε_e are admittance, length, and substrate dielectric constant, respectively. Admittance can be calculated by the reactance and resistance of the stubs by the equation given below;

$$Y_i = \frac{1}{(jwC_i)^{-1} + jwL_i + R_i} \qquad Eq.2$$

Where the C_i, L_i, R_i, w are intrinsic capacitance, inductance, resistance and angular frequency.

Before jump into the design and fabrication further we had to optimize our transmission line and the substrate properties had to be defined where we can implement or try further experiments and designs to get responsive low loss circuitry.

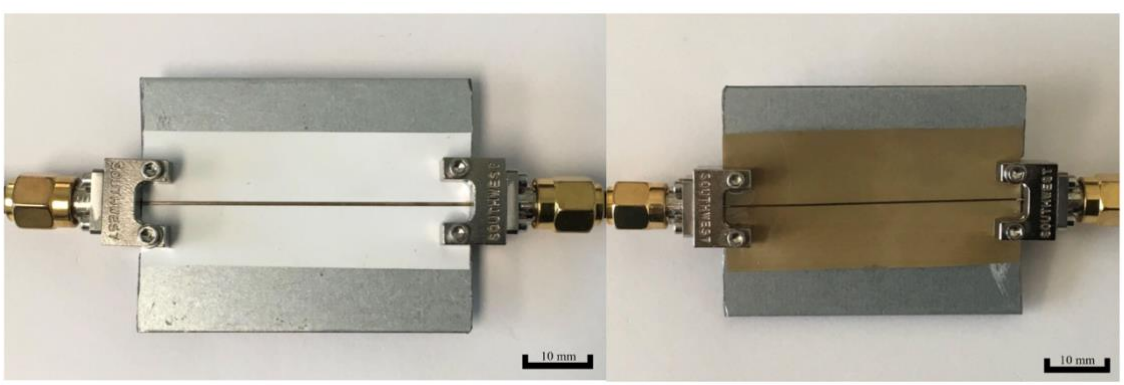

Figure 13: Microstrip lines designed on PET and polyester film in several thicknesses

Multiple microstrip lines and substrates are used to observe which substrate has more convenient for our purpose and what size of the transmission lines will be on these designs to match with the characteristic impedance of the equipment as it seen from figure above. We have designed 300um to 3mm thickness lines, and we have designed on paper, PET, PP, PE, and vinyl substrates. We have found 0.7mm thickness on PET has the best matching impedance and best antenna and resonator design. PET has an advantage over all for best deposition on. The performance has changed accordingly.

We have provided and proved that the five stubs have better quality factor than the 3 and more stubs that the paper has claimed. Our equivalent drawing is given below,

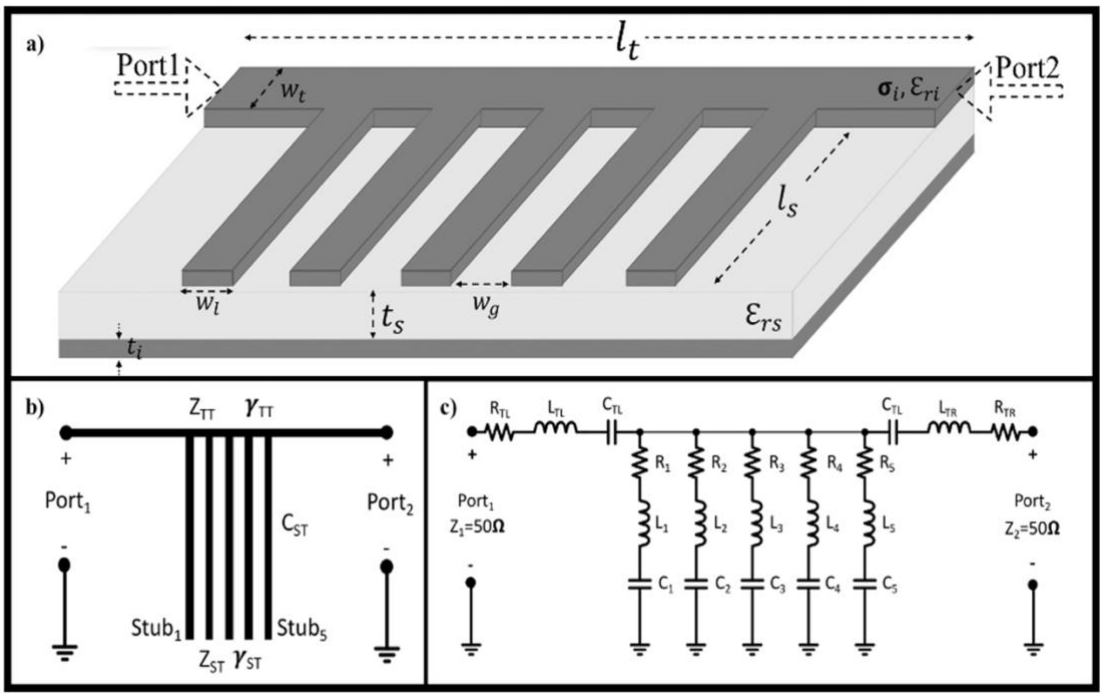

Figure 14: a) Designed 3D schematics of the resonator on a microstrip line, b) impedance and 2D structural position of the stubs, c) their equivalent circuit affecting the resonance frequency and their quality factor.

As it is seen from figure above, there are five stubs parallel to each other connected to the same transmission line respectively at the same distance. The dielectric constant of the substrate and conductivity of the material have been calculated by the VNA and LCR meter. PET dielectric constant has been measured by the LCR meter at lower frequency levels and provided adequate result as a 3.18. We have used Mitsubishi PET paper substrate specifically designed for inkjet printing and silver nanoparticles deposited on both sides. One side has the design while the reverse side having the ground. The distance between stubs needs to be more than 500 microns, where the printing resolution and their capacitive effect allow us. If they are less than 450 microns, we observed dramatically decreased quality factor and more frequency shift towards to higher frequencies. In the figure, their inner inductive effect also suppresses the obtained reflection, and magnetic response flattens the resonance peak and decreases the performance of the stubs. In detail, each stub has proximity coupling with the stubs nearby by three couples. These three groups has a part of the other three groups nearer to them. Center stub of the 3 groups has the dominant effect and pair with other 3 for further interaction. Their third stage of interaction has the best resonance and quality formation, according to our experiment. Previously, there is a paper discussed why three stub resonators are better than one and two. We have proof of a concept of why five stub resonators are better than all other versions. Therefore, we have designed all our designs and resonators by simply using 5 of them.

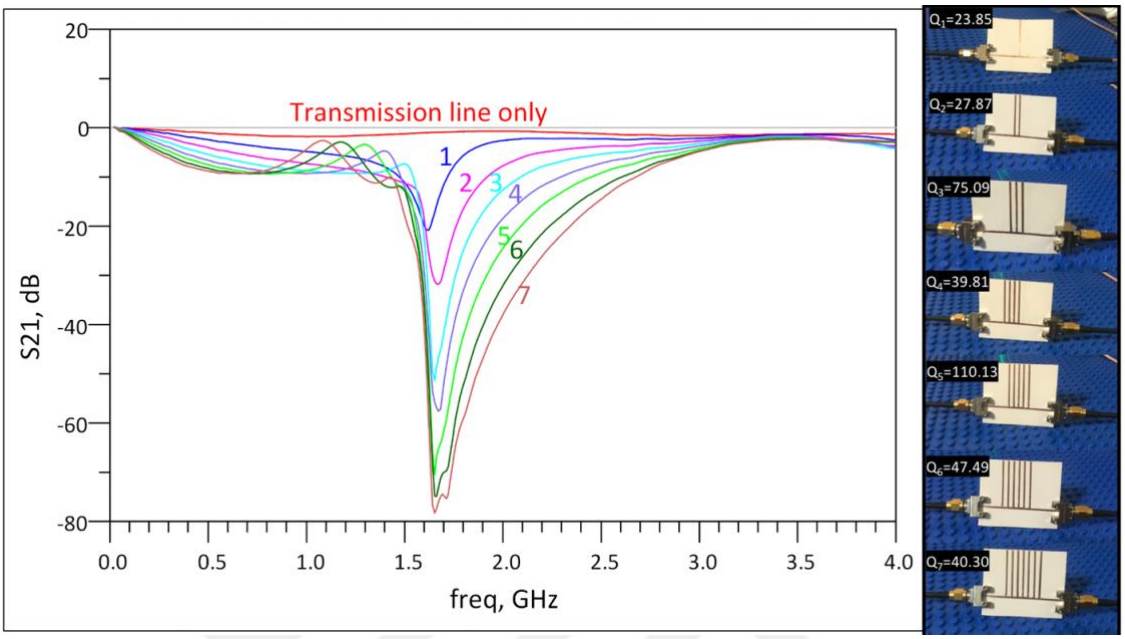

Figure 15: Stubs resonant frequencies by the numbers of the stubs allocated on the same substrate and their quality factors defined by their resonance frequency and 3dB signal decrease method.

In the figure, stubs groups have their identical responses, and their coupling effects change their operational performance. The best quality factor has observed in five stubs group from our experiment. Actually, we had observed this phanomena multiple times when we started to add additional subs to have better quality signals where we can perform our sensors capable to get small changes from the target. Five stubs group is the best while three stubs follow it. Three might be an alternative where high quality factors are not a concern, and the cost is very high for each stubs. As we tried to explain previously, their interaction and coupling with each other are dominant when they have smaller w_g values as it seen from the figure.

We have used these stubs group to create a multiplexed sensor that can detect two or more variables simultaneously on the same transmission line. Therefore, we have

cascaded three different lengthen five-stubs. Our structure resembles to a log periodic antenna. Actually, the principle and the method look identical to log periodic antenna only having a smaller size and multiple stubs located on one line and perform various points of resonance frequencies.

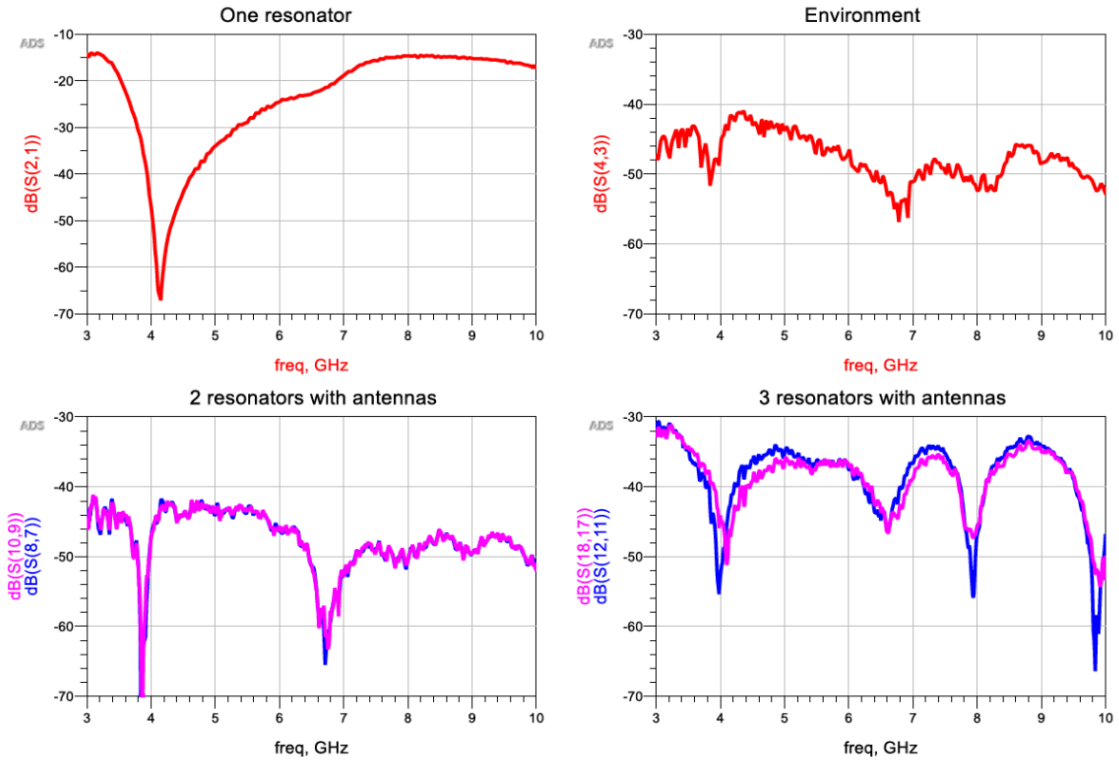

Figure 16: Multiplexed resonators and their frequency vs gain responses

When a stub resonator multiplexed, their resonance frequencies cascade with each other while their impedances are affecting their performance and resonance frequency. In the figure above, one stubs group resonator and two stub group resonators, and three resonators group have investigated and measured. Their resonant frequencies and responses are observed as expected from our designs. They have shown three

distinguished resonance frequencies related to their lengths. When we cascaded them, we also watched their gain decrease while their central resonant frequency shifts slightly. We have removed the environmental noise from all our measurements to avoid more errors while reading. Frequency shift gives information about temperature change, and amplitude change obtains information about moisture level.

3. MULTIPLEXED UWB (ULTRA WIDE-BAND) SENSOR

This work presents an adequate low-cost paper soil moisture and temperature multiplexed wireless sensor on paper. Our inkjet printed on PET substrate sensors have a cost-efficient dependable response. Our multiplexed sensors have unique characteristics to provide effective sensing in outdoor conditions, and experiments are performed in real soil scenarios. The designed sensors are compatible with ultrahigh frequency level communication components that can be implement into an ultra-wideband antenna.

3.1. Introduction

Soil moisture and temperature monitoring is required for sustainable farming and improve the yield.[49, 50] Furthermore, low cost sensing is necessary to perform continuous moisture monitoring integrated with advanced setup to optimize consumption and adequate irrigation and maximize growth speed and cultivation efficiency.[51] Moreover, moisture and the temperature of the soil can vary by irrigation pattern and instantaneous weather condition. To optimize the soil condition, continuous live data have to be obtained from many implemented sensors. There are many applications and commercially available sensors that can sense the state of the soil.[52,53,54] However, their expensive fabrication and the cost per unit limit their usage of them in the field at a significant quantity. There are other individual sensors are also available in the market, however, none of them is using just one signal spectrum to monitor multiple analog signal spectrum changes.[54,55] We have achieved a multiplexing sensor design and operation

detection of moisture and temperature of the soil that suitable for future chipless and wireless applications.

The current state of the art for temperature sensors involves the use of capacitive sensing and operation at low frequency to detect changes in DC capacitance and low frequency reactance. Besides, the art of the moisture sensors is to monitor the conductivity response of soil between two electrodes and measures the TDR characteristics. However, their measurements have also been done in very low frequency levels that do not provide the capability to directly integrate into a chipless high frequency operating systems that can have the advantage of wireless networks[54,55]. We have used a similar approach to perform our sensors at UWB (Ultra wide band) antenna frequency levels to enable future UWB network implementations on smartphones[56].

Stub type resonators have their own advantage over the spiral resonators versions in terms of the quality factor. The helical resonators are more susceptible to noises and implementation of them outside of an isolated condition. Overall, passive and chipless RFID sensors are sensitive to any changes in the sensors and the EM field. One sensor affects others in terms of the characteristic impedance and overall performance. The changes in output signal shifts all resonant frequencies, and gain will be decreased dramatically[57]. We have proposed a novel way to use the multiplexed resonators to detect changes in the environment simultaneously despite an interference between resonators. The method and further experimental explanations will be discussed in the results section.

We have achieved low-cost fabrication by using inkjet printers and low-cost harsh environment resistant substrates. We have used water-resistant silver nanoparticle-based ink and plastic substrate. We believe being disposable and low cost per unit will allow our soil sensors to be more prevalent and easier to be fabricated. In addition to its low cost, we have improved the current resonator topology [58,59,60,61] and present a better way to increase the quality factor for acceptable sensing level.

3.2. Materials and Methods

The sensor has been designed, and measurement results processed in Advance Design System by Keysight. The fabrication was made by a material inkjet printer from Fujifilm Dimatix. The substrate is a Mitsubishi PTA100 Inkjet printer PET film. We have used Novacentrix JSADEV291 nanosilver inkjet ink which has polyurethane as a bending agent and is durable in harsh weather conditions where we intend to use the sensors in the agricultural field.

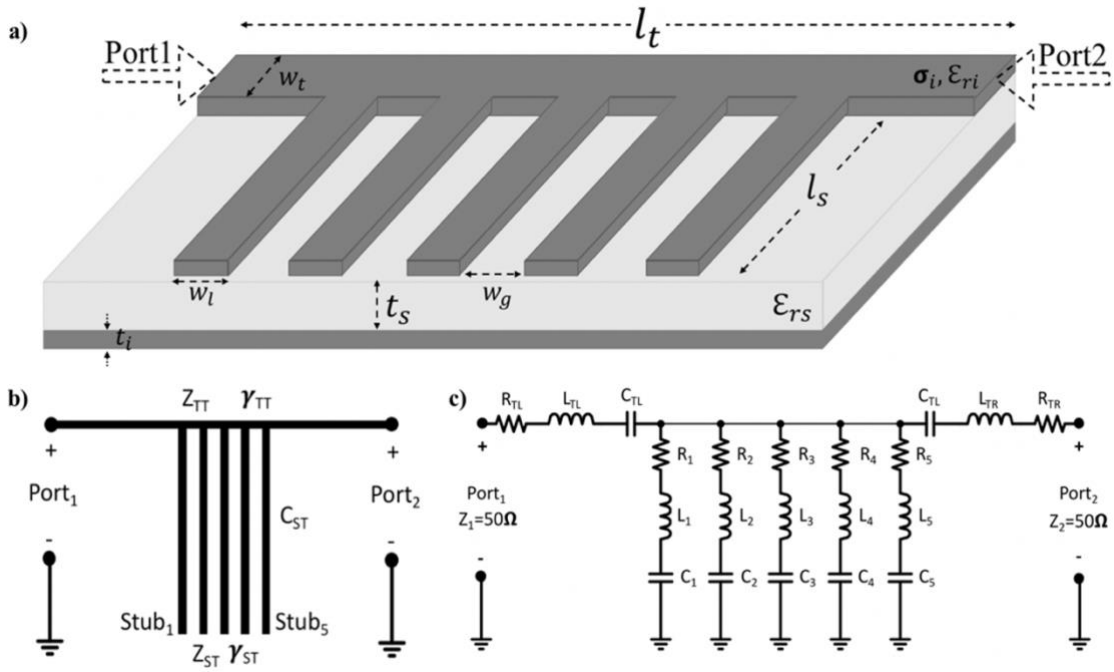

Figure 17: a) Fabricated five stubs microstrip line resonator on pet substrate b) Schematical representation of the stubs impedance and conductance c) Equivalent circuit schematics of the printed circuit network for multiplied stubs

The figure 1a has a fabricated illustration for a stub-type resonator and representing its characteristic parameters affecting the overall performance and the circuit response in high frequencies. Multiple resonator designs and measurements have been done to define the most quality factor resonant by optimizing w_g, t_i, w_t, and w_l parameters to provide a 50ohm network impedance match to deliver a higher gain. Stubs' admittance and their capacitive characteristic have been investigated and calculated by their reflected S11 and transmitted S21 values received by a portable vector network analyzer (PicoVNA 106). In figure 1c, the equivalent circuit of the multiple stubs' schematic presented as the RLC response of each stub.[1] To define the best impedance match with the inkjet printing, we fabricated multiple wt and ti simple transmission lines and tested their S21

responses/losses. With our specific ink, substrate, and the dimensions, we defined the silver deposition thickness (ti) at 10um ±0.65 and line width (wt) at 700um ±30 (Supplemental Section2) to provide desired 50ohm impedance match. In addition, the forward transmission matrix response of the stubs and transmission line have been investigated and explained in previous works[2,3]. In design, the stubs are printed on a polyethylene substrate. Testing with a paper substrate, it needs to be careful not to bend and not to push because of the thickness of the PET inkjet paper substrate is 250um which makes it delicate to any forces. Microwave level connectors are bulky and heavy and out of a limit for a paper to carry on. To avoid bending and unintended deformation, we have installed a plastic substrate to keep the sensor plane stable and solid and able to dip into the soil. To define the size and shapes, we have limitations from the printer, the silver nanoparticle ink (SNP), the substrate, the curing process, and environmental effects. One limit is in material printer quality and resolution. Deposition from the printer multiple times creates an unstable transmission line, and the near line contamination increases. Therefore, we have used at the highest deposition limit of the printer deposition setting and the highest volume 10pL cartridge nozzles. We have achieved up to 10micron silver deposition after sintering. We have kept wg more than 800um, which avoids any further capacitive interferences at high frequencies up to 10GHz, where we applied the most elevated silver deposition at a single printing. Before printing, to avoid any static particle contamination, we sprayed liquid multipurpose Staticide, and dried it on the surfaces of the printing plane and the substrate.

The conductivity of the ink we used is calculated by the kelvin 4 probe measurement method on a source meter (Keithley 2450 Sourcemeter), where it has measured 1.304 x 10^6 S/m. Loss tangent has been measured and calculated from equivalent series resistors values from an LCR meter (BK Precision 880) as 0.0322°.

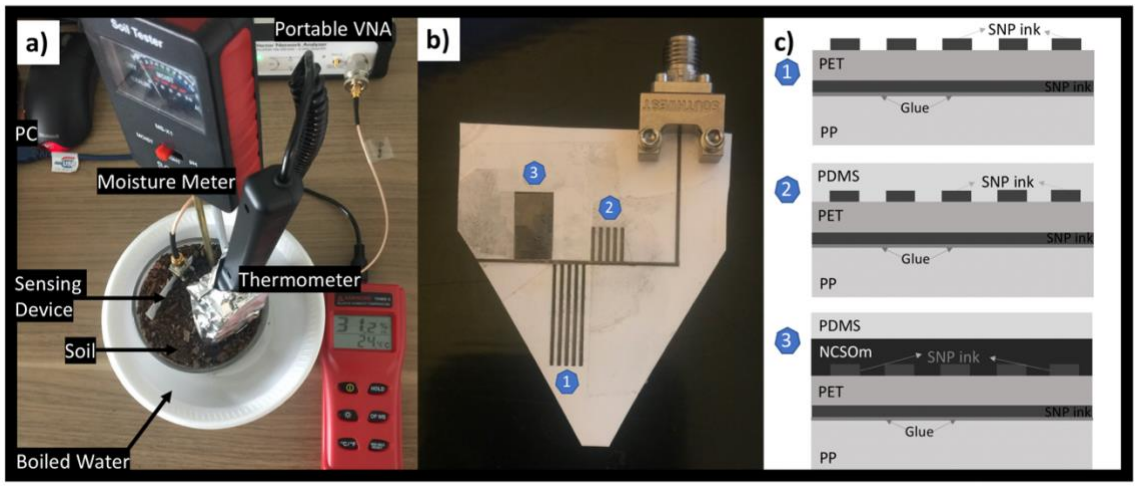

Figure 18: a) Testing setup for the multiplexed soil sensor, b) The sensor before dipping into the soil, c) Cross-sectional cut view and layers depositions on the PET substrate.

The traces are printed by the Fujifilm Dimatix Material Printer 2830 with Novacentrix JS ADEV 291 ink. The silver nanoparticle ink has additional polymers to make it water resistant after curing. The parameters of the material printer are given in the supplement file section 1. Before inkjet printing, Staticide sprayed on the substrate surface and the printer printing plate surface. It let it to be air dried. After printing, the devices were cured in an oven at 110°C for two hours. After the silver ink sintering process, we have deposited plenty amount of ceramic and oxide particle paste on the printed resonator #3 as it is seen in figure2b. To avoid contamination of other spaces on the sensor plane, we have covered

the surface with surface safe tape from 3M. The paste (NCSOm) is a mixture of thermally conductive nitrides, ceramic and oxides, and conductive silver flakes with epoxy paste. We have mixed commercially available Arctic Silver 5 thermal compound with, MG Chemicals 8330S Silver Epoxy paste at a weighted mixture ratio (1:1). After the paste deposition, we have removed the tape. Then, it has cured in the oven for 2 hours at 80C. After curing, we have placed a surface safe 3M tape to cover #1 sensor and connector section (before a connector is installed), and we have spin coated Polydimethylsiloxane (PDMS) to all device. We have removed the tapes and cured the device in the oven for a day at 65C. After curing, polypropylene substrate is cut and epoxy glued on the backside of the multiplexed sensors plane to keep the sensors strong and solid before dipping into the soil. In the last step, the microwave connector has installed on the sensor connector section.

The sensor dips into the soil. The connector does not touch to the soil surface to avoid any high frequency interferences with the wet soil. A precision thermometer probe has placed inside of the soil to monitor temperature changes by cold and boiled water. Moisture has been observed by a commercially available galvanic soil moisture sensor to define the changes in the received signal from the printed sensor. A portable vector network analyzer (PicoVNA 106) has connected with the sensor, and a portable personal computer has been used to monitor changes in the meantime. All-purpose natural soil from Dr.Earth has been used for real soil scenarios. For the wireless measurements, we had a setup, as seen in the figure below,

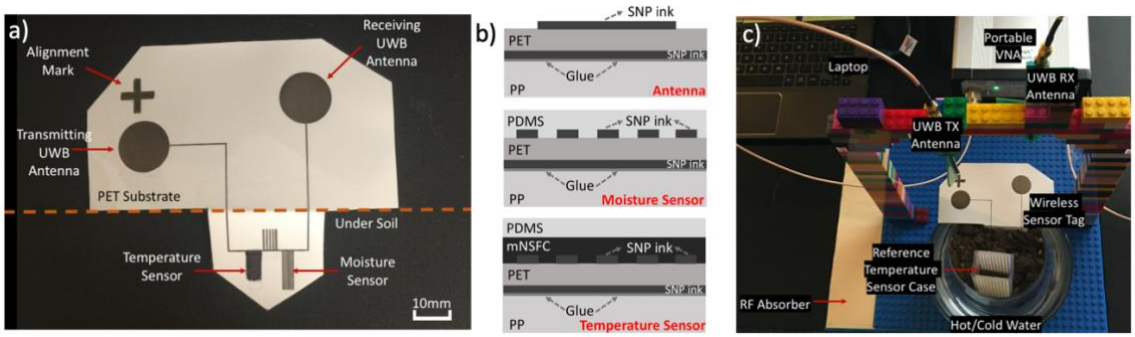

Figure 19: a) Printed and prepared wireless sensor unit, b) Cross-sectional view and parts of the paper sensor, c) Experimental setup for the wireless measurement

A wireless ability has been achieved by an ultra-wide band antenna (UWB). UWB antennas are connected in 90 degrees in phase difference. Since the antennas have a symmetrical resembles, the transmitter and receiver antennas are pointed directly on these antennas. In addition, to avoiding any interferences, RF absorbers are placed in almost every direction. In the figure, the multiplexed sensor has printed on a PET substrate. For the wireless measurements, we have established an RF absorber under the testing setup, and we have used RF absorbers in all covered boxes to cover all structures for any environmental interferences and reflections from any fields as it seen in figure below.

Figure 20: All RF Absorber covered box

Also, we have measured temperature and moisture as a reference to commercially available probes to optimize and monitor changes in frequency and amplitude.

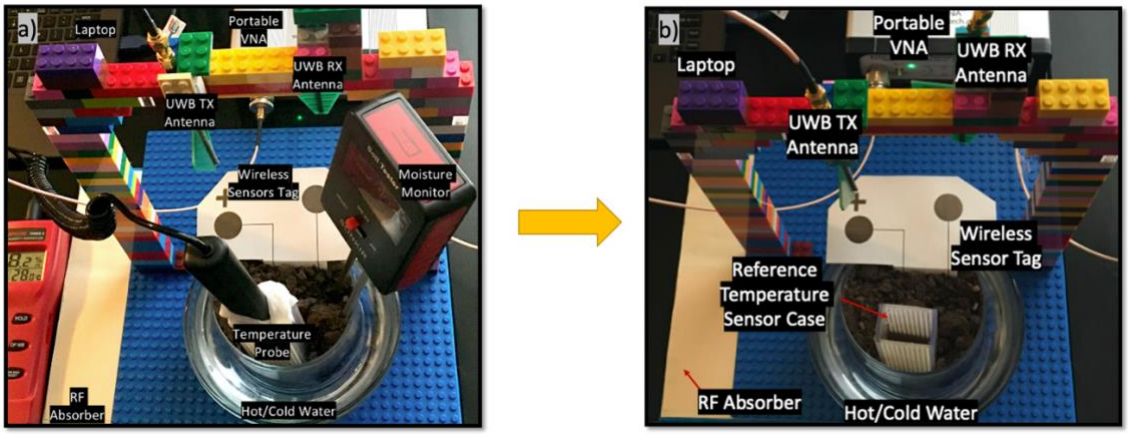

Figure 21: a) Experimental Setup with other sensor probes b) Experimental Setup monitoring sensors removed and ready to perform the wireless measurement

To avoid any reflection from probes and external measurement components, we have removed them before measuring reflection and transmission from the wireless multiplexed sensors tag. This experimental setup depicted in figure 21a ensures sensors removed measurements can be done after removed in figure 21b and covered with an absorber box from the figure 20.

The printed UWB antenna is also available to measure the salinity of the water, where the droplet has to be placed in the middle of the designed antenna.

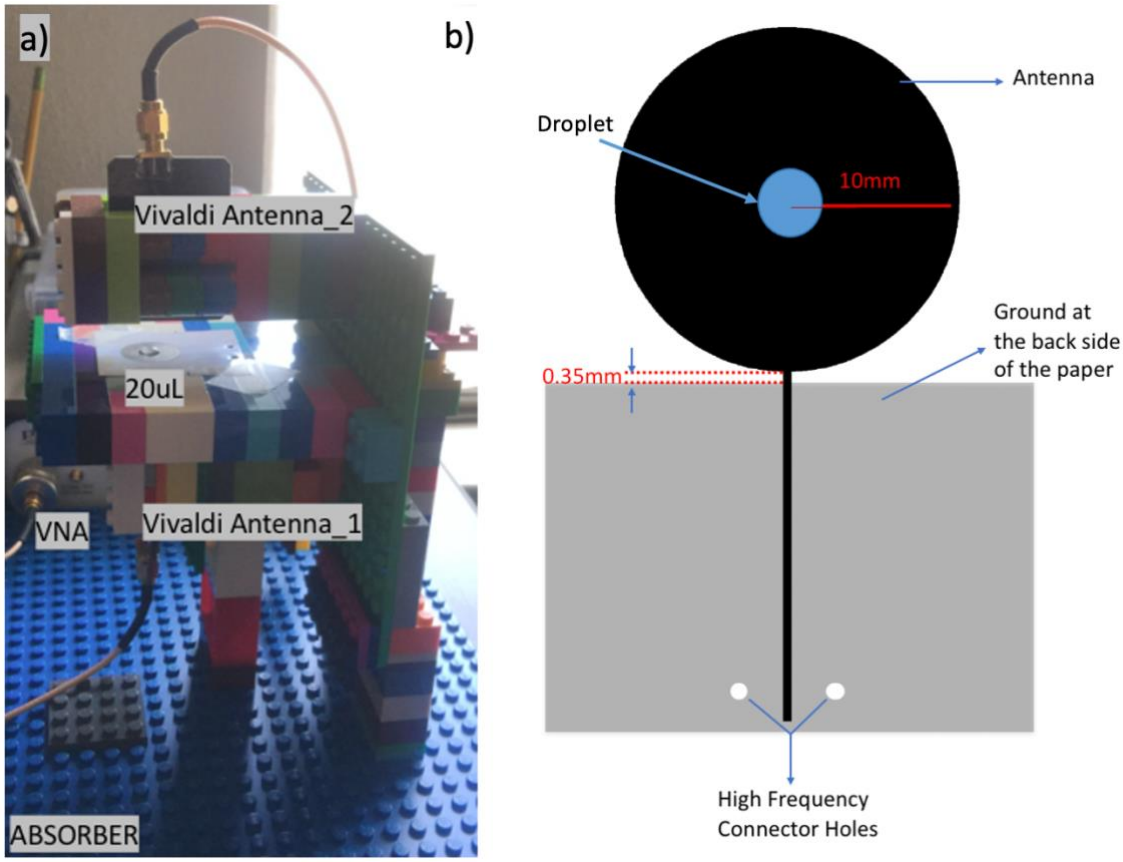

Figure 22: a) Salinity experiment setup, b) UWB antenna design and the water droplet illustration

The all RF absorber box was placed on the whole tasting set up and provided an isolated chamber from environmental wireless noises. 20 uL DI water droplet mixed in several salt concentrations has placed on the middle center of the UWB antenna. And measured their S21 values to observe changes in the wireless transmitted signal as in seen figure 22a above. The figure 22b illustrates the design of the UWB antenna and the droplet placed in the middle of it.

4. UHF TAG SENSORS

Using UWB antennas at super high frequency levels have issues with environmental effect and noise interferences. Therefore, lover the resonance frequency has more advantage over the information loss, especially for chipless and Batteryless applications. Consequently, we have an RFID tag design, that can sense gas concentrations inside of an encapsulated airtight chamber. We weren't able to use the Super High Frequency (SHF) tag in this application because of the high noise levels inside the chamber, and the absorber box cannot cover all testing sections without having any metal parts existing in (which is not applicable for proper measurement).

We have a molecularly imprinted UHF tag sensor for sensing ammonia as an example.

4.1. Molecular Imprinting

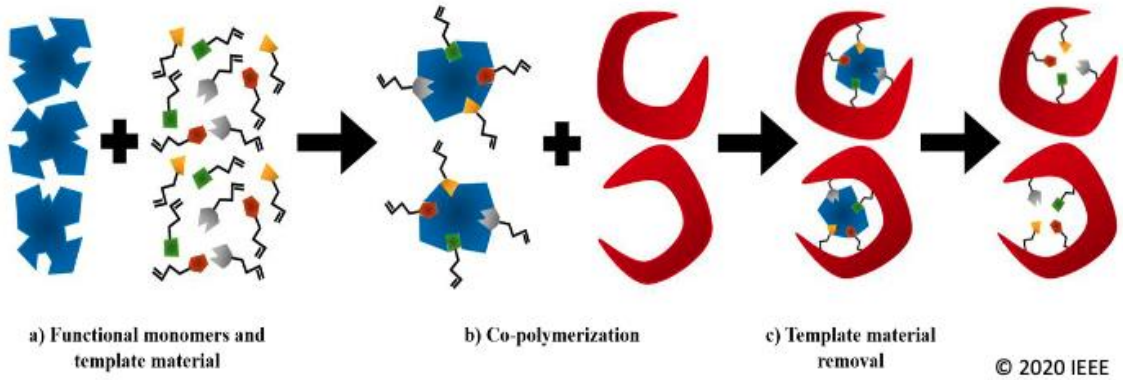

Figure 23: Molecular printing principles and methods a) solution mixed with the functional monomers (blue) and template materials, b) Co-polymerization of Functional monomers with templates. Molecular recognition modification has been made and, c) Removing the template material © 2020 IEEE "Adapted from [45]".

Fundamental basics of molecular imprinting has been shown in figure 23. As it is seen from the figure, polymerization can be achieved by using monomers and target elements with a basic polymerization process. First of all, 500 uL of aniline (99%, Sigma, USA), 2mL of 36.8% (w/v) hydrochloric acid (HCl, Macron, USA), and 100 mg of target material were mixed with deionized (DI) water to prepare a total of 10 mL of the monomer solution. [45] In our case we have mixed with ammonia as a target material inside of the solution to create target material detection and recognition site. We have used a PET film as a substrate. We have deposited the monomer solution on the polyethylene terephthalate. To make surface slightly hydrophilic, we have used oxygen plasma treatment on the PET substrate. To achieve proper deposition, we kept the substrate inside of the oxygen plasma chamber for 1 minute. The color we were targeting was pinker rather than purple since pink has more effect on nitrogen rather than purple effecting mostly oxygen. Continuous vigororus stirring has been applied during the application since the polyaniline and aniline particles are tend to settle at the bottom. Heterogenous mixture and solutions cause more irregular and unexpected conductivity therefore we have stir the sample at the highest settings. Oxidant solution has been prepared by mixing 1218 uL HCl and 818 mg ammonium persulfate. Then the rest is mixed with deionized water for a total of 8 mL solution. [45] When we mixed and put all materials in together we had 18 mL solution ready to sample and use in any substrates or applications. All particles and soluble materials are dissolved inside of the solution, and it became more homogeneous and ready to deposit any substrates for further testing. Oxidation process has to be prepared slowly dropping of the oxidant on the material since fast addition can cause occasional mixing

and irregular patterns. [45] Polymerization process has lasted around 30 minutes and after the process achieved, we observed color changes from the clear to black. The material or any designs or substrate is washed ethanol since there can be any residues and acids could remain on the top fo the modified sensor. Finally, the design washed with DI water to remove any other residual materials. We have used air drying method in our designs since the expansion and shrinking can cause unwanted cracks which it decreases the quality and/or causes malfunctioned structures. [45]

4.2. Electrodes Printing

We have performed electrode printing on PET substrate and/or other polymer substrates like polyester film, even their surface hydrophobic. The hydrophobicity is temporarily changed by applying oxygen plasma treatment on the surface as we discussed previously. After the printing, the deposited material thermal treatment was planned and appropriately performed.

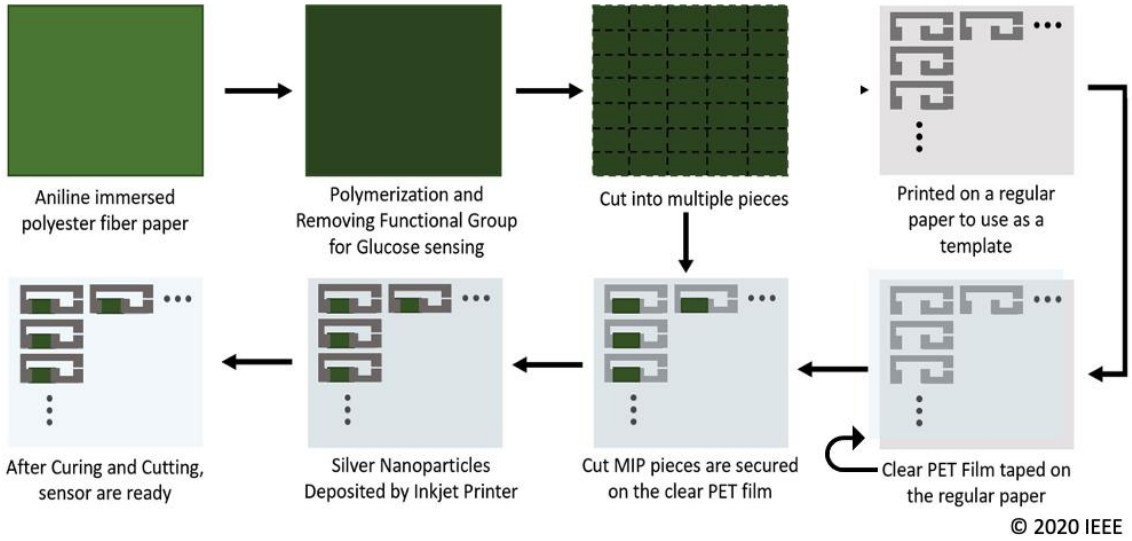

Figure 24: Fujifilm Dimatix material printer electrode printing process schematics. Silver nanoparticles are deposited on the polyethylene terephthalate and/or any other polyester materials. In a conventional oven it has been cured for 120°C for an

hour. Sintering helped to evaporate the solvents in the ink. Polyaniline strips are integrated with the silver electrodes. Conductive silver flakes paste has been applied added on the corner parts to avoid any discontinuity © 2020 IEEE "Modified from [45]"

Molecularly imprinted polyaniline paper strips are placed on the Fujifilm Dimatix material printed electrodes as it seen in the figure 24. Both used substrates are flexible and polyester based polymer material. Electrodes are printed by a material inkjet printer and we have shared the properties and the printing presets with the important methods' to perform healthy and proper printing. The designed electrodes, antennas almost all conductive printings are were printed on the PET film and/or other polyester papers or polymer substrates by an inkjet printer (Fujifilm Dimatix Material Printer 2830) using water and UV resist silver nanoparticle ink (JS ADEV 291, Nova Centrix, USA) . [45]

4.3. UHF Tag Sensor Setup

To combine the affinity detection of bacterial alcohol VOC with wireless signal transmission, the MIP-conductive polymer sensing element will be integrated with an ultra-high frequency (UHF)-RFID tag (Figure 25).

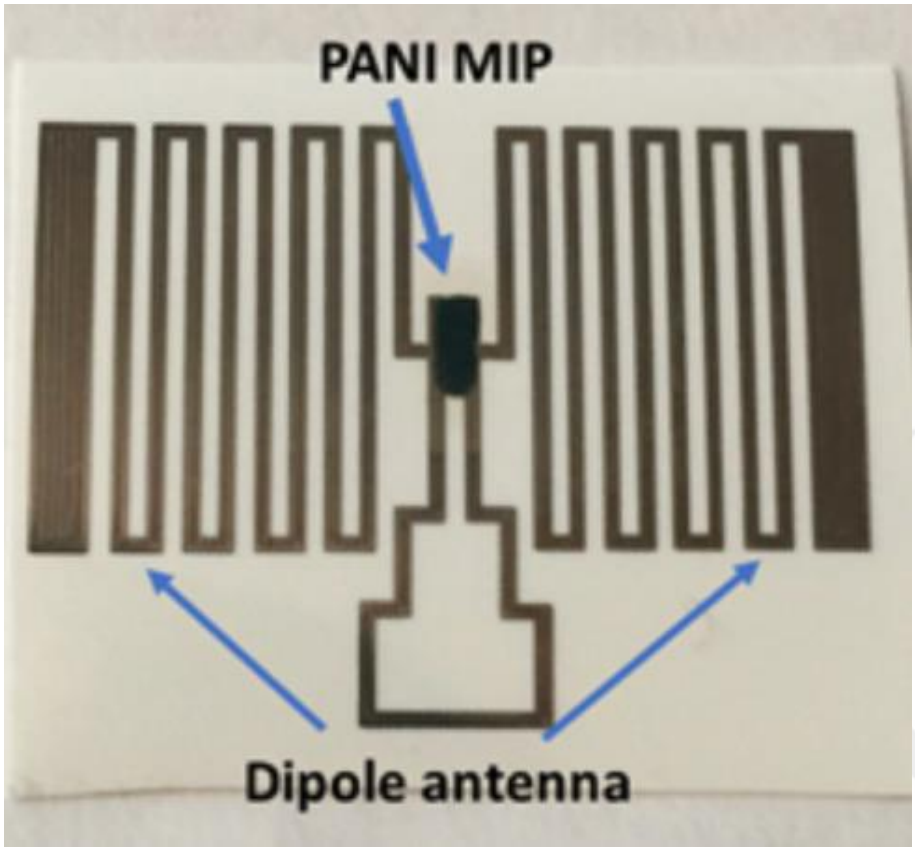

Figure 25: Wireless and battery-less paper sensor, schematic diagram of wireless and battery-less paper sensor. Dipole antenna receives the signal from the source antenna, and RF signals proceed through the MIP sensing element and back to the source antenna

The paper sensor has a dipole antenna that flanks the MIP-PANI component as it seen from the figure above. The UHF has been selected for this proposed work because it has a more extended communication range and can penetrate through the plastic wall through the VOC chamber for sensing signal communication. The entire paper sensor device will be fabricated using the inkjet printing protocol we have developed. The design parameters, including dimensions of a dipole antenna, PANI sensing element, will be optimized. To validate integrated sensing and wireless signal transmission, the MIP-

PANI-UHF-RFID paper sensor is placed inside of vapor chamber, as shown in Figure, and an external RFID antenna will transmit RF signals to sense the VOC concentrations. The circularly polarized RFID antenna (MTI-242025) is positioned outside of the VOC chamber to communicate with the paper sensor in the chamber.

We have used and tried multiple dipole antennas in several sizes, lengths, thickness, substrates. After a couple of dozens of experiments and fabrications, we have found the optimized thickness in the transmission line previously defined. All antenna parts and designs are used to be in the same dimension and printing settings.

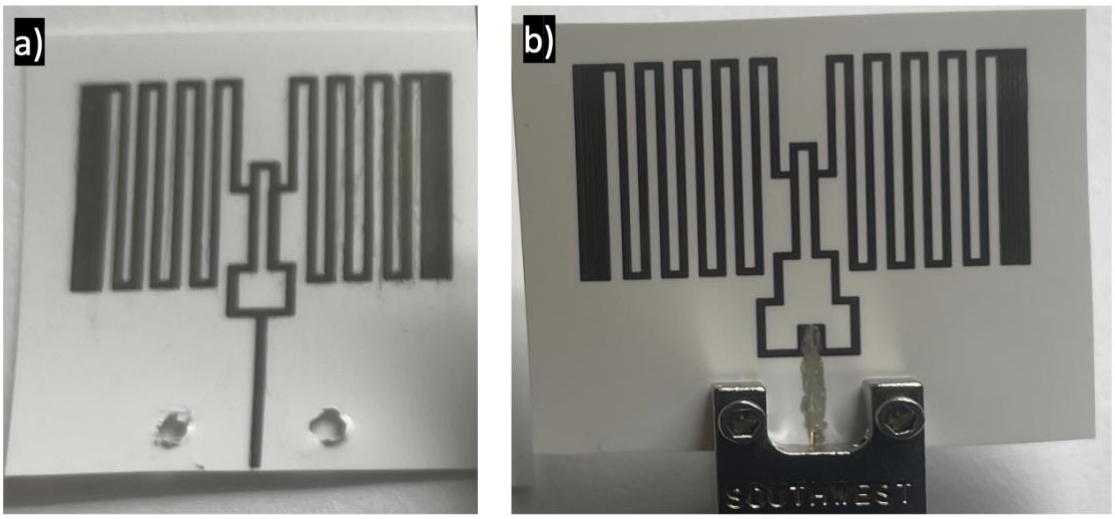

Figure 26: a) Designed and first worked UHF tag with better quality factor and resonance at 1100MHz b) Ultimate version of the UHF tags where it can operate at 940MHz

As it seems from the figure 26 a and b , we have improved our printing and our design by adding one more curved arm (figure 26b) to meet in the frequency range of the global UHF antenna. We have tested and printed multiple versions and compared their resonance where only the figure served as the best performance and impedance match.

The only issue with the tag is caused by the vertical printing from an inkjet material printer. The printer can't print in the vectorial plane; it only prints in one plane. The one plane brings quality and reliability issues on these material printors. The dipole antenna design was as seen in the figure below

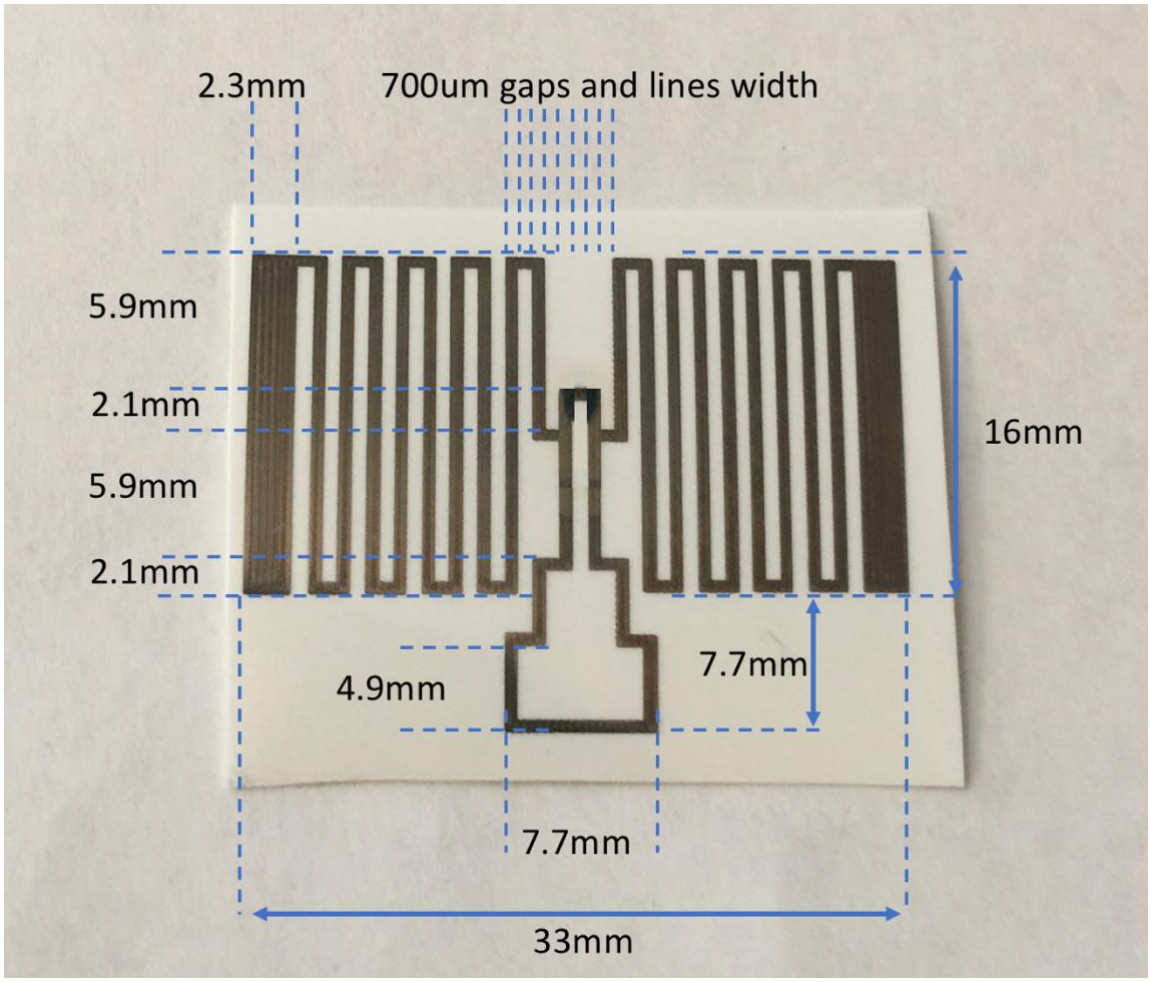

Figure 27: UHF level tag design and its dimensions in detail for reproducibility and comparison.

The sizes of the design have been identified and measured multiple times with different methods since the transmission line experiments are ensured the characteristic

impedance match and overall performance of the circuitry. The width, length, the distance between lines are optimized by the limits of the printer and electrical applicability with the backscattering response of the tag. All related dimensions are given in the figure above.

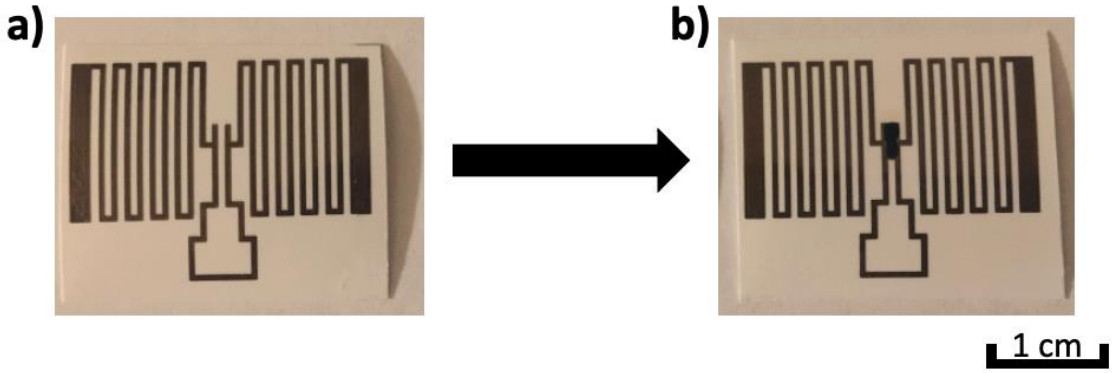

Figure 28: a) Printed UHF tag b) MIP PANI deposited on the gap between dipole antennas

As it is seen from the figure, we have deposited Molecularly imprinted polyaniline on the tag where it will be sensitive to the ammonia changes in the environment.

An incoming RF signal from the RFID antenna is transmitted through the plastic wall of the VOC chamber to the paper sensor at which RF signals are received by dipole antennas and pass through the MIP-PANI sensing element. The sensing information from the paper sensor is transmitted back to the RFID antenna as signal loss and analyzed by Vector Network Analyzer (VNA). As a relevant example for beef spoilage, we have demonstrated the detection of NH_3 vapor using the paper sensor and the VOC chamber.

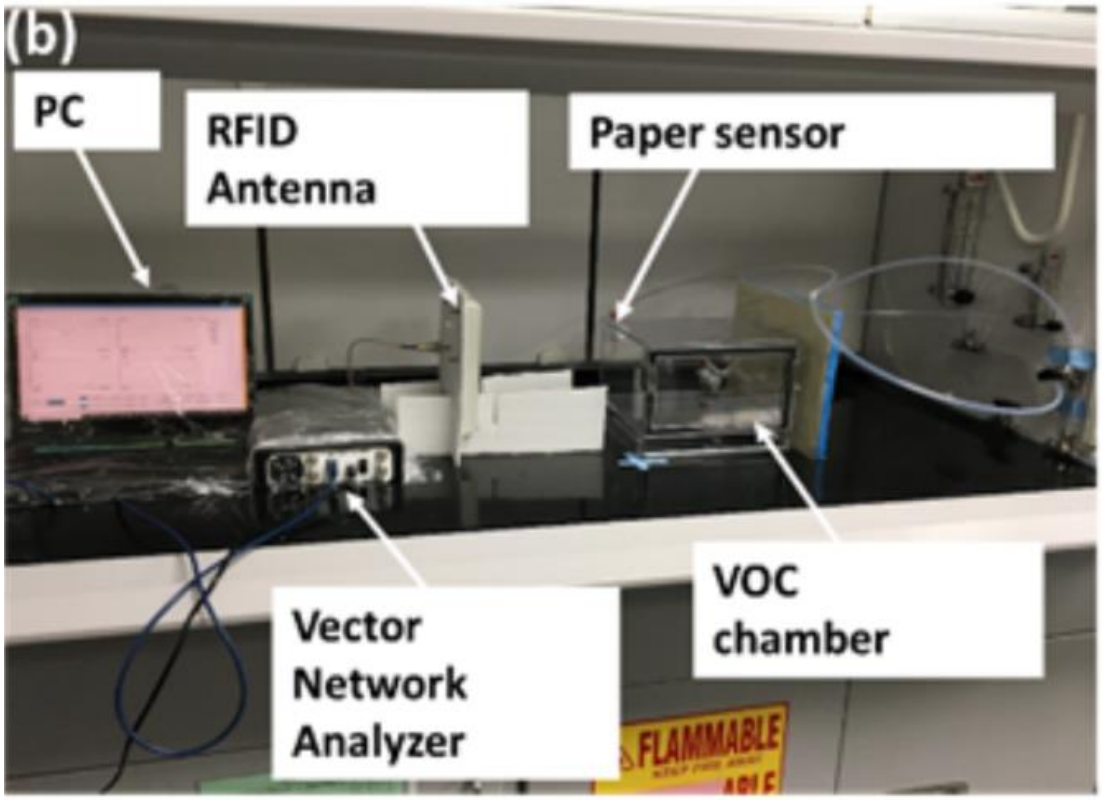

Figure 29: Image of the VOC detection experiment set up. Wireless paper sensor is located on the inside of the chamber wall to monitor the VOC concentration from food spoilage.

The NH 3 MIP component was printed onto PANI conductive polymer to generate the paper sensor, which was placed in the VOC chamber, with a 30 cm distance to the RFID detector in figure 29. The graph for reflective coefficient as a function of transmitting frequency is shown in the PC. The reflective coefficient under the atmospheric environment of the VOC chamber (blue line) contains three resonant configurations (0.8, 0.9, and 1.0 GHz). An injection of NH 3 vapor (2000ppm) into the VOC chamber is quickly detected as a decrease in the magnitude of decibels (red line). We can follow this approach to optimize the paper sensor configurations.

4.4. Wireless UHF Tag for Plant Drought Stress

We have designed and fabricated additional interdigitated designs for the wireless ultra high frequency level corn plant health monitoring. The method and the fabrication techniques have been discussed in this section. The size of the tag was optimized previously, and we have used the same structure by adding interdigitated sensing element section on the tag itself. To achieve it, the design has been calculated and measured related to the oscillation frequency. Since the only substrate changes, the signal response doesn't change noticeably. To make it possible for the deposition on the polyimide tape sticky side, we have used surface plasma treatment. During the treatment, we mostly used pinkish color treatment rather than purple by adjusting oxygen input. In this way, the sticky surface of the polyimide tape changed from being excessive hydrophobic to acceptable hydrophilic, where I was able to deposit and transfer the design on the PI tape.

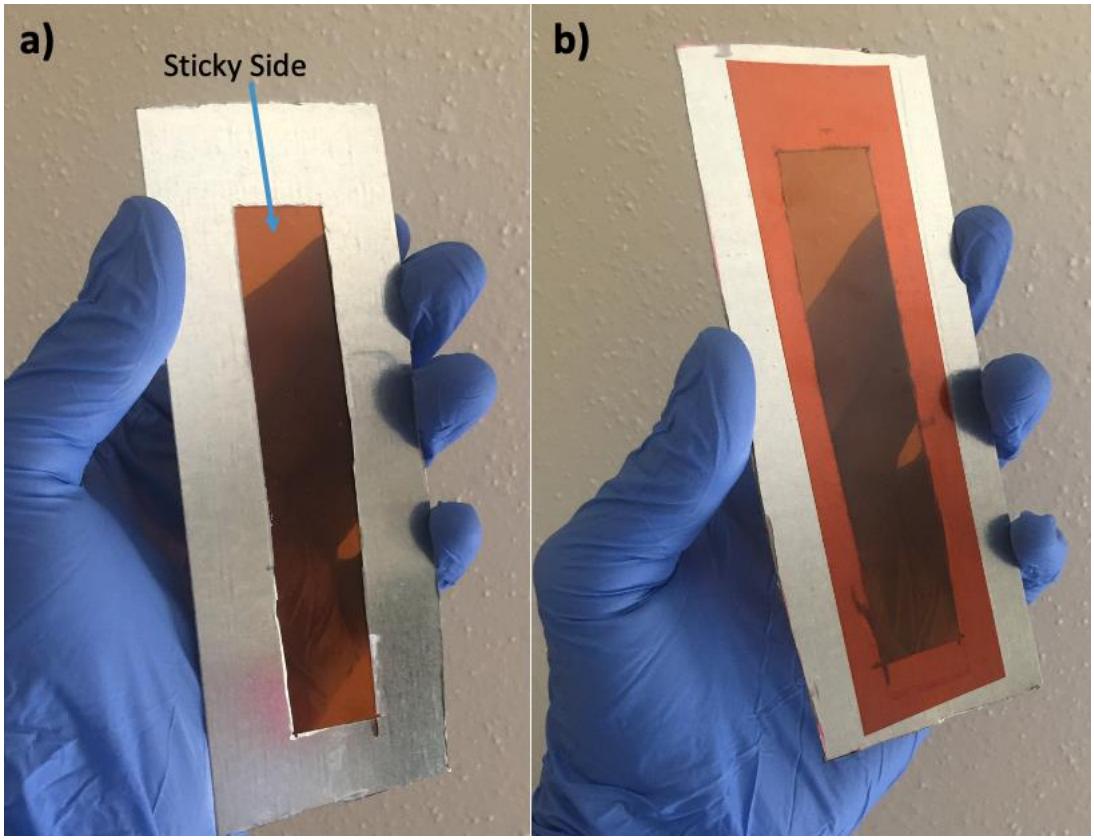

Figure 30: Metal template for plasma treatment before printing and high temperature oven curing a) Printed sticky front side b) Opposite side view of the tape.

As it is seen from the figure, we have used a steel metal plate and cut the center section as a rectangle shape to make it possible for the deposition in this section. Using a steel sheet also has an advantage over curing since polyimide can go up to 192 degrees of Celsius. The metal template has been secured for very high-temperature annealing/ curing after printing.

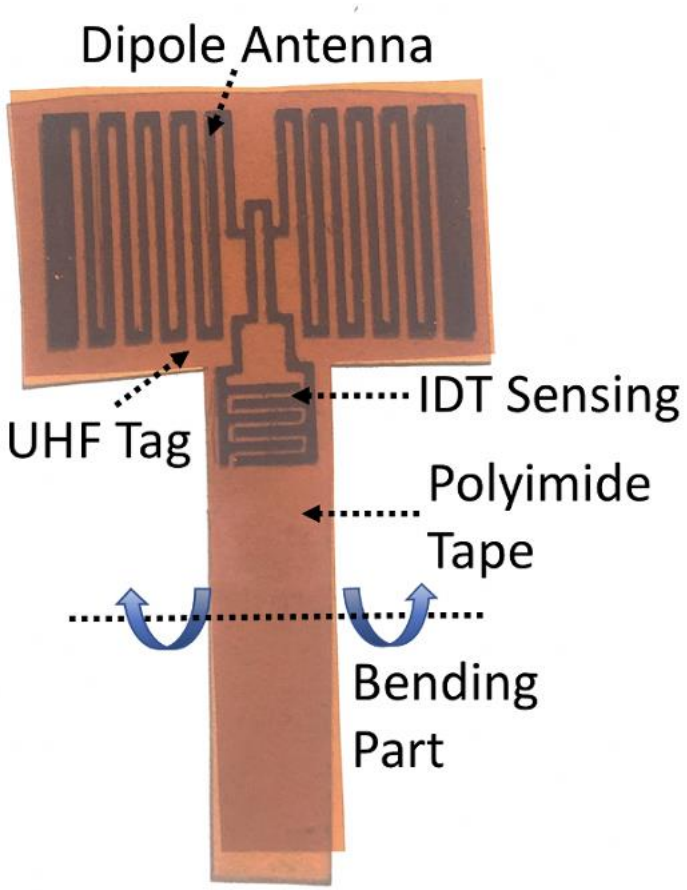

Figure 31: UHF level wireless IDT sensor design for sensing plant abiotic stress (drought)

As it has been seen from the figure, our design consists of a dipole antenna IDT sensing unit on a polyimide tape. Polyimide tape has been used since it has the best durability in low cost plastic substrates. Our curing temperature goes up to 140 C degrees, and these temperatures are not suitable for other substrates. To perform proper deposition (printing) on the sticky surface of the tape, we have performed oxygen plasma treatment to make the surface better hydrophilic and even particle (droplet) distribution. Bending part is used to create proper attachment on the corn leaf and tried to be kept as small as

possible since thicker than 1 cm IDT design and bending part causes deformation on the leaf in time. In addition to, the leaves of the corn plant are fragile at the time of V1-V2-V3; therefore, we can't increase the sensor weight load more and need to be light to avoid any inclination and/or bending. It is always better to design a more compact and less-weight load with a smaller surface overrun on the plant.

The performance of the tag itself has discussed in the results section. The setup for the experiment and set up discussions are in the below.

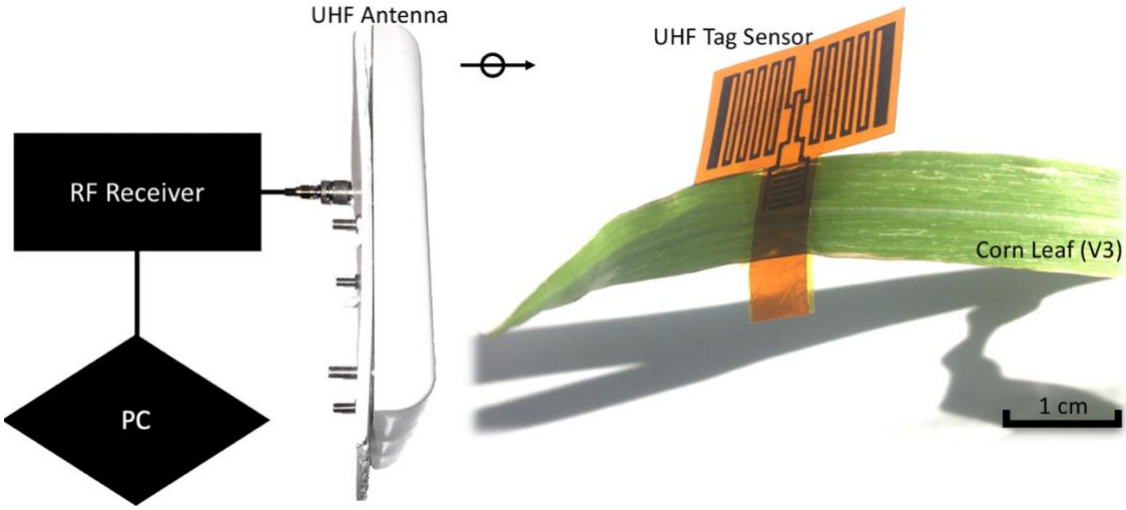

Figure 32: UHF Plant Stress Monitoring Tag Experimental Setup

In our testing setup depicted above, we have used a VNA as a receiver, and we have used a right hand circular polarized global frequency operated wide band UHF antenna that has a distance of 25 cm from the UHF tag sensor. The operational global wideband UHF antenna range is from 865 MHz to 956 MHZ, and average gain is 7.0 dBc in this range. Elevation beamwidth and azimuth beamwidths are 72 and 74 degrees, respectively. We have used absorbers under and behind the corn leaf when we perform

the measurements to avoid interferences and signal propagations from other resources related to the and considered to beamwidths provided from the antenna datasheet. Our UHF tag sensor has placed on the V3 growth rate corn leaf, and performed wireless measurements without moving the leaves and changing the positions because of avoiding any signal gain errors. For this purpose, every time, each measurement, we put the samples in the same positions that we have done before from looking at the images we have taken previously and the place we have marked. Not only position but also the distance matters for our purpose. We have to be sure that the position, the distance, the angle similar to the previous measurements.

5. LF LEVEL PLANT HEALTH MONITORING

Wireless applications ultra-high frequencies and super-high frequencies can be performed by many tags or small antenna applications. However, when wireless sensing goes to lower frequency levels, transmission without any additional amplifier becomes hard to accomplish, and distance becomes a near field where only inductive coupling involves in. Inductive couplings perform by coils where those coils are long enough to resonate at the expected operational frequency. The distance and the power are pretty limited in these applications. Therefore, especially in passive tag applications, it is avoided chiefly or not practical. However, these resonant frequencies can be used as a sensing element, and electrodes or any designs can perform as sensors. There are multiple plant health and plant stress reasons.

5.1. Introduction

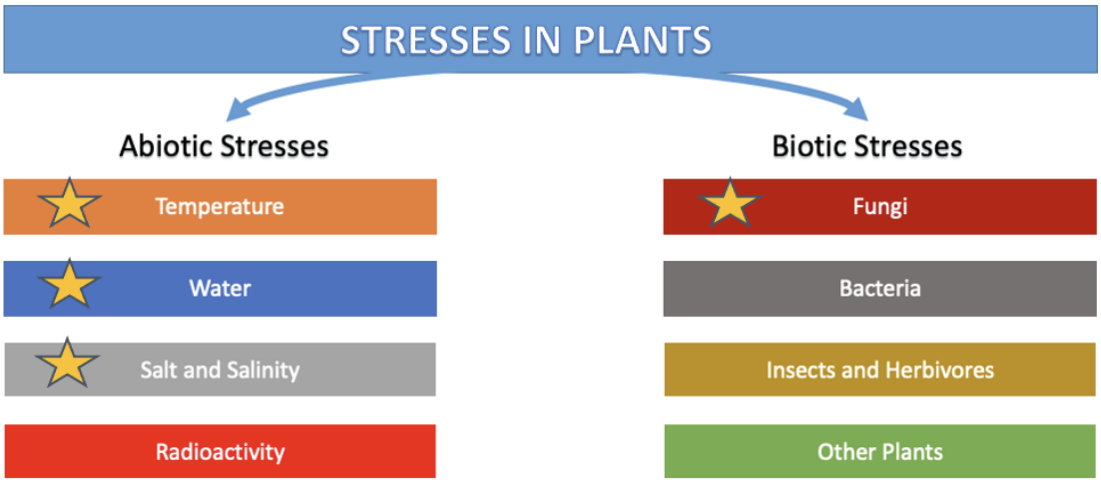

Figure 33: Stress reasons in plants

From the figure 33, we have used water as a abiotic stress and fungi for biotic stresses to compare the changes and differentiate and understand the changes in the targeted plant.

5.2. Abiotic and Biotic Stress Sensor and System Design

We have designed an impedance sensor to perform reactance and capacitance measurements at targeted frequency. The sensor electrode has three electrodes independently located side by side. The purpose of the having multiple electrodes or any electrode matrix is to reduce the measurement errors and perform more reliable results. However, our first design and fabrication started with the capacitive measurements of our designed hand-held clamp.

The principle behind sensing is basically sandwiched leaf between conductive probes having a signal generated and received simultaneously by the vector network analyzer or LCR meter. Scanned (Generated) signal can be different by the settings. We kept the scanned frequency range from 50kHz to 400kHz for portable vector network analyzer and 1kHz,10kHz, and 100kHz from a precision LCR meter. However, we defined 100kHz for the LCR meter as the most readable results and saturates faster than lower frequencies and available to compare readings from the LCR meter and the VNA as a joint operational range.

The readings from the VNA have been processed in ADS (Advanced Circuit Systems) and Y11 (Admittance) used for this basic calculation to obtain capacitance at the scanned frequency range. The equation was *imag(Y(1,1))/(2*pi*freq)* . The readings from an LCR meter were irregular, and has to wait to settle in a certain capacitance and

resistance readings. However, after 2minutes of waiting for each measurement, we obtained reliable data from the meter and processed it for further investigation. Sensing limits are defined by measurement resolution and accuracy of the meter or analyzer and the size of the capacitor surface with the distance between the opposite electrodes from the basic capacitor equation.

$$C = \frac{\varepsilon_0 A}{d} \qquad \text{Eq.5.1}$$

Where d is the distance between electrodes and A is the area of the capacitor. ε_0 Is dielectric constant for dc capacitance where 8.84×10^{-12}, but if we apply AC signal, it comes with additional which is frequency dependentε_r''. Frequency dependent dielectric constant is collected by an LCR meter and estimated for high frequencies to design electrodes at operational capacitive and detection ranges limits of the devices.

We also obtained the reactance (X) of the measurements from the vector analysis of the signal and the LCR meter separately.

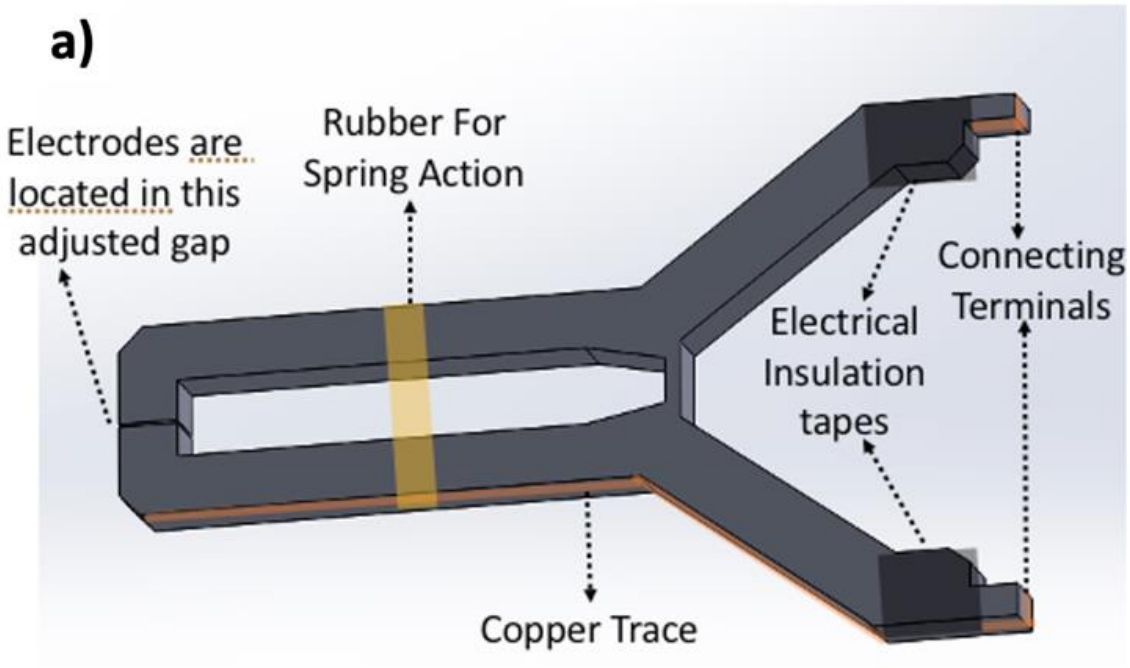

Figure 34: Schematic of a handheld with described parts

As it is seen in the figure, the electrodes are made by copper tape, and this copper tape can be etched and fabricated by any basic Printed circuit board (PCB) etching techniques. We have used rubber for spring-like action when the 3D printed handheld electrode clamped on a corn leaf. Electrical insulation tapes were for to avoid any deformation from connection terminals. The adjusted gap for this application is 200um ± 20um, where the leaves of a V1- V2 level corn have matching thickness. For these measurements, there were infected plants with Fusarium verticillioides fungi infected six samples, and 6 healthy plants are used to compare and measure.

Figure 35: Printed handheld probes for precise measurement

3D printed probes have copper tape electrodes at the tip measurement part and have a rubber for spring action and keep corn leaves at the tip without damaging and slipping as it seen from figure 35. Calvin probes are attached to the terminals of the handheld device, and electrical insulation probes were there to avoid any deformations on the copper tape while sticking on the measured leaves. As it is seen from the figure, corn leaves are at the level of the V3 growing phase and mean that each corn plant has three leaves. Usually, two more giant leaves are targeted for the measurement since the third one grows from the middle as a weak and small leaf that is more delicate.

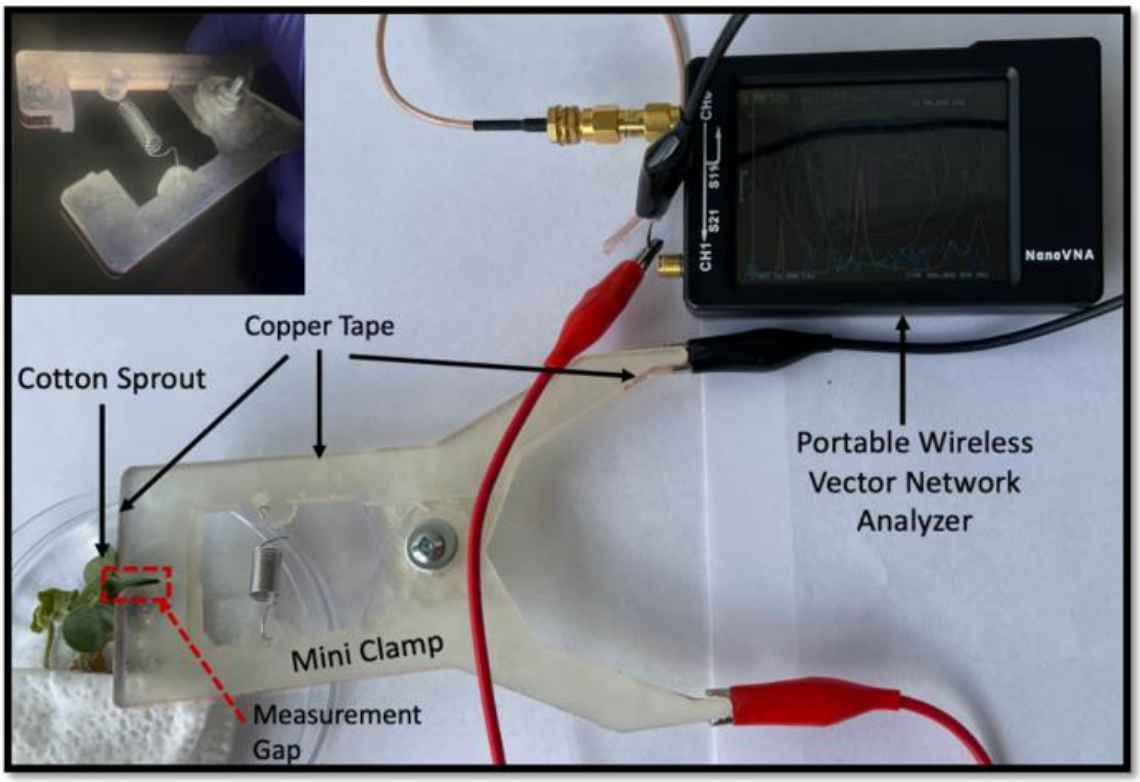

Figure 36: Experimental setup for plant health monitoring (cotton) testing setup of the handheld device with complete wireless configuration and connection through portable wireless VNA

From the figure, in this experiment, we have a 300um gap designed plant health monitoring clamp between electrodes, especially for a cotton seedling. A portable vector network analyzer has an operational range from 50 kHz to 1 GHz and can connect through WIFI. Only CH1 connectin was used on the VNA since we looked forward to measuring reflection from the electrode where it was designed as a capacitor. The copper tape has electrodes on the tip. There are three electrodes in the tip of the measurement gap at the each surface. The surfaces are placed parallel to each other, and all electrodes couples with their counter-side electrodes.

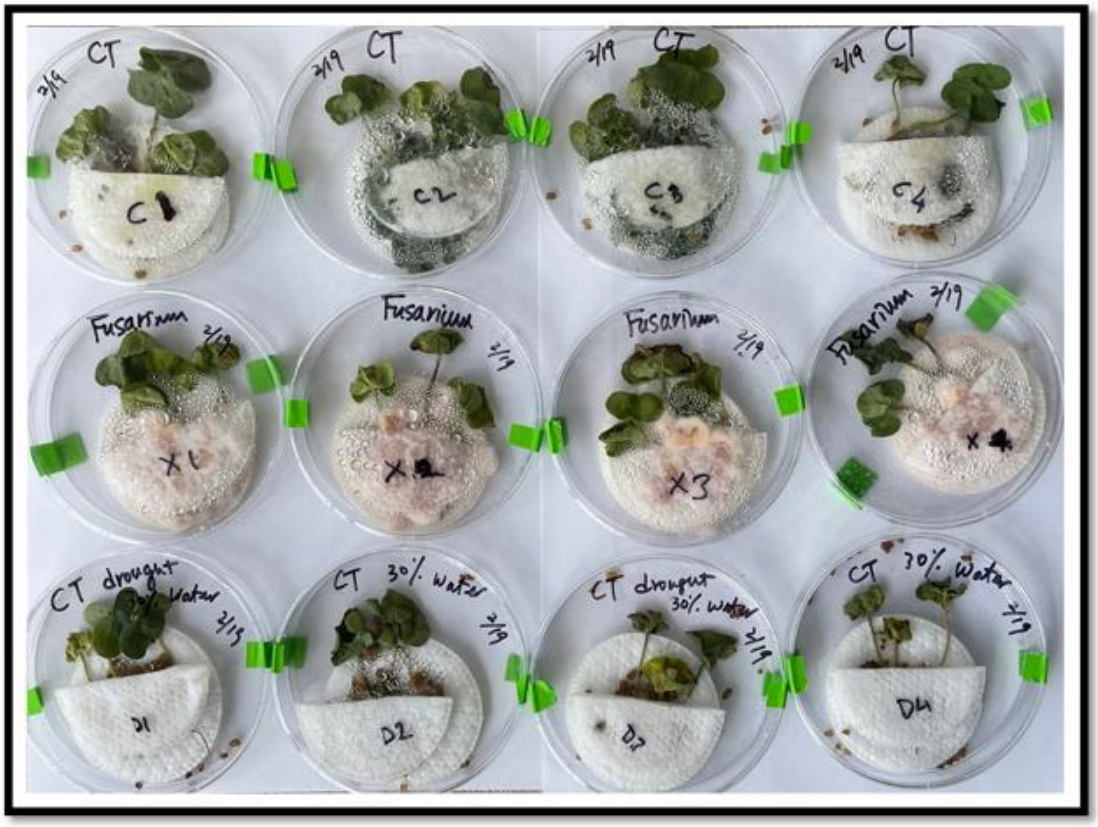

Figure 37: Cotton seedlings for plant abiotic and biotic stress monitoring

As it is seen from the figure, Fusarium oxysporum f.sp. vasinfectum race 4 (Fungal Inoculum prepared on autoclaved oatmeal) has added and infected to the cotton samples. Multiple electrodes are located at the tip of the clamp for more accurate measurements. For testing purposes, the samples were 12 samples with three other plants in each petri dish, a total of 36 cotton plants in total, 12 of them are control group watered regularly, 12 were infected, and 12 of them are water deficient in observing drought effect on plants. After the measurements, drought-abiotic stress was investigated more deeply to understand the effect on plants and reflection to our result. Therefore, we have prepared

18 samples in different water concentrations with continuously watered samples to compare changes inf every measurement and understand the reliability of the each experiment.

Figure 38: Cotton seedlings for drought test b) Cotton seedling sample in a petri dish

There were three samples 25% water only (watered on the first day of the measurements), three samples of 50% water only (watered on the first day of the measurements), three samples of 75% water only (watered on the first day of the measurements), three samples of 100% water only (watered on the first day of the measurements), three samples of 10% water (watered on the first day of the measurements) and periodically watered, the total of 15 cotton seedlings. In figure 38, there are 18 samples where the last three samples were dead on the first day. We also performed plant health monitoring for drought recovery by avoiding watering these 100% watered and continuous watering cotton seedlings samples after 10 days of measurement. The 0.3 mL distilled water was added every other day. Especially we have chosen 0.3 mL

directly injected on the seedling roots located section where we can avoid excessive watering and interferences of the data with the accumulated water resistance.

6. RESULTS AND DISCUSSION

The measurements and results with initial experiments of UWB antenna wireless multiplexed soil humidity, and moisture sensor and UHF tag gas sensor and UHF tag wireless plant drought stress experiment, and LF capacitive electrode plant health measurements are presented and discussed in this section.

6.1. Wireless Multiplexed Temperature and Moisture Sensors Measurements

We have multiple measurements to ensure soil humidity and moisture measurements that can represent as a multiplexed sensor on the same chipless batteryless wireless plane and perform passive communication between the tag and the TX (transmitter) and RX (receiver).

6.1.1. UWB Antenna Tests and Measurements

Ultra wide band antenna has been designed from an existing paper; however, the antenna has an advantage over all published alternatives in its operational frequency range capability, which is from 2.2 GHz to 17 GHz. This is, so far, the most extended communication range among published journal papers.[46-48]

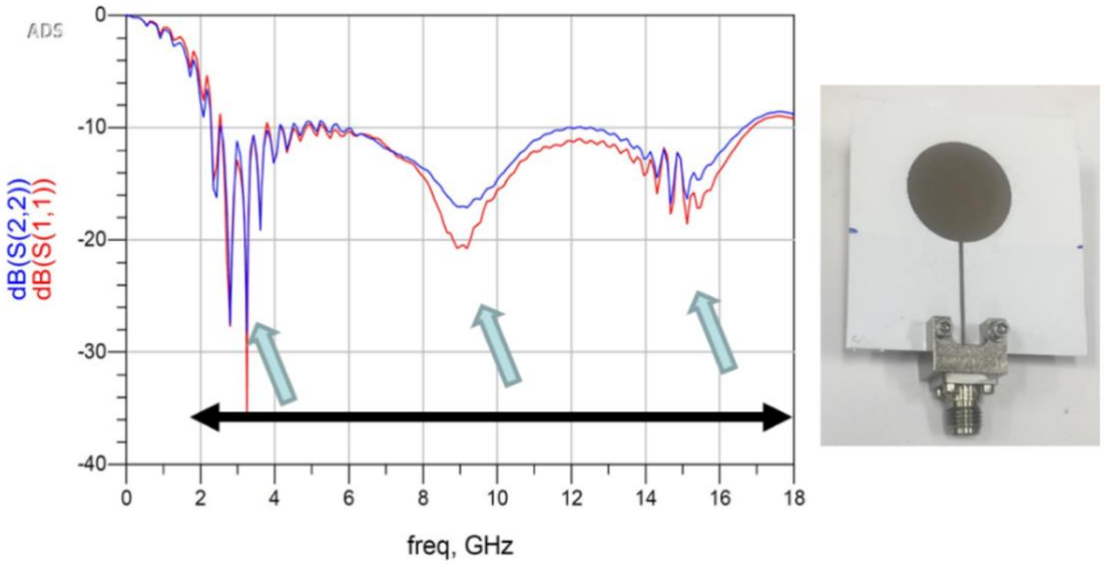

Figure 39: Graph for antenna reflection S11 data and the printed antenna.

From the figure, the -10 dB range is broad for a paper substrate antenna. We observed effective operational range from 2.3 GHz to 16.7 GHz. Additional curing and printing improvements result in better sensitivity as it seen in the graph. DB(S(1,1)) has better improved reflection depicted in the graph. One of the printed and tested antenna is shown in the figure 39.

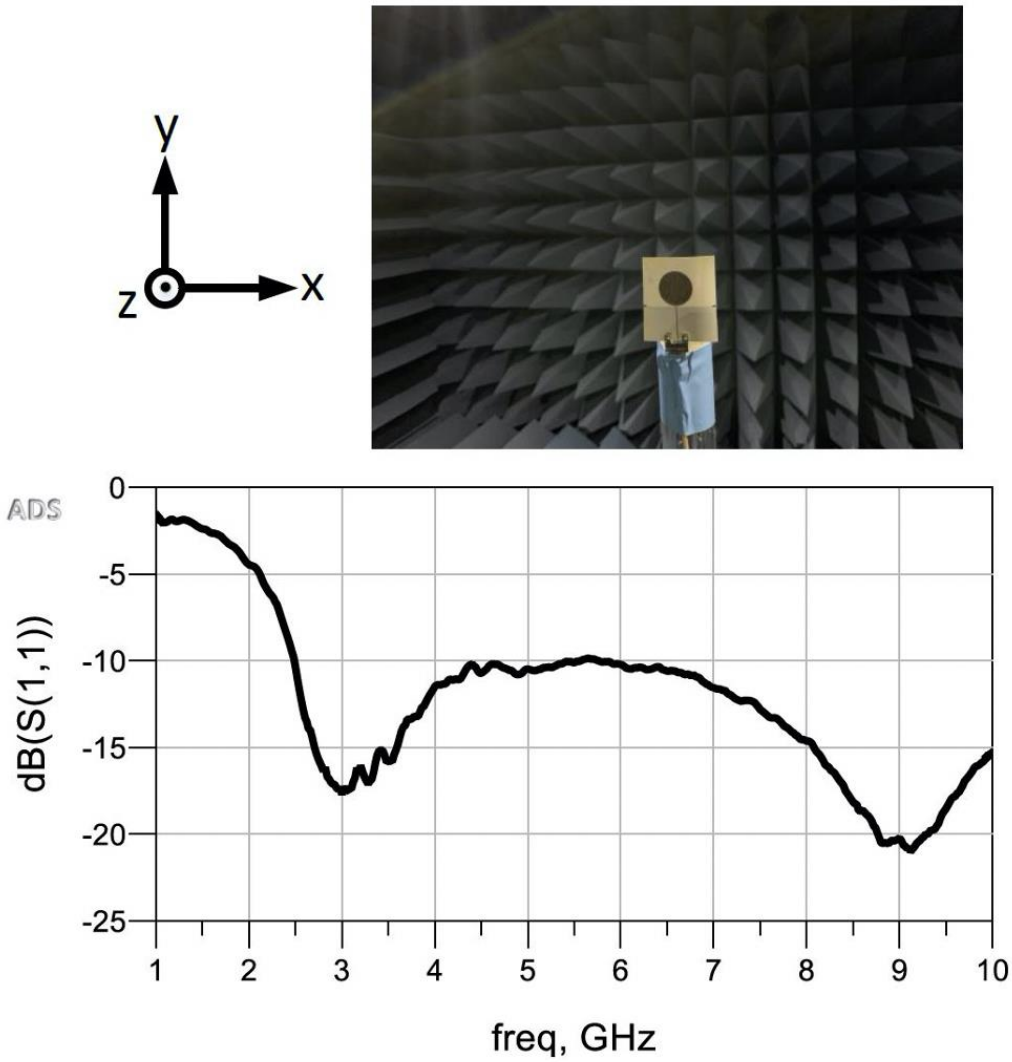

Figure 40: Anechoic chamber measurements of the UWB antenna

As with the figure, anechoic chamber measurement matched with our VNA measurements, and performed as expected. As we consider -10dB as a threshold of an acceptable antenna reflection gain, the antenna design on PET paper ranges from 2.4GHz to 17GHz. This UWB range provides us an opportunity to implement resonators or other circuit elements on the antenna and can be processed effectively. In addition, to these

measurements, we have tested its reflection and radiation pattern in the anechoic chamber.

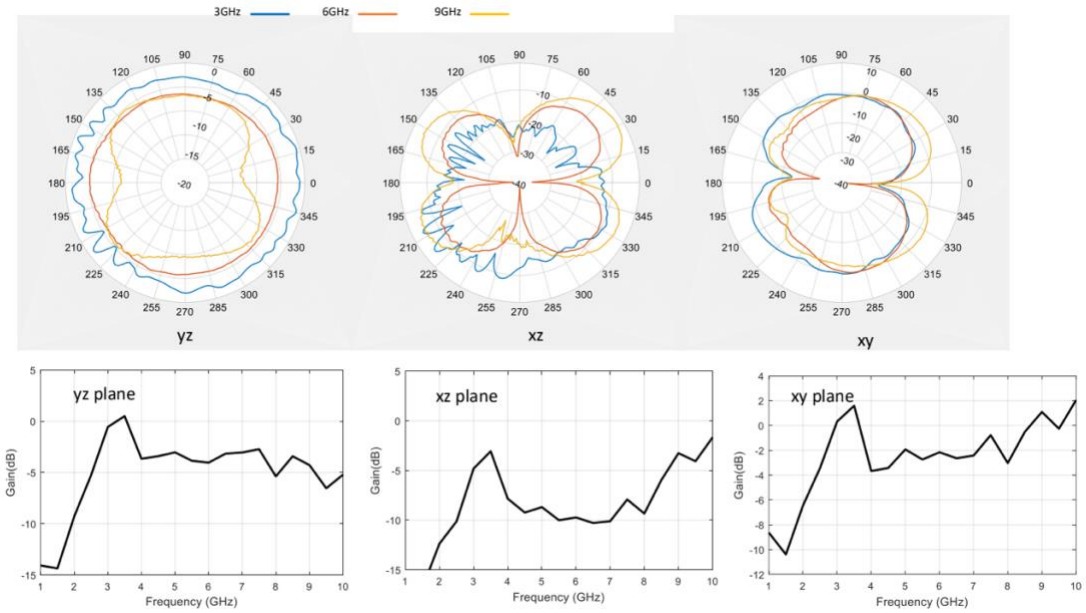

Figure 41: Anechoic Chamber measurements of the UWB antenna and its radiation pattern at three planes (yz, xz, xy)

As it seen in the figures, the antenna has a reliable reflection at x-direction and polarization. The polarization relates to two parts which are linear polarization and vertical polarization. This radiation pattern gives us an idea about the antenna's performance and its radiation direction and how it receives the signal or radiation (energy) from other resources. From the figure, yz plane is the vertical plane which is also called as elevation plane, and xy plane is the horizontal plane where it also called the azimuth plane. The results from the measurements encouraged us to operate primarily between 3.5 to 8.5 GHz level where we have designed our stub type resonators integrated into this antenna.

6.1.2. Stub Resonators Design and Measurement Results

This is the first of its kind a multiplexed sensor in analog measurements since the measurements can affect the whole circuitry. To avoid it, treatments and design methods are applied to decrease the error caused by other analog sensory parts. We have achieved this by using frequency and gain. For additional data, it can be used phase or Q factors in other resonators depends on the application. We have effectively measured the soil moisture and temperature.

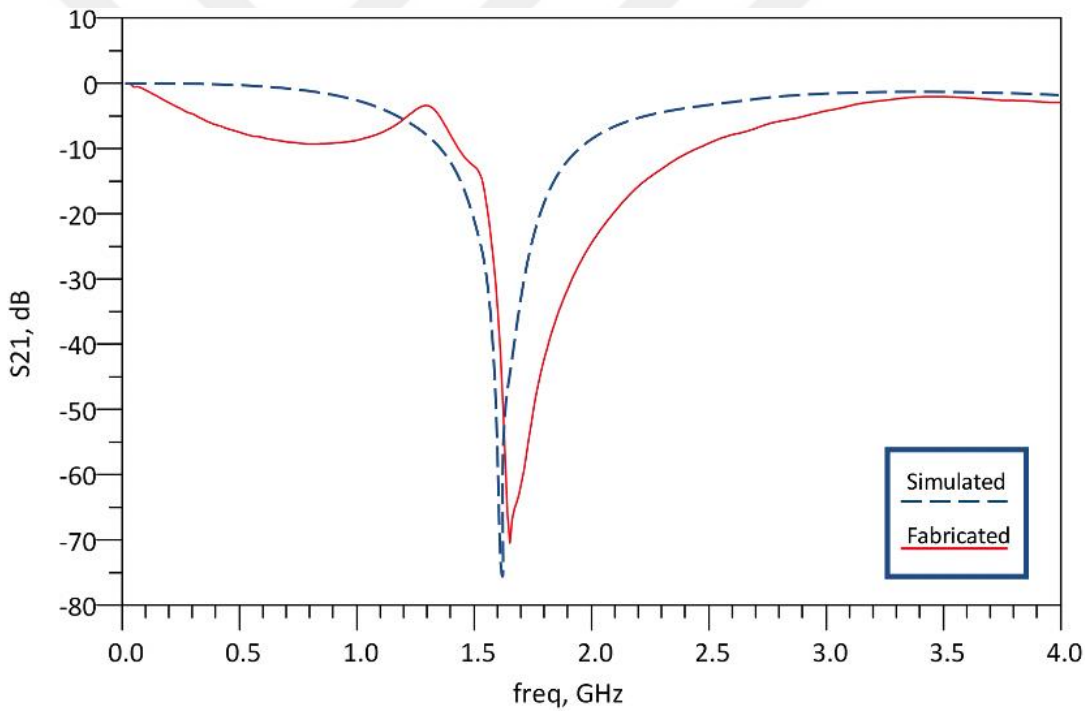

Figure 42: Stub type resonator simulation and measurement (5 Stubs)

From the figure 42, we have observed a reliable and expected fabrication with our simulation. The simulation has been made in HFSS and fabricated stub measured with a VNA. We measured the quality factor as 407.21 but estimated 110.13. This has been caused by the inner fabrication effects and surface roughness of the deposited silver. The

central resonant frequency of the stubs was simulated at 1.613 GHz but measured at 1.639 GHz. This has been caused by the edge effect of the depositions where the deposition from a material printer does not have a perfect and immaculate edge. Cleaner the edge and rectangular the shape will have the best matching measurement with the simulation. However, there are limitations we have discussed in the UWB antenna section. Multiple resonators have been tested, and measurements are compared. In figure 3, a number of the stubs and their transmitted signal and resonance profile has been presented, and the quality of the signal has been measured as it is seen in the figure. We observed the quality factor is highest in 5 stubs that are parallel and connected to a transmission line. Magnetic resonance has multiplied by the numbers of the stubs added to the system. However, we measured the quality factor (Q), which decreases and forms another resonance point in stubs number six and seven. Therefore, additional internal resonance and stubs interactions become more problem also the size of the sensor becomes unpractical if we follow to increase the number of the stubs. Individual sensors' responses and their measurements are discussed in this section. Their behavior and response when multiplexing in sensing have been investigated and compared. Simulated five stubs resonator has the highest quality factor. Our simulation and fabrication measurements match with each other. Frequency shift and the quality factor variations are the results of the printing quality, surface roughness, and the connection contact effect with related instrumentation. We believe the irregular sub 1.3 GHz errors are caused by the capacitive coupling effect of the stubs and their crosstalk. However, increasing the distance between stubs cause further issues with the quality factor where the transmission line involves and

decreases the quality factor dramatically. Therefore, crosstalk is not an issue as long as the quality factor has the highest possibility. Limitation of the fabrication and crosstalk defines the distance between these stubs. Less than 500um results in excessive crosstalk and improper resonance at higher frequencies. Simulations can not give these effects to investigate because there are more non-linear effects than a simulation program can handle. For example, curing nonlinearity in conductive ink, printed irregular edge effect of the conductive ink, conductive ink metal particle aggregation, ohmic and capacitive contact on the connectors and the ink material, printing statics causing metal nanoparticles to spread nearby printed lines, and so forth.

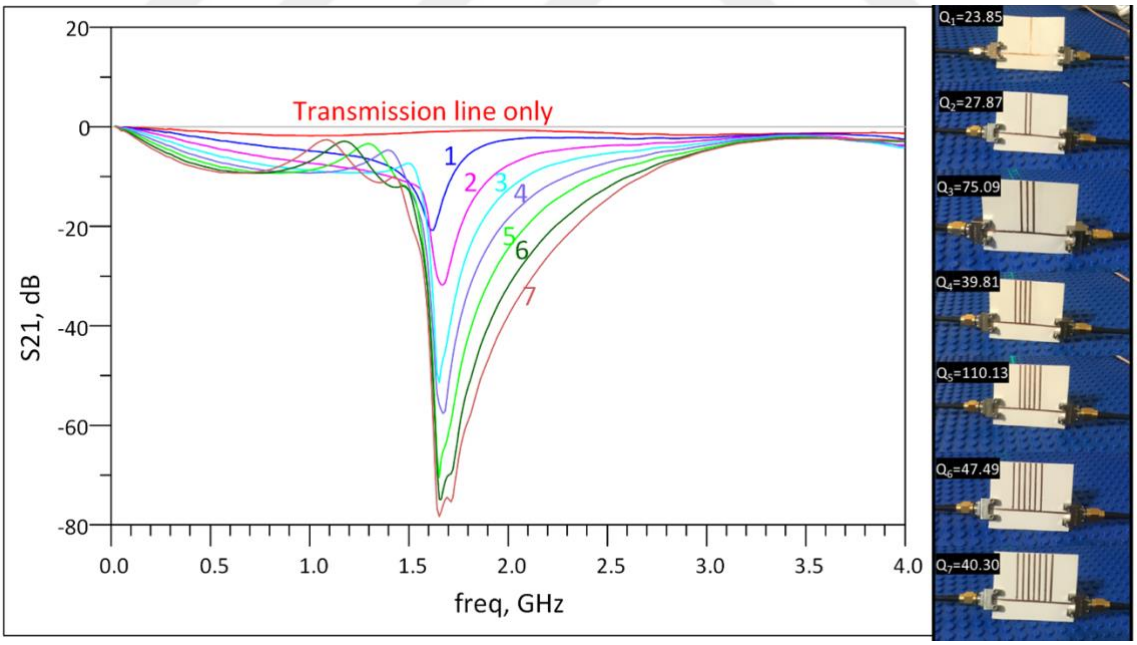

Figure 43: Stubs resonance frequencies vs to gain and their quality factors

As it is seen from the figure, we have tested seven stubs in different numbers; the stubs are 1, 2, 3, 4, 5, 6, 7 stubs configurations, respectively. These configurations are

tested by a VNA and processed the data in ADS. From the measurement, it is evident that the highest quality factor is obtained from the five stubs configuration, and it has been measured 120.13. The calculation for the quality factor was made possible by the 3 dB method, where we have counted 3dB corner frequencies (lower and upper cutoff frequencies) and resonant frequency. Simply resonant frequency divided by the 3dB cutoff frequencies difference. We also observed three stubs performed decently; however, five stubs resonator was the highest quality and made our different designs and testing on this resonator configuration. In the figure, you might notice there is an additional peak that comes with the 6 and 7 stubs configuration. In these two configurations, the transmission line length and fabrication imperfections contribute to secondary resonant peaks on the resonator and decrease the quality factor of the composition.

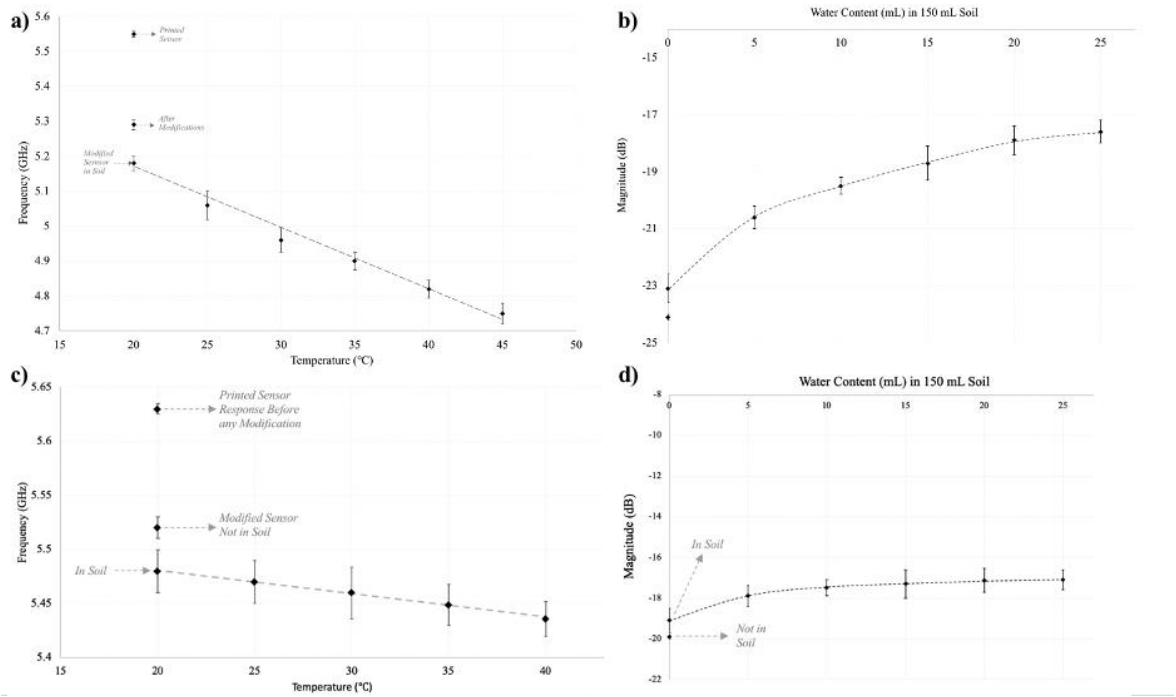

Figure 44: a) Not multiplexed stubs group temperature sensor performance b) not multiplexed sensor response to the water content in soil c) Multiplexed version of the

stubs group temperature sensor response to the temperature changes in the soil d) multiplexed sensor response of the moisture sensor

As it seen from the figure, this figure is about the measurement from a non-wireless multiplexed sensors, and the readings show changes between the printed sensor and its response change after modification and slight difference when the sensor is put into the soil. The sensors' frequencies shift when they have dipped into the ground. Also, magnitude changes are observed when we dip into the soil. The first results are from one resonator. However, the results c and d are with a multiplexed sensor. The quality factor decreased a little by the cascading; therefore, we made some modifications and improved the quality of the resonators by adding ceramic and silver nanoparticles we have discussed previously and covering with PDMS the parts those not exposed and directly contribute to moisture measurements. Basically, only the moisture sensing stubs design configuration was not covered with the PDMS layer. We observed magnitude changes by the increase of the moisture (water content) in the soil. For the observation, we have waited 30 minutes to settle the heat distributed inside the soil. From the measurements and results, we have found that the temperature has a significant effect on the frequency shifts. When it has more heat under the soil, it shifts towards to lower frequencies. Both single and multiplexed versions presented reliable and promising results. Therefore, we have continued to perform wireless sensing after.

6.1.3. Wireless Soil Measurements for Super High-Frequency Levels

Wireless soil measurements were not as easy and did not have more quality factor than our wired measurements as expected. Therefore, the measurements and data processing tools can increase the correct estimations and meet with our validations.

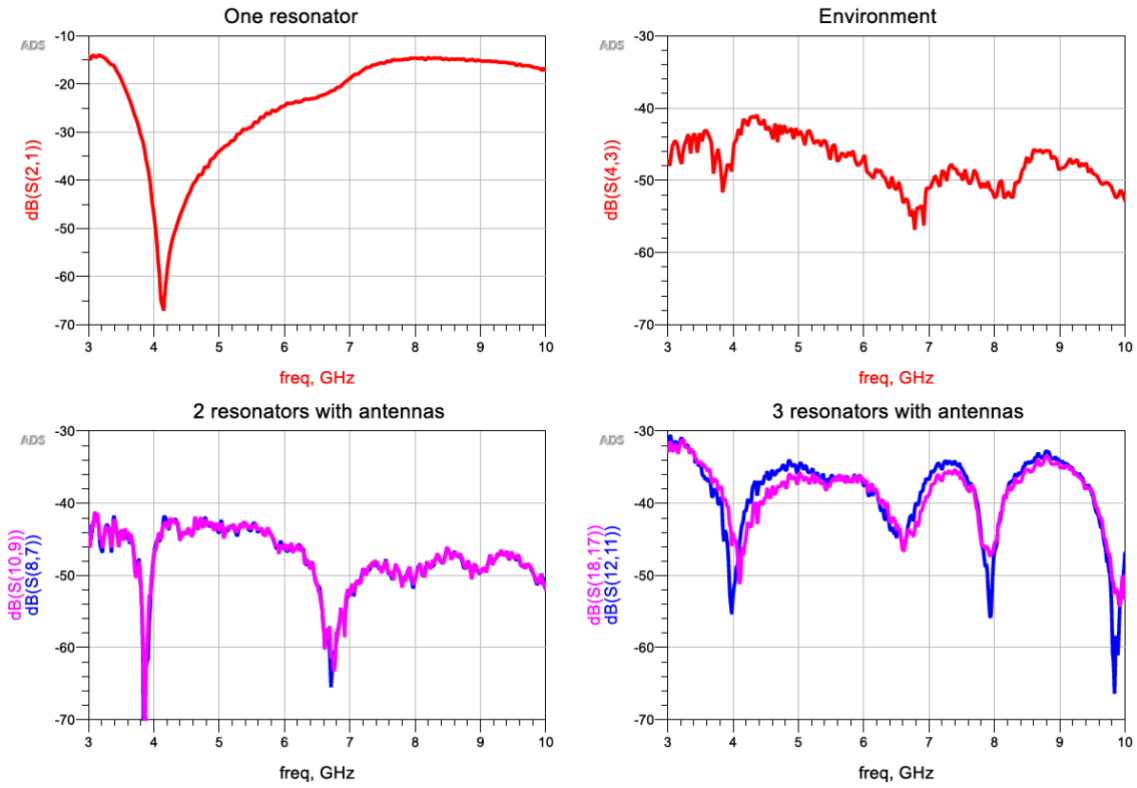

Figure 45: Multiplexed Resonators and their frequency and gain responses

From the figure, we have processed data and made a measurement for each configuration. These configurations were one resonator with two UWB antennas, two resonators with two UWB antennas, three resonators with two UWB antennas. These three configurations are tested wirelessly by the UWB transmitter and receiver from a VNA. To decrease the noise from the environment, we have subtracted environmental measurements from the tag measurements. Our wireless multiplexed sensor measurements

were promising, and as it is seen in the figure, they had dependable results and resonant frequency peaks for further testing and measurement in a real case scenario. The frequency has slightly shifted when new resonators were added into the circuit. However, these shifts are negligible and inside the operational frequency range. Resonators are investigated separately and measured their responses. We have collected S21 data for the multiple resonators with a subtraction of the environmental noise. These resonators have interconnected analog responses that show effects on each other. However, as discussed in the design and applications, we have modified the sensors in the design and fabrication section. As it is seen from the figure, their connections and overall resonance responses are slightly changed or shifted. Blue and pink measurements are from the same multiplexed sensor. Blue measurement has a particular position where pink measurement has 1mmx1mm off from the alignment and 5cm more distant. As it from the figure, the analog response of the multiplexed sensor can be measured and collected without any filtering or pre signal processing. Three resonators' responses are as it seen in figure d. The fourth peak around 9.8GHz is an internal oscillation harmonic that occur at high frequencies. Precise positioning and the UHF+SHF absorbers are required at further multiplexing, as shown in figure d.

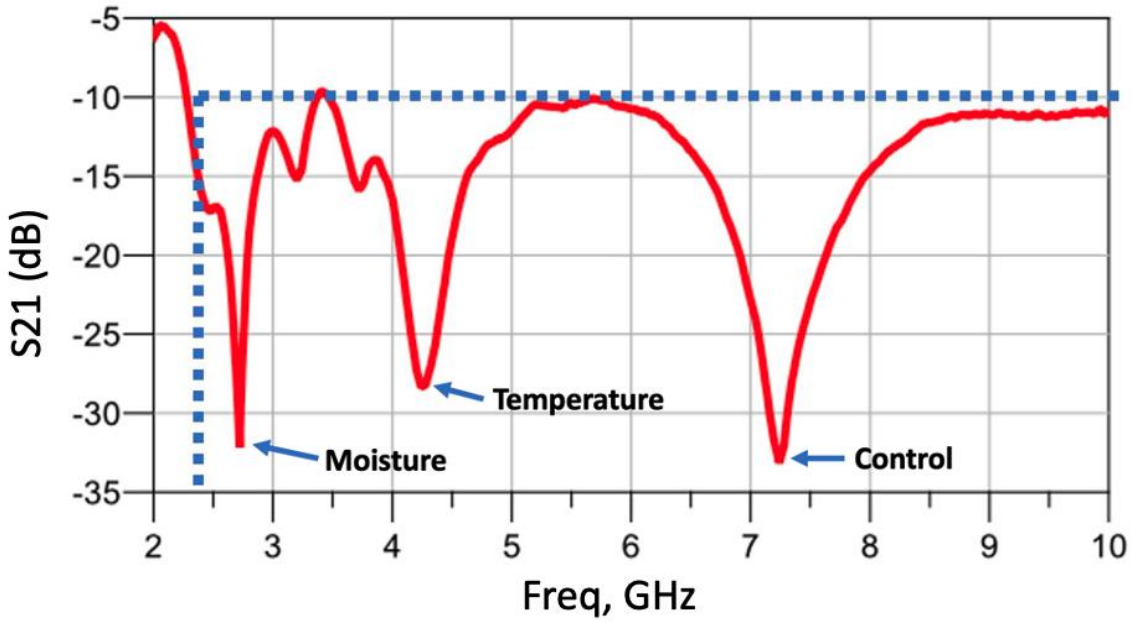

Figure 46: S21 Response of the antenna for wireless sensing and its temperature, moisture and control resonance frequency peaks

For the moisture detection and measurement we have used the most extended stubs configuration and used it to observe the gain changes in dB from S21 measurements. Temperature changes are observed in the changes in frequency and peak frequency of the measurement shown in the figure used to measure the changes in the temperature of the soil. The control measurement was there to observe overall frequency shifts and amplitude loss during the changes in the environment. It has been used to monitor and understand the effect on a comprehensive system. However, it can be used for to increase the quality of the measurement (by using machine learning algorithms) and decrease the errors.

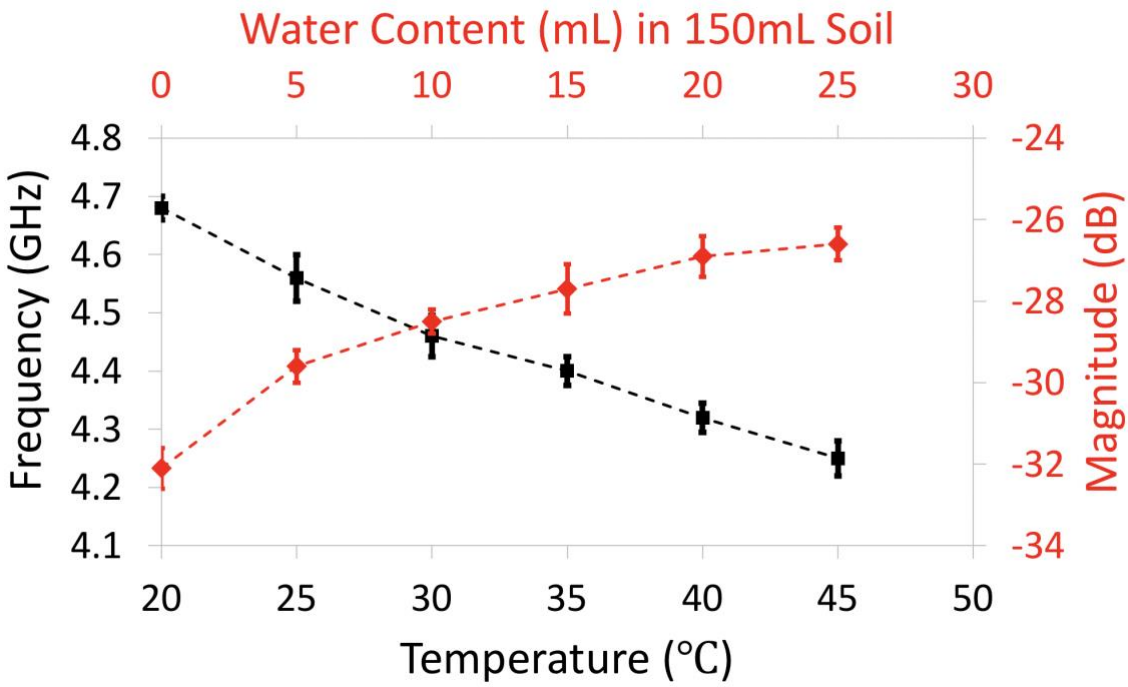

Figure 47: Water content and temperature changes in magnitude and frequency, respectively, for wireless sensing.

From the figure, we had observed linear response when the temperature changes (increases), and also magnitude change observed in a reliable result that we could process the measurement for saturation points. Moisture has a more non-linear effect on the sensors since the response and the moisture of the soil are not exactly precise in every exposure, and the moisture (wetting) also happens under the soil is not fast and causes moisture levels to change, and additional water soluble minerals involve in. Cascaded moisture, temperature, and control resonators are used to monitor the soil environmental characteristics in several scenarios. Related to our measurements, we have observed changes in frequency dominates changes in magnitude in temperature changes. The received signal magnitude changes more with the changes in the water content. To

improve these phenomena, we have modified the sensors with an additional deposition and modifications to contribute to the shift for optimum monitoring. In the figure, moisture and temperature have their own specific resonance frequency with a control oscillation. The measured transmitted data has been processed, and changes in peaks in moisture and changes in frequency in temperature have been measured and recorded. According to the water content, modifications and changes in temperature had more impact on the magnitude and the frequency, respectively. Magnitude has increased by the increase of the water content. Besides, frequency has been shifted by the changes in soil temperature.

6.1.4. SHF Salinity Measurement

In addition to all, we have been tested this UWB antenna itself for wireless salinity measurement.

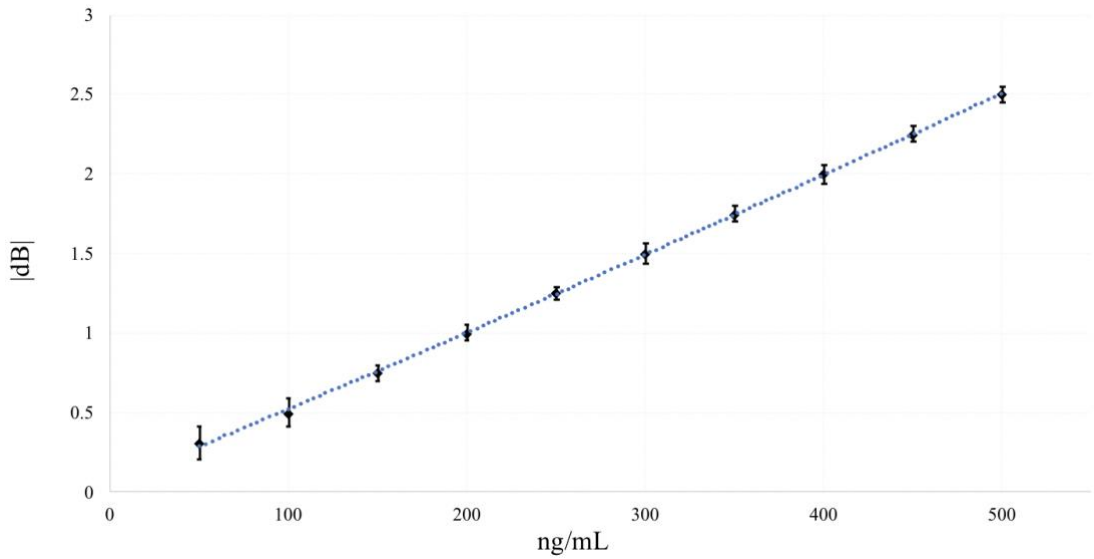

Figure 48: Wireless S21 changes in the gain by the salt content in the water droplet.

The measurement setup and design configurations are in the UWB antenna section and discussed. In this measurement seen in the figure 48, results we have been ensured by the usability of the existing antenna can be used to monitor salinity in a single droplet. We also calculated the limit of detection from the measurements and calculated it as 24.97 ng/mL. The droplet has been placed center of the antenna and measured wirelessly. With this method, any salinity of the liquid can be measured without interacting with an electrode. The resolution and the limit of the detection might be lower than the connected versions. However, this measurement and the technique have an advantage over the corrosive materials and low cost passive wireless capability.

6.2. UHF Level Sensing and Measurement Results with Discussion

We have designed new sensors for lower frequency levels since super high frequencies require more absorbers and likely to use encapsulated structures, and they are susceptible to any changes in the environment. We have done wireless gas sensing and the wireless plant stress monitoring.

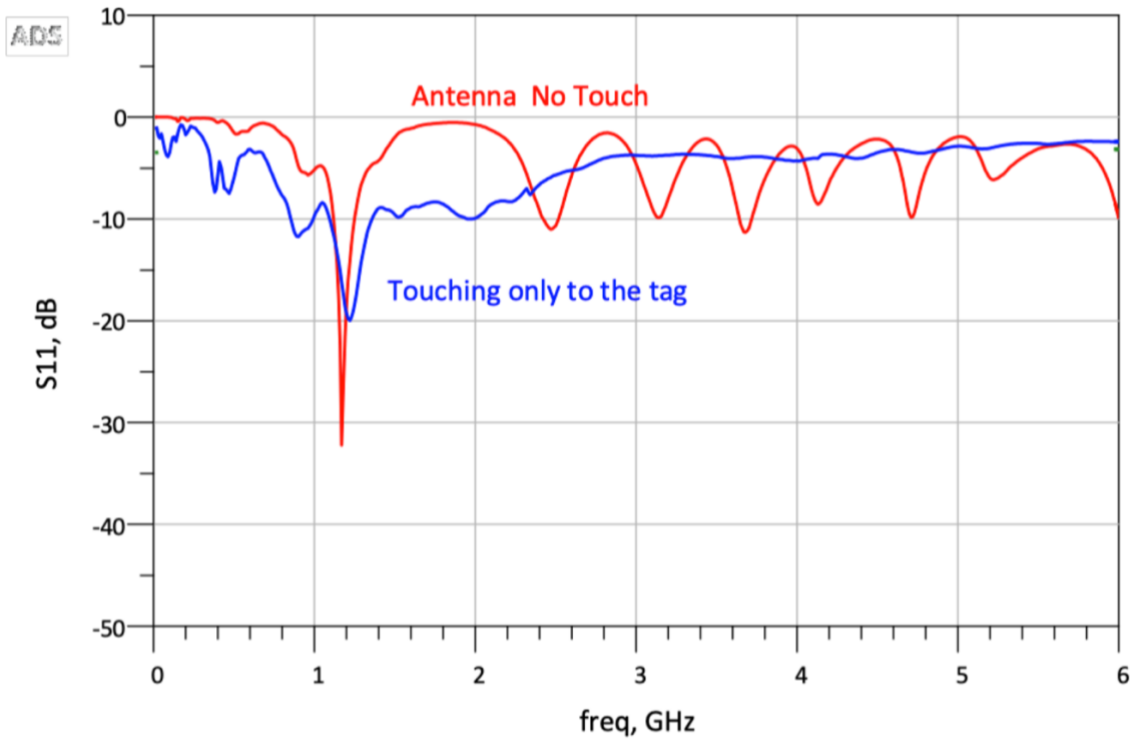

Figure 49: Fabricated UHF tag version 1 (shorter dipole antennas)

From figure 49, shorter dipole antenna S11 resonance reflection occurs at 1.1 GHz. The higher frequency ripples are caused by the printing quality in a vertical direction, since, the each folded line represents higher frequencies, and with a shorter length, they create reflective resonance at those frequencies. However, the highest resonance frequency occurs at the complete dipole antenna and thousand times more robust than the ripples. The difference between touching and non-touching is the human body has its own magnetic field. This test ensures the surface of the transmission lines or antennas is not very smooth; our magnetic body interference dissipates the ripples at high frequency levels since their effect is caused by a wavy printing in a vertical direction. The printing impurity in a vertical plane is the reason for the frequency ripple effect where the vertical printing

has an issue with a wavy surface and increased ohmic shape (lower conductivity). Therefore, at each curved section acts as an independent antenna parts having its own resonant frequency related to its length. According to this observation, having a printed super high-frequency tag with a method (90-degree rotation) introduced in the fabrication section prevents these unwanted ripples and noises in super-high frequencies. However, we are not concerned about the UHF level monitoring in our tags where we haven't used multiplexed resonators. Our approach has improved the quality of the printing but also provided a new method in testing and observations of the printed RF tags.

6.2.1. UHF Wireless Gas Sensing

Our designed tag is able to operate between UHF levels from 300 MHz to 3 GHz. We have designed our tag for chipless and batteryless low-cost wireless sensing. The design and experimental setup are discussed before.

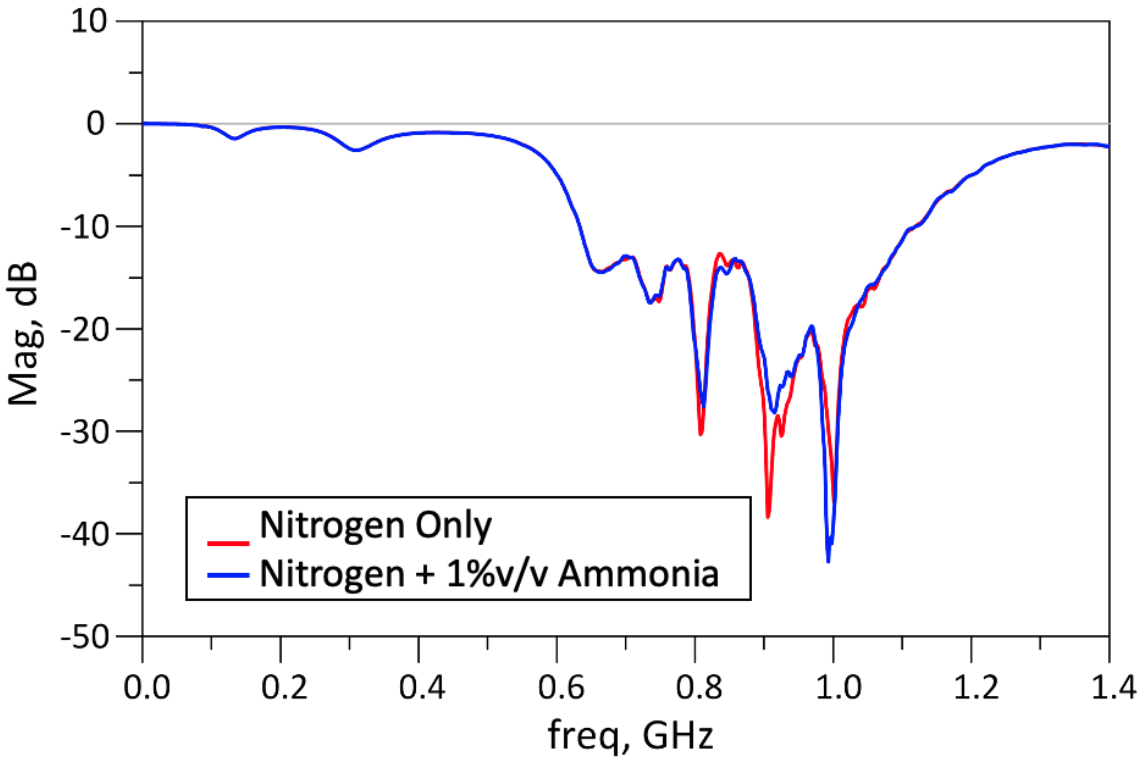

Figure 50: Nitrogen only and nitrogen with ammonia measurements from the setup at a particular concentration.

Without changing anything in the chamber, just with the changes in the ammonia gas changes, we observed changes in our received signal as it seen in figure 50 above. This result encouraged us to measure other concentrations. Ammonia molecules attached to PANI particles where it becomes less conductive the impedance increases, and the gain decreases dramatically. This change is observed to measure the concentration in the chamber. 99% nitrogen and 1% ammonia concentration configuration were promising for us to observe ppm levels, and we pursued the ppm levels measurements for the wireless ammonia sensing.

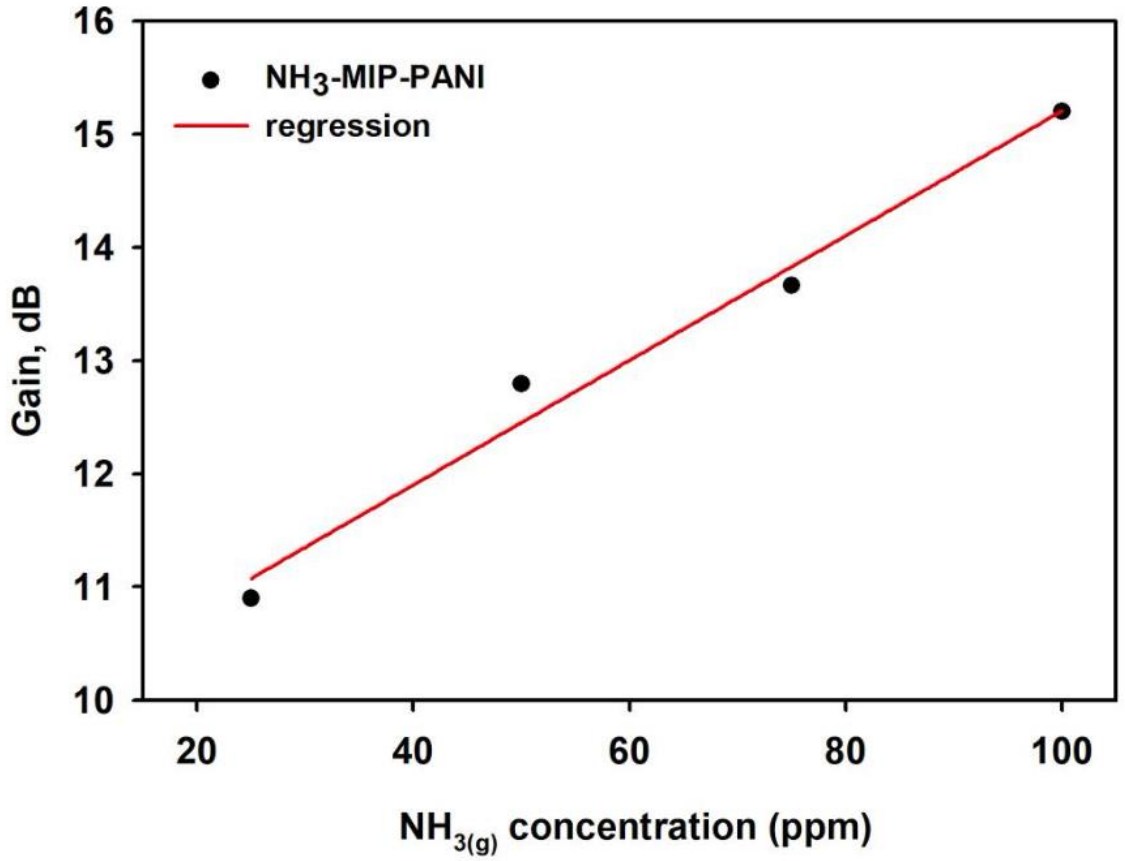

Figure 51: Molecular imprinted wireless sensor measurement in several ammonia concentrations

As seen in the figure, our measurements presented linear response and reliable wireless reflections where we can process the changes in the gain as a factor of ammonia concentration. PANI is very reactive to the ammonia and changed the overall impedance of the circuitry. We have observed more gain changes where the concentration increases. This increase was linear and reliable for further calculations, in which we have calculated the limit of detection of the sensor. This result has encouraged us to create more molecularly printed electrodes and observe changes in the frequency or the gain. The

measurement concentration of the samples was 25 ppm, 50 ppm, 75 ppm, and 100 ppm, respectively.

6.2.2. UHF Level Wireless Plant Stress Monitoring

Ultra-high frequency level wireless sensing has been achieved with that tag that can resonate between UHF levels. And we have integrated an interdigitated electrode design to see the overall tag response. The design and the methods are discussed in the design and fabrication of the UHF level sensors section. We measured magnitude changes from the first reference measurement to other time measurements.

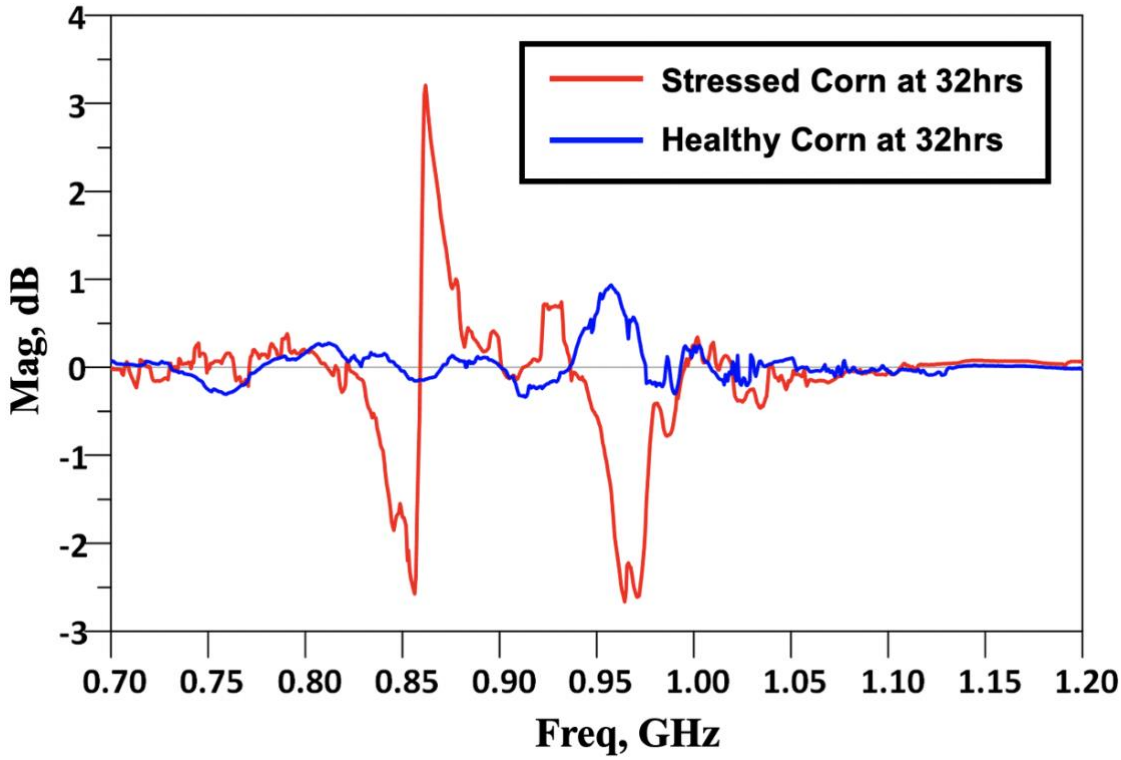

Figure 52: Stressed and healthy corn response in wireless measurements.

Stressed and not stressed responses of the corn plants are measured wirelessly and their changes of the responses 8 hours interval measured and subtracted from the first measurement. Healthy corns did not have similar fluctuations in measurements, and stressed group corns had noticeable fluctuations between 830 MHz to 1 GHz. Therefore, we have calculated and compared their averaged fluctuations of healthy and unhealthy (stressed by drought) corn plants. We observed positive averaged amplitude in dB at healthy plants and negative dB averaged levels in stressed plants. Therefore, we focused more on averaged signal rather than the resonance peaks since they can be deceiving some other environmental noises. As it is seen from the figure above, it looks there is a peak at 0.86 GHz. However, we found its not correct if we average the whole signal. The change should affect the overall response of the tag rather than only one resonance point like in the gas sensor. Gas sensor had a more precise amplitude change than the interdigitated measurement of the plant.

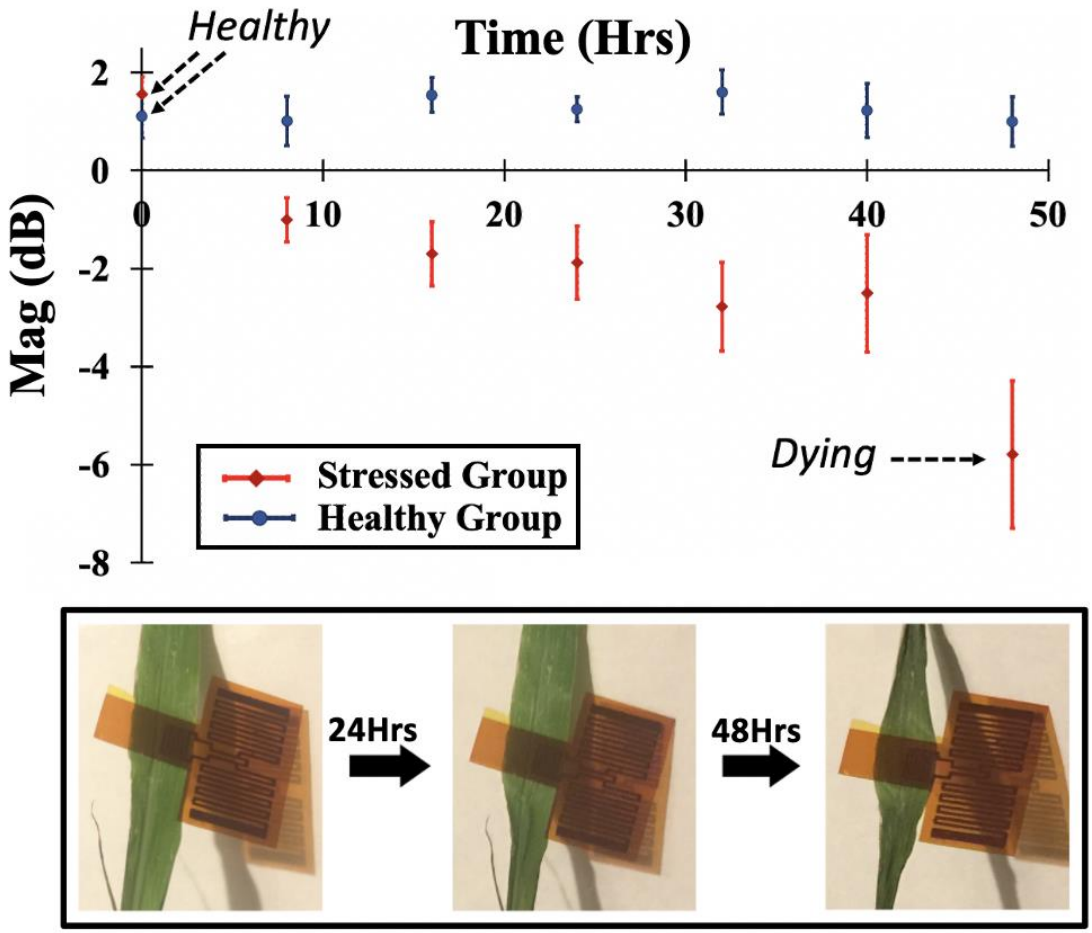

Figure 53: Healthy and stressed plants averaged magnitude results from UHF wireless sensing tag

As it is seen from the figure, the stressed group of the corn samples was dead after 48 hours from the water scarcity. And those healthy corns and the stressed group had similar measurement point right after the stressed group corns were not watered regularly like the healthy ones. Measurements results have changed, and the difference between healthy and stressed increased dramatically. We have observed the changes and performed early stress detection in 10 hours before the stress becomes noticeable after 24 hrs. The

measured time intervals were 8 hours, 16 hours, 24 hours, 32 hours, 40 hours, and 48 hours respectively. We have presented a successful wireless drought stress monitoring for corn plants.

6.3. LF Level Plant Health Sensing

Low-frequency level measurements are tried to observe the biotic and abiotic stress level in the plant; for this purpose, we have obtained capacitance and resistance in 100kHz where the frequency is standard inthe LCR meter and the VNA we have used.

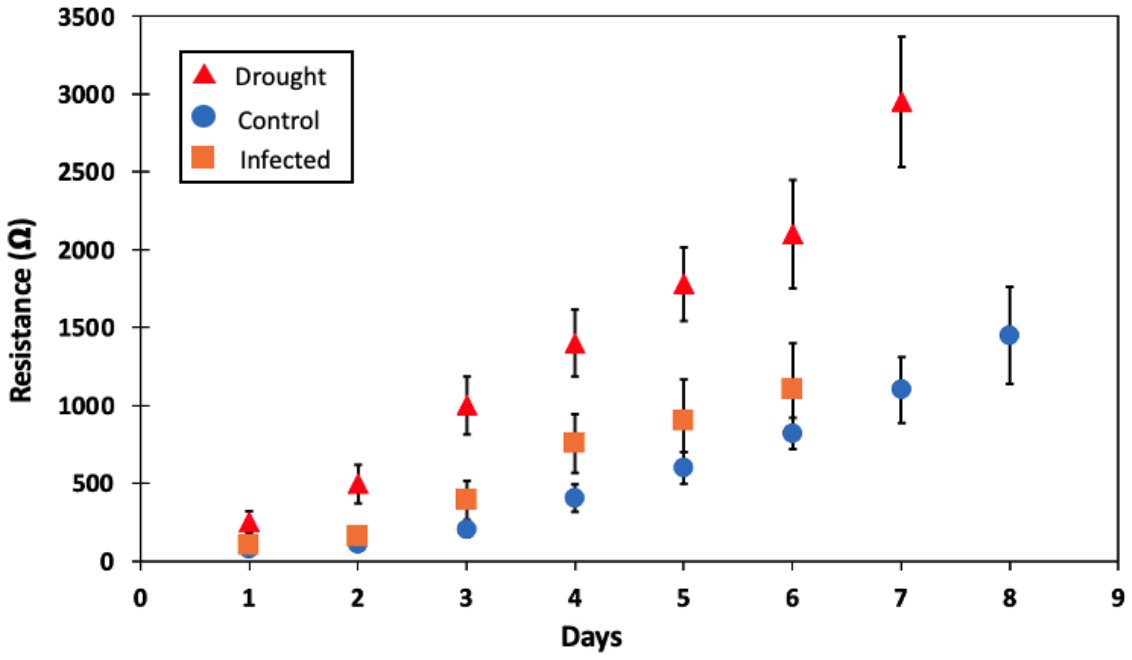

Figure 54: Measured resistance from the cotton samples

From the figure, we have observed resistance changes in all samples. However, the resistance changes from the drought testing samples were much more significant than those control and infected samples. Resistance error has increased over time since the

testing setup, and light might have very tiny changes by the position of the seedlings, and more it will be affected by the growth rate differences between each sample.

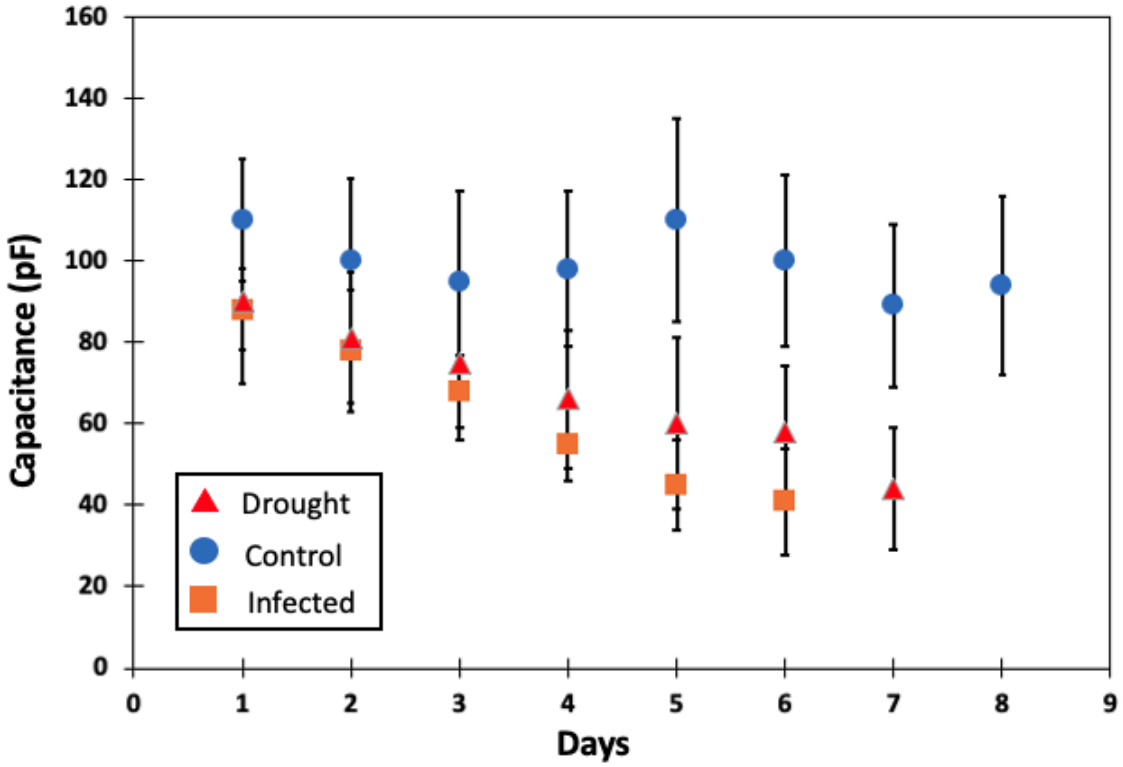

Figure 55: Measured capacitance from the cotton samples

The measured capacitance is related to the size of the electrode and the thickness of the leaf; for this purpose we kept the distance fixed for the cotton to avoid any damaging and pressures effect our measurements. We observed capacitance differences between control and the rest. Drought and infection do not differentiate in capacitance. However, with this method we observed the changes in capacitance on control groups of cotton seedlings as it seen from figure 55. This means that we can detect the samples which are healthy and under stress.

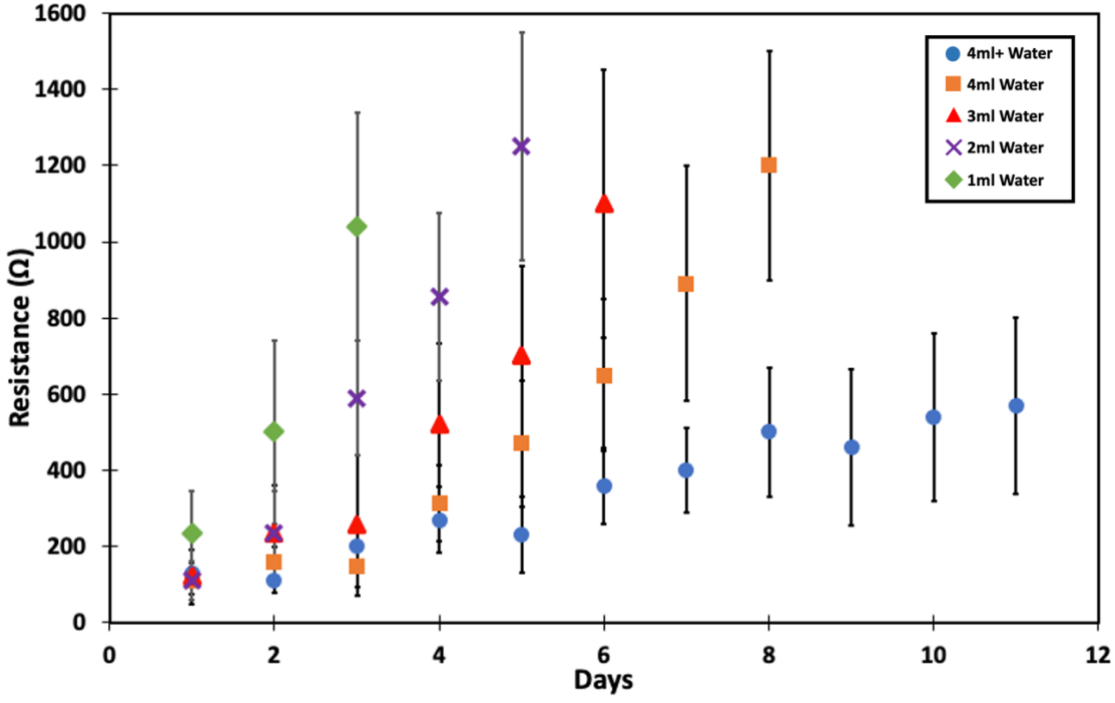

Figure 56: Resistance Measurements for abiotic drought stress on cotton seedlings

We have observed abiotic stress differences in several water concentrations cotton seedlings where the 4mL considered 100% watering as shown in the figure above. The testing samples were varied by their water content and their continuous watering. The testing setup and testing samples comparisons are given in the previous section. We observed tremendous changes in resistance when a plant has a resistance jump and found that this is a meaning of dying in couple days if it was not watered. We measured and compared different water concentrations to see if it provides us a similar jump between in those samples. And as it is depicted from figure 56, we found more abrupt changes in the

resistance before they worsen. This phenomenon is caused by the dramatic changes in the leaves when the plant is overstressed.

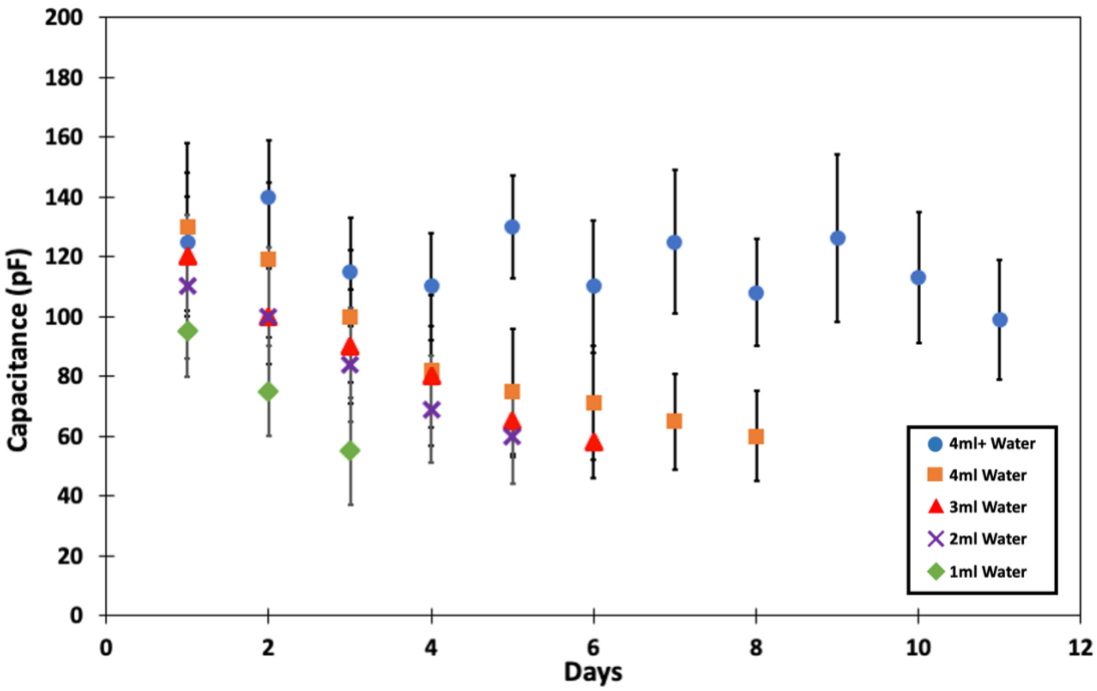

Figure 57: Capacitance measurement of abiotic drought stress on cotton seedlings

We have observed the stressed seedlings has more capacitive decrease by the time as it seen from results figure above. This measurement again distinguishes healthy, and the stressed as expected and matches with our previous measurements and discussions. Capacitance decrease in overall in time too, where the plant thickness changes by the growth, as we discussed from the basic capacitance equation.

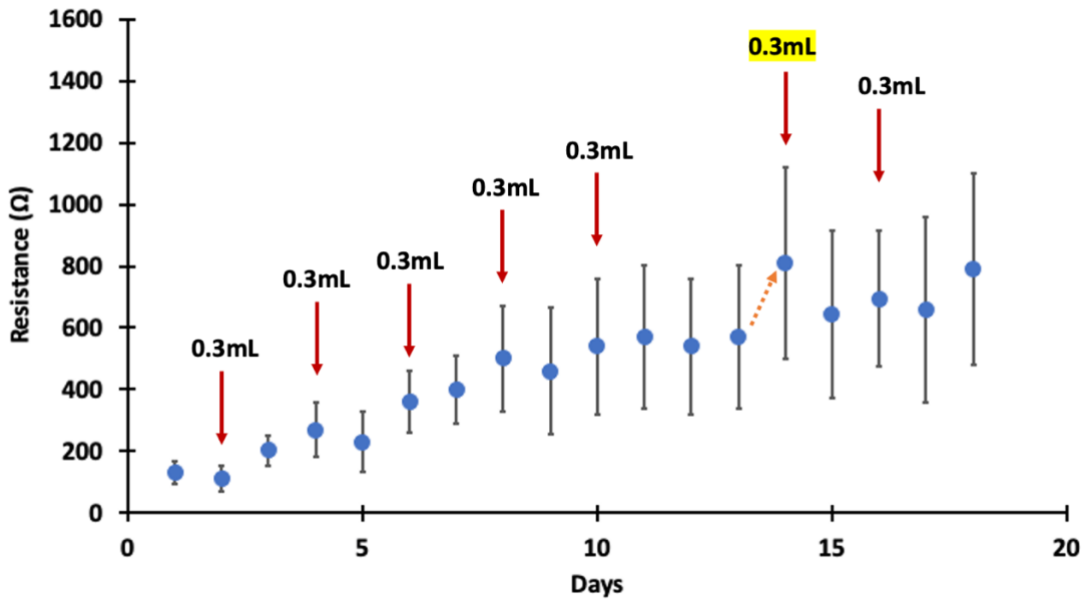

Figure 58: Measured resistance at 100 kHz of abiotic drought stress on cotton seedlings

As seen in the figure the arrows show the added water was 0.3 mL, and the samples watered periodically until the day ten after the watering, it has not received any water and the stress level of the plant measured by simply measuring the resistance. We found on the day 14 tremendous changes in resistance as a percentage and realized it would be dead in a couple of days if it does not get any water. Therefore, we have watered and observed the changes along with the measurements. It has recovered in 2 days and continued the regular growing chart. The threshold level for the excessive stress in plants is the measurement dependent where the continuous measurement changes in time. We observed extreme changes in resistance, where the escalation/slope more than 40°. When in passes specific escalation rate it denotes us to add more water; otherwise the plan will be deformed and cannot be recovered.

7. CONCLUSIONS

This research described and explained a multiplexing, wireless and batteryless sensors with an effective plant health monitoring in detail. The sensors are made by ultra-low-cost materials and performed effectively in sensing. The sensor is powered when a signal is received by the RF wireless communication antenna and takes measurements of a medium being monitored by the sensor. Data corresponding to the measurements is then transmitted from the sensor via the RF wireless communication antenna. Our UWB SHF level antenna soil moisture and temperature sensor tag has an ability to be multiplexed and used in outdoor conditions. UHF level gas and plant stress monitoring tag has an advantage to qualify as an effective commercial sensor and can be used for multiple medium detections. In addition to all, we have proved LF level electrodes can be used to distinguish biotic and abiotic stress in plants with the method and approach we have described and demonstrated.

REFERENCES

[1] Mannoor, M. S., Tao, H., Clayton, J. D., Sengupta, A., Kaplan, D. L., Naik, R. R., ... & McAlpine, M. C. "Graphene-based wireless bacteria detection on tooth enamel." *Nature communications*, 3, 763, 2012.

[2] Larpant, N., Pham, A. D., Shafaat, A., Gonzalez-Martinez, J. F., Sotres, J., Sjöholm, J., ... & Ruzgas, T. "Sensing by wireless reading Ag/AgCl redox conversion on RFID tag: Universal, battery-less biosensor design," *Scientific reports*, *9*(1), 1-9, 2019.

[3] Xie, M. Z., Wang, L. F., Dong, L., Deng, W. J., & Huang, Q. A. "Low cost paper-based LC wireless humidity sensors and distance-insensitive readout system." *IEEE Sensors Journal*, 19(12), 4717-4725, 2019.

[4] Hojaiji, H., Kalantarian, H., Bui, A. A., King, C. E., & Sarrafzadeh, M. "Temperature and humidity calibration of a low-cost wireless dust sensor for real-time monitoring." *IEEE sensors applications symposium* (SAS) (pp. 1-6). March 2017.

[5] Zheng L, Wang L, Sun H, Zhang M, Li M "Real-time evaluation of corn leaf water content based on the electrical property of leaf." *Comput Electron Agric* 112:102–109, 2015.

[6] Bogena, H. R., Huisman, J. A., Oberdörster, C., & Vereecken, H. "Evaluation of a low-cost soil water content sensor for wireless network applications." *Journal of Hydrology*, 344(1-2), 32-42, 2007.

[7] Harun, A. N., Kassim, M. R. M., Mat, I., & Ramli, S. S. “Precision irrigation using wireless sensor network.” *International Conference on Smart Sensors and Application (ICSSA)* (pp. 71-75). IEEE, May 2015.

[8] Ruiz-Garcia, L., Lunadei, L., Barreiro, P., & Robla, I. “A review of wireless sensor technologies and applications in agriculture and food industry: state of the art and current trends.” *sensors*, 9(6), 4728-4750, 2009.

[9] Ojha, T., Misra, S., & Raghuwanshi, N. S. “Wireless sensor networks for agriculture: The state-of-the-art in practice and future challenges.” *Computers and Electronics in Agriculture*, 118, 66-84, 2015.

[10] Palazzi, V., Gelati, F., Vaglioni, U., Alimenti, F., Mezzanotte, P., & Roselli, L. “Leaf-compatible autonomous RFID-based wireless temperature sensors for precision agriculture” *IEEE Topical Conference on Wireless Sensors and Sensor Networks (WiSNet)* (pp. 1-4). IEEE, January 2019.

[11] Amin, M., Ramzan, R., & Siddiqui, O. “Slow wave applications of electromagnetically induced transparency in microstrip resonator”, *Scientific reports*, 8(1), 1-13, 2018.

[12] Visconti, P., De Fazio, R., Primiceri, P., Cafagna, D., Strazzella, S., & Giannoccaro, N. I. “A Solar-Powered Fertigation System based on Low-Cost Wireless Sensor Network Remotely Controlled by Farmer for Irrigation Cycles and Crops Growth Optimization.” *International Journal of Electronics and Telecommunications*, *66*(1), 59-68, 2020.

[13] Yang, L., Rida, A., Vyas, R., & Tentzeris, M. M. “RFID tag and RF structures on a paper substrate using inkjet-printing technology.” *IEEE transactions on microwave theory and techniques*, *55*(12), 2894-2901, 2007.

[14] Orecchini, G., Alimenti, F., Palazzari, V., Rida, A., Tentzeris, M. M., & Roselli, L. ”Design and fabrication of ultra-low cost radio frequency identification antennas and tags exploiting paper substrates and inkjet printing technology.” *IET microwaves, antennas & propagation*, *5*(8), 993-1001, 2011.

[15] Kim, S., Kawahara, Y., Georgiadis, A., Collado, A., & Tentzeris, M. M. “Low-cost inkjet-printed fully passive RFID tags using metamaterial-inspired antennas for capacitive sensing applications.” *2013 IEEE MTT-S International Microwave Symposium Digest (MTT)* (pp. 1-4). IEEE, June 2013.

[16] Zhang, J., Tian, G. Y., Marindra, A. M., Sunny, A. I., & Zhao, A. B. “A review of passive RFID tag antenna-based sensors and systems for structural health monitoring applications.” *Sensors*, *17*(2), 265, 2017.

[17] Riheen, M. A., Saha, T. K., & Sekhar, P. K. “Inkjet printing on PET substrate.” *Journal of the Electrochemical Society*, *166*(9), B3036, 2019.

[18] Van Osch, T. H., Perelaer, J., de Laat, A. W., & Schubert, U. S. “Inkjet printing of narrow conductive tracks on untreated polymeric substrates.” *Advanced Materials*, *20*(2), 343-345, 2008.

[19] Ferrández-Pastor, F. J., García-Chamizo, J. M., Nieto-Hidalgo, M., Mora-Pascual, J., & Mora-Martínez, J. “Developing ubiquitous sensor network

platform using internet of things: Application in precision agriculture," *Sensors*, *16*(7), 1141, 2016.

[20] Engel, K. H., Frenzel, T., & Miller, A. "Current and future benefits from the use of GM technology in food production." *Toxicology letters*, *127*(1-3), 329-336, 2002.

[21] Badgley, C., Moghtader, J., Quintero, E., Zakem, E., Chappell, M. J., Aviles-Vazquez, K., ... & Perfecto, I. "Organic agriculture and the global food supply." *Renewable agriculture and food systems*, 86-108, 2007.

[22] Crist, E., Mora, C., & Engelman, R. "The interaction of human population, food production, and biodiversity protection." *Science*, *356*(6335), 260-264, 2017.

[23] Abbasi, A. Z., Islam, N., & Shaikh, Z. A. "A review of wireless sensors and networks' applications in agriculture." *Computer Standards & Interfaces*, *36*(2), 263-270, 2014.

[24] Adamchuk, V. I., Hummel, J. W., Morgan, M. T., & Upadhyaya, S. K. "On-the-go soil sensors for precision agriculture," *Computers and electronics in agriculture*, *44*(1), 71-91, 2004.

[25] Antonacci, A., Arduini, F., Moscone, D., Palleschi, G., & Scognamiglio, V. "Nanostructured (Bio) sensors for smart agriculture." *TrAC Trends in Analytical Chemistry*, *98*, 95-103, 2018.

[26] Muangprathub, J., Boonnam, N., Kajornkasirat, S., Lekbangpong, N., Wanichsombat, A., & Nillaor, P. “IoT and agriculture data analysis for smart farm.” *Computers and electronics in agriculture*, *156*, 467-474, 2019.

[27] Ghafar-Zadeh, E.“Wireless integrated biosensors for point-of-care diagnostic applications.” *Sensors*, *15*(2), 3236-3261, 2015.

[28] Srbinovska, M., Gavrovski, C., Dimcev, V., Krkoleva, A., & Borozan, V. “Environmental parameters monitoring in precision agriculture using wireless sensor networks.” *Journal of cleaner production*, *88*, 297-307, 2015.

[29] Riquelme, J. L., Soto, F., Suardíaz, J., Sánchez, P., Iborra, A., & Vera, J. A. “Wireless sensor networks for precision horticulture in Southern Spain.” *Computers and electronics in agriculture*, *68*(1), 25-35, 2009.

[30] Ruiz-Garcia, L., Lunadei, L., Barreiro, P., & Robla, I. “A review of wireless sensor technologies and applications in agriculture and food industry: state of the art and current trends.” *sensors*, *9*(6), 4728-4750, 2009.

[31] Ferri, J., Lidón-Roger, J. V., Moreno, J., Martinez, G., & Garcia-Breijo, E. “A wearable textile 2D touchpad sensor based on screen-printing technology.” *Materials*, *10*(12), 1450, 2017.

[32] Wei, Y., Torah, R., Yang, K., Beeby, S., & Tudor, J. “Screen printing of a capacitive cantilever-based motion sensor on fabric using a novel sacrificial layer process for smart fabric applications.” *Measurement Science and Technology*, *24*(7), 075104, 2013.

[33] Dincel, O., Ueta, T., & Kameoka, J. “Acoustic driven microbubble motor device.” *Sensors and Actuators A: Physical*, *295*, 343-347, 2019.

[34] Chen, Z., Wright, C., Dincel, O., Chi, T. Y., & Kameoka, J. “A Low-Cost Paper Glucose Sensor with Molecularly Imprinted Polyaniline Electrode.” *Sensors*, *20*(4), 1098, 2020.

[35] Li, Z., & Bhadra, S. “A 3-bit fully inkjet-printed flexible chipless RFID for wireless concentration measurements of liquid solutions.” *Sensors and Actuators A: Physical*, *299*, 111581, 2019.

[36] Parra, L., Sendra, S., Lloret, J., & Rodrigues, J. J.“Low cost wireless sensor network for salinity monitoring in mangrove forests.” In *SENSORS, 2014 IEEE* (pp. 126-129). IEEE, November 2014.

[37] Manzari, S., Occhiuzzi, C., Nawale, S., Catini, A., Di Natale, C., & Marrocco, G. “Polymer-doped UHF RFID tag for wireless-sensing of humidity” In *2012 IEEE International Conference on RFID (RFID)* (pp. 124-129). IEEE, April 2012.

[38] Zou, Z., Chen, Q., Uysal, I., & Zheng, L.”Radio frequency identification enabled wireless sensing for intelligent food logistics.” *Philosophical Transactions of the Royal Society A: Mathematical, Physical and Engineering Sciences*, *372*, 20130313, 2014.

[39] Bhattacharyya, R., Floerkemeier, C., & Sarma, S. “Low-cost, ubiquitous RFID-tag-antenna-based sensing.” *Proceedings of the IEEE*, *98*(9), 1593-1600, 2010.

[40] Kim, S. G., Jun, J., Lee, J. S., & Jang, J. “A highly sensitive wireless nitrogen dioxide gas sensor based on an organic conductive nanocomposite paste.” *Journal of materials chemistry A*, *7*(14), 8451-8459, 2019.

[41] Hussein, H. M., Rinaldi, M., Onabajo, M., & Cassella, C. “A chip-less and battery-less subharmonic tag for wireless sensing with parametrically enhanced sensitivity and dynamic range.” *Scientific reports*, *11*(1), 1-11, 2021.

[42] Bhattacharyya, R., Floerkemeier, C., & Sarma, S. “RFID tag antenna based temperature sensing.” In *2010 IEEE International Conference on RFID (IEEE RFID 2010)*(pp. 8-15). IEEE, April 2010.

[43] Hsieh, L. H., & Chang, K.”Equivalent lumped elements G, L, C, and unloaded Q's of closed-and open-loop ring resonators.” *IEEE transactions on microwave theory and techniques*, *50*(2), 453-460, 2002.

[44] Wang, X., Zhang, J., Yu, Z., Mao, S., Periaswamy, S. C., & Patton, J. “On remote temperature sensing using commercial UHF RFID tags.” *IEEE Internet of Things Journal*, *6*(6), 10715-10727, 2019.

[45] Chen, Z., Chi, T. Y., Dincel, O., Tong, L., & Kameoka, J. “A Low-cost and Enzyme-free Glucose Paper Sensor” In *2020 42nd Annual International Conference of the IEEE Engineering in Medicine & Biology Society (EMBC)* (pp. 4097-4100). IEEE, July 2020.

[46] Cook, B. S., & Shamim, A. “Inkjet printing of novel wideband and high gain antennas on low-cost paper substrate.” *IEEE Transactions on Antennas and Propagation*, *60*(9), 4148-4156, 2012.

[47] Shaker, G., Safavi-Naeini, S., Sangary, N., & Tentzeris, M. M. “Inkjet printing of ultrawideband (UWB) antennas on paper-based substrates.” *IEEE Antennas and Wireless Propagation Letters*, *10*, 111-114, 2011.

[48] Choi, S. H., Park, J. K., Kim, S. K., & Park, J. Y. “A new ultra-wideband antenna for UWB applications.” *Microwave and optical technology letters*, *40*(5), 399-401, 2004.

[49] Henderson-Sellers, A. ”Soil moisture: A critical focus for global change studies.” *Global and Planetary Change*, *13*(1-4), 3-9, 1996.

[50] Hay, R. K. M., & Wilson, G. T. “Leaf appearance and extension in field-grown winter wheat plants: the importance of soil temperature during vegetative growth.” *The Journal of Agricultural Science*, *99*(2), 403-410, 1982.

[51] Fares, A., & Alva, A. K. “Evaluation of capacitance probes for optimal irrigation of citrus through soil moisture monitoring in an entisol profile,” *Irrigation Science*, *19*(2), 57-64, 2000.

[52] Zazueta, F. S., & Xin, J. “Soil moisture sensors.” *Soil Sci*, *73*, 391-401, 1994.

[53] “Verdmo Pro SOIL,” *Verdmo Pro*. [Online]. Available: https://www.verdmopro.com/verdmo-pro-soil. [Accessed: 10-May-2021].

[54] “Hobo Inc. Soil Moisture Data Loggers & Sensors,” *Soil Moisture Data Loggers & Sensors | Onset Data Loggers*. [Online]. Available: https://www.onsetcomp.com/products/data-loggers-sensors/soil-moisture/. [Accessed: 10-May-2021].

[55] “ Onset Inc. HOBOnet T12 Soil Moisture/Temp/EC Sensor,” *TEROS 12 Soil Sensor*. [Online]. Available: https://www.onsetcomp.com/products/sensors/rxw-t12-xxx. [Accessed: 10-May-2021].

[56] Elobaid, H. A. E., Rahim, S. K. A., Himdi, M., Castel, X., & Kasgari, M. A. “A transparent and flexible polymer-fabric tissue UWB antenna for future wireless networks” *IEEE Antennas and Wireless Propagation Letters*, *16*, 1333-1336, 2016.

[57] Lee, H. J., Park, K. K., Oralkan, Ö., Kupnik, M., & Khuri-Yakub, B. T. (2014). “A multichannel oscillator for a resonant chemical sensor system” *IEEE Transactions on Industrial Electronics*, *61*(10), 5632-5640, 2014.

[58] Shang, X., Wang, Y., Xia, W., & Lancaster, M. J. “Novel multiplexer topologies based on all-resonator structures.” *IEEE Transactions on Microwave Theory and Techniques*, *61*(11), 3838-3845, 2013.

[59] Bahar, A. A. M., Zakaria, Z., Ab Rashid, S. R., Isa, A. A. M., & Alahnomi, R. A. “High-efficiency microwave planar resonator sensor based on bridge split ring topology.” *IEEE microwave and wireless components letters*, *27*(6), 545-547, 2017.

[60] Carroll, J. M., & Chang, K. “Microstrip mode suppression ring resonator”, *Electronics Letters*, *30*(22), 1861-1862, 1994.

[61] Seyfert, F., & Bila, S.“General synthesis techniques for coupled resonator networks.” *IEEE Microwave Magazine*, *8*(5), 98-104, 2007.

APPENDIX A

EDX AND SEM IMAGES

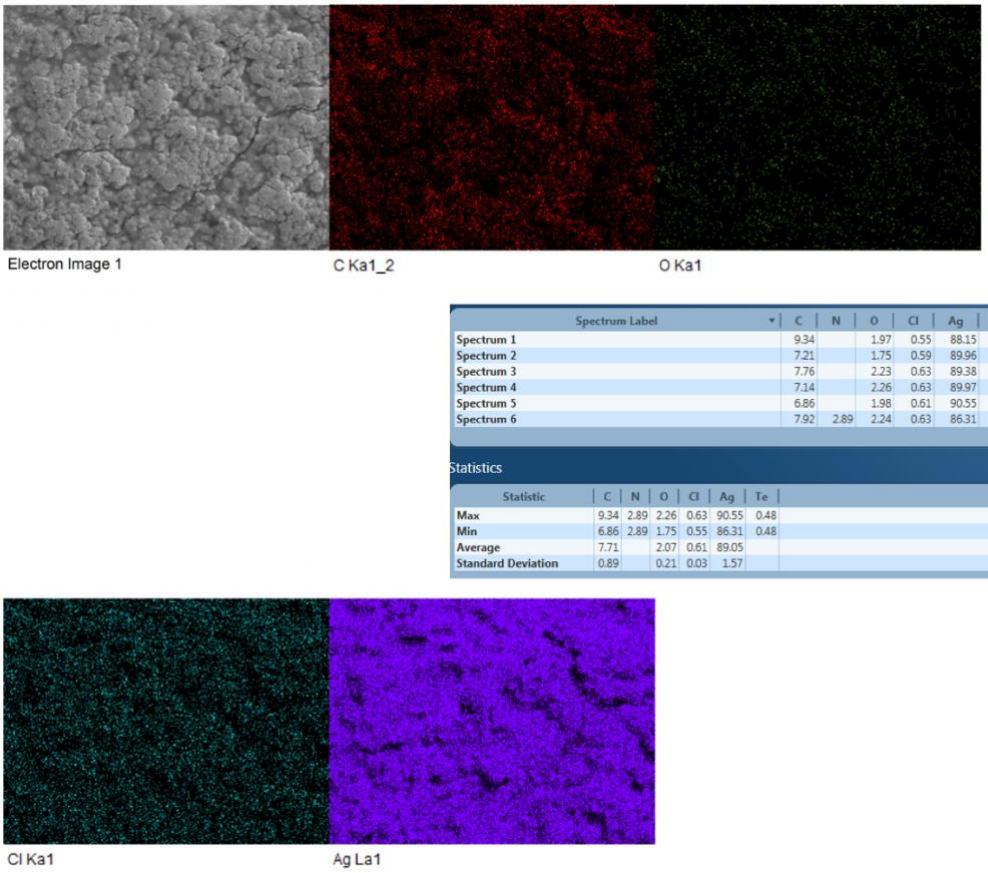

Spectrum Label	C	N	O	Cl	Ag	Te	Total
Spectrum 1	9.34		1.97	0.55	88.15		100.00
Spectrum 2	7.21		1.75	0.59	89.96	0.48	100.00
Spectrum 3	7.76		2.23	0.63	89.38		100.00
Spectrum 4	7.14		2.26	0.63	89.97		100.00
Spectrum 5	6.86		1.98	0.61	90.55		100.00
Spectrum 6	7.92	2.89	2.24	0.63	86.31		100.00

Statistics

Statistic	C	N	O	Cl	Ag	Te
Max	9.34	2.89	2.26	0.63	90.55	0.48
Min	6.86	2.89	1.75	0.55	86.31	0.48
Average	7.71		2.07	0.61	89.05	
Standard Deviation	0.89		0.21	0.03	1.57	

Figure 59: EDX measurement and SEM images with Silver, Chloride, Oxygen, Carbon atoms in the sample

In figure, the material content for silver nanoparticle ink and the materials distinguishment to understand the compounds and the molecules. EDX measurement gives detailed knowledge for further molecular imprinting techniques and its ability to integrate with existing inkjet products.

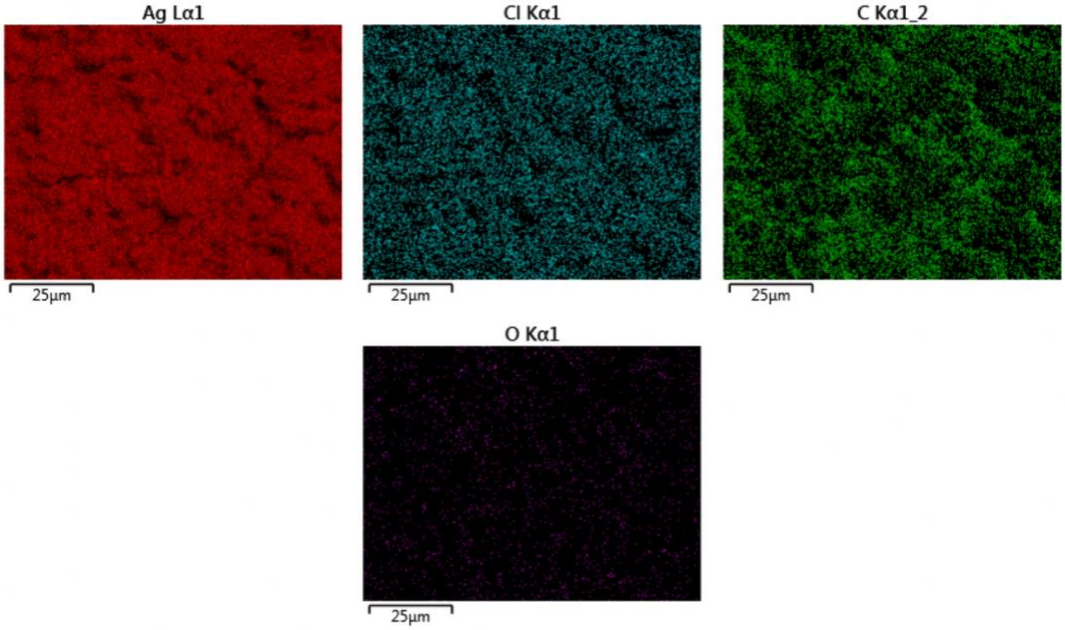

Figure 60: Silver, Chloride, Carbon and Oxygen atoms in the ink sample

In figure 60, Silver, chloride and carbon materials with a rare concentration of oxygen molecules observed in the sample ink we considered this migh be caused from oxidation and humidity (water) content.

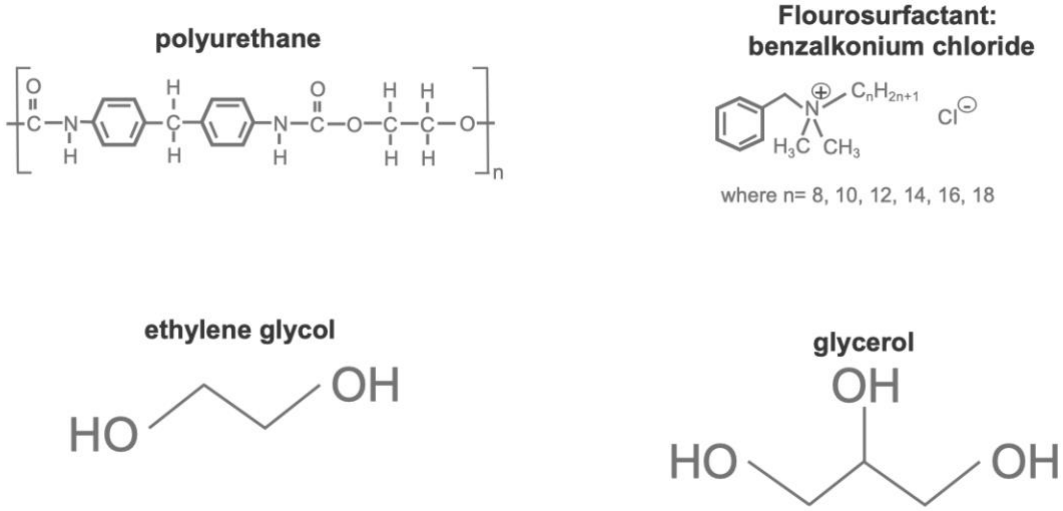

Figure 61: Polyurethane, Ethylene glycol, Flourosurfactant (Benzalkonium Chloride), and Glycerol Chemical Structures

Figure 61, demonstrates the chemical structure and the material content we have found a cured silver nanoparticle inkjet ink.

APPENDIX B

ENHANCEMENTS IN FABRICATION

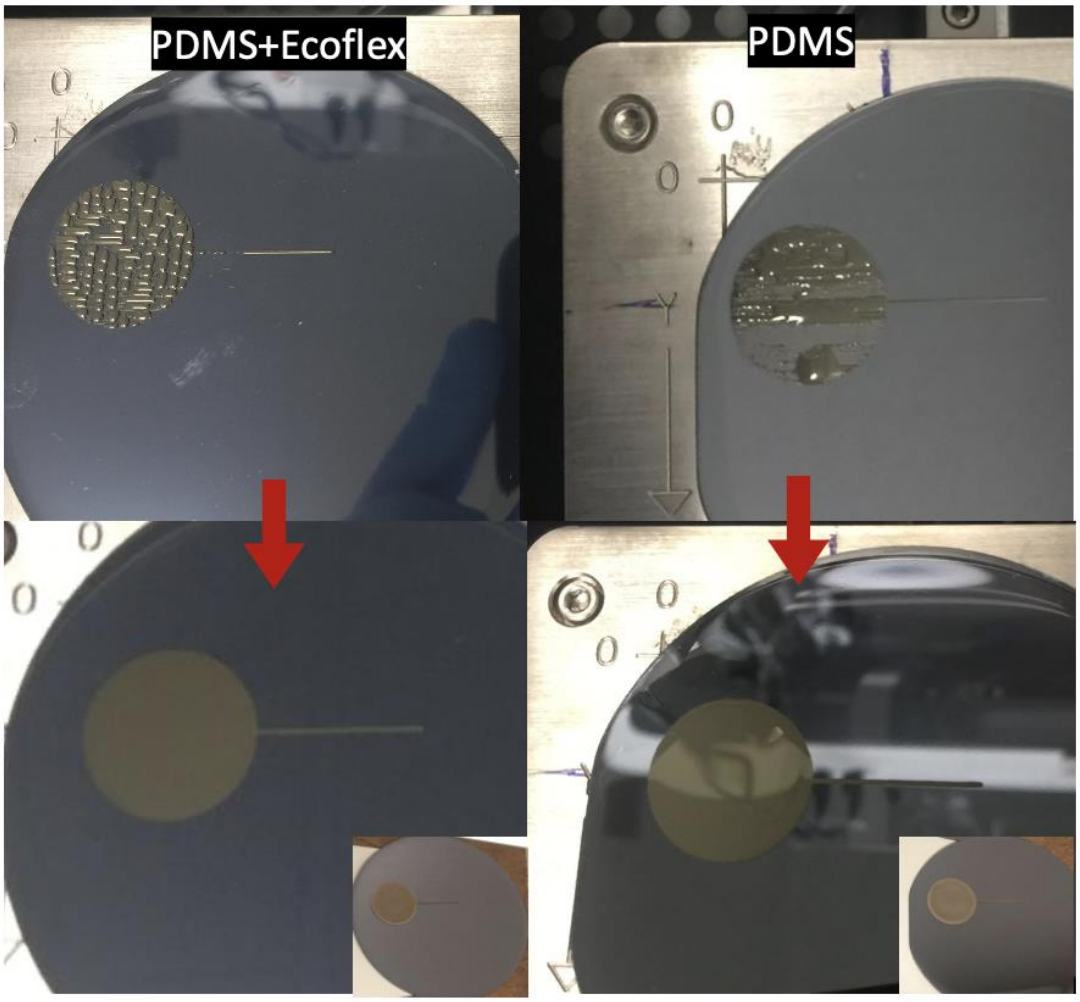

Figure 62: Ultra wide band antenna design on PDMS and PDMS Ecoflex mixed samples

We have tried to print the ultra wide band antenna design on the ecoflex PDMS (polydimethylsiloxane) mixture or PDMS only layers. As seen in the figure above, the

hydrophobicity did not allowed to proper deposition of the silver nano particals on the top. However, we have performed oxygen plasma treatment for two minutes especially at the pink color not purple.

APPENDIX C

DEVICES USED IN FABRICATION

EnvisionTec Perfactory 3D printer has been used for fine printings and molding. Formlabs 3D printer for bigger size covers and designs.

Figure 63: a) Stereolithography 3D printer b) Material inkjet printer c) Spin coater

Oven has been used for curing process of the deposited silver ink at 140C or 110C depends on the sensor and the application. Plasma treatment chamber has been used for making surface hydrophilic. Spin coater from figure 64c has been used to cover the surface of the sensor area to avoid any direct contact with soil. Dimatix material printer is used to deposit silver nano particles (figure 64b). Stereolithography 3D printer has been used to create holders and covers.

Figure 64: Devices are used for cleaning and curing processes a) Ultrasonic Cleaner b) Optical Curing Flashing Machine c) Hand Vacuum d) Scale e) Oven

Vacuum tank and hand vacuum vessel used to de-bubbling the PDMS and Ecoflex in the figure above. RCL meter used to optimize the capacitive sensor probes in plant health monitoring. We have used 6 different VNAs from $100 to $400000. They are Keysight PNA in an anechoic chamber and ENA series in Dr. Entesari Lab, Field fox series handheld in Zachery Engineering lab, Pico VNA in our lab, VNWA3 from SDR kits, and NanoVNA. Stereoscopes and microscopes to observe the printing quality. 4 probes method kelvin probes are used to measure the quality of the printing and curing.

Multimeter is used to test continuities and basic DC resistance. Low-frequency LCR meter has been used to observe the capacitive and reactive response of the designed capacitive electrodes in several frequencies and compare them with the VNA measurements.